STRATHCLYDE INSTITUTE OF PHARMACY & BIOMEDICAL SCIENCES

University of Strathclyde Science

Self-assembling silk hydrogels as a mesenchymal stem cell support matrix for stroke

Osama Abdulaziz Ibrahim
201469442

Strathclyde Institute of Pharmacy and Biomedical

Sciences

March 2018

DECLARATION BY RESEARCHER

‘I declare that, except where specifically indicated, all the work presented in this thesis is my own and I am the sole author of all parts.’

Signed: _____

Date: _____

ABSTRACT

Advanced cell therapies require robust delivery materials, and silk is a promising contender. This biopolymer already has a long clinical track record and can be assembled into a range of material formats, including hydrogels (Chapter 1). The hypothesis of this thesis was that reverse engineered silk could be programmed to form a self-assembling silk hydrogel for stem cell delivery. Therefore, the aim of this thesis was to optimise self-assembling silk hydrogels as a mesenchymal stem cell (MSC)-support matrix for stroke treatment. Sonication energy was used to programme the transition of the silk (1 to 5% w/v) secondary structure from a random coil to a stable β-sheet configuration (Chapter 3). This allowed the fine tuning of self-assembling silk hydrogels to achieve space conformity in the absence of any silk hydrogel swelling (Chapter 3) and to support uniform cell distribution as well as cell viability (Chapter 4). Embedded cells underwent significant proliferation over 14 days, with the best proliferation achieved with 2% w/v hydrogels. Embedded MSCs showed significantly better viability after injection through a 30G needle when the gels were in the pre-gelled state versus post-gelled state (Chapter 4). Silk hydrogels with physical characteristics that matched those of brain tissue showed good space conformity after stereotaxic injection into an ischaemic stroke lesion in mice (Chapter 5). Overall, this thesis demonstrates that silk hydrogel is a promising cell delivery (MSC) platform for central nervous system diseases, especially stroke.

ACKNOWLEDGEMENTS

Firstly, I am grateful to The Almighty God for establishing me to complete this project.

I am extremely grateful to my principle supervisor Dr. Hilary Carswell for her support and guidance. The thesis would not have been possible without her help, support and patience. Her timely advice, scholarly advice and scientific approach have assisted me to accomplish the project. I am deeply grateful to her constant encouragement and great guidance in the detailed work. Her understanding of this field and her tireless work ethic has been an immense inspiration. The fact that her door was always open and her encouraging guidance helped this thesis greatly along the way. Thanks Hilary for always asking and caring about my well-being and for always meeting me with a smile when I was in need of your help with all sorts of questions and issues.

I would like to extend my sincere thanks to my co-supervisor Dr. Philipp Seib who provides me invaluable contribution and experimental advices to the work presented in this thesis. His ambitious, hard work, meticulous scrutiny and unsurpassed knowledge about all aspects of my research help me a lot to do this project.

Immeasurable thanks extend to my colleagues, Dr Craig McKittrick, Thidarat Wongpinyochit, John Totten and Abdulhadi Burzangi for their supports, encouragements, suggestions, motivations, valuable and intensive

discussions, suggestions and most importantly being good and special friends. I am lucky enough to have a smart person in my life (Abdulfattah Alhazmi), who has supported me throughout this thesis. All of them helped me a lot in most of the experimental issues. I can't thank you enough for helping me throughout this experience.

I wish to thank my family, my brother and sisters. A big and warm thanks to my parents for supporting me spiritually throughout this project and in my life in general. Words cannot express how grateful I am for all of the sacrifices that they have made on my behalf. Their prayer for me was what sustained me thus far, they are the most important people in my world and I dedicate this thesis to them.

Finally, the biggest thanks go to my wife Sumaya for always wanting the best for me, and for being willing to do everything to make that happen! Thank you for always believing in me and for managing and enduring so much at home days and nights, and at the same time being so wonderful with our children, throughout the years and in this final critical phase, I love you. May the last words be dedicated to our two children, Lamar and Fahad, who I had while doing my PhD research. I feel so grateful that I have you. Thank you for being my wonderful children. You have already given me so many fantastic moments and are constantly reminding me what is important in life. May God bless all of you.

TABLE OF CONTENTS

LIST OF TABLES

LIST OF EQUATIONS

LIST OF FIGURES

LIST OF ABBREVIATIONS

AB	AlamarBlue
ANOVA	Analysis of variance
BBB	Blood brain barrier
bFGF	Basic fibroblast growth factor
CD	Circular Dichroism
CNS	Central nervous system
DMSO	Dimethylsulfoxide
DNA	Deoxyribonucleic acid
ECM	Extracellular matrix
EDTA	Ethylene diamine triacetic acid
ESC	Embryonic stem cells
FACS	Fluorescence-activated cell sorting
FBS	Foetal bovine serum
FCS	Foetal calf serum
FDA	The American Food and Drug Administration
FTIR	Fourier transform infrared spectroscopy
HCL	Hydrochloride
IKVAV	Isoleucine-lysine-valine-alanine-valine
ILT	Intraluminal thread
LCCA	Left common carotid artery
LECA	Left external carotid artery
LICA	Left internal carotid artery
MCA	Middle cerebral artery

MRI	Magnetic resonance imaging
MSC	Mesenchymal stem cells
MTT	3-(4,5-dimethylthiazol-2-YL)-2,5-diphenyltetrazolium bromide
NSC	Neural stem cell
P	*p*-value
PBS	Phosphate buffered saline
PES	Polyethersulfone
PFA	Paraformaldehyde
PMT	Photomultiplier tube
RCF	Relative centrifugal force
ROS	The reactive oxygen species
SEM	Scanning electron microscope
SF	Silk fibroin
SGZ	Subgranular zone
SVZ	Subventricular zone
TIA	Transient ischaemic attack
tMCAO	Transient Middle Cerebral Artery Occlusion
TRITC	Tetramethylrhodamine-isothiocyanate

CHAPTER 1. INTRODUCTION

1.1 Introduction to stroke.

In the human body, mainly in adults, organs and tissues might be damaged and lose their functions by a wide range of diseases and injuries such as degenerative diseases, trauma, inflammation or any other conditions. The body's self-repair ability usually is limited without any medical intervention. Some damaged tissue cannot be regenerated effectively by itself, such as in the central nervous system (CNS). In addition, the repairing process can involve producing scar tissues instead of restoring the function of tissues and normal structure (Teo and Ramakrishna, 2006, Sun et al., 2016b).

There are more than 100,000 stroke cases in the United Kingdom every year; meaning one case every 5 minutes in the UK and every 2 seconds in the world (StrokeAssociation, 2018). Stroke is the fourth leading cause of death in UK. People surviving from stroke currently in the UK is estimated to be ~1.2 million. Stroke is considered to be the leading cause of disability. Almost two thirds of stroke survivors leave the hospital with a disability. Black people are twice as likely to have a stroke compared to white people (StrokeAssociation, 2018). The stroke is promoted to the lay person as a brain attack; the essential nutrients and oxygen are carried by blood and without blood the brain cells could be damaged or die and this damage leads to different effects on human, such as thinking, moving and communicating, depending on where it happens in the brain (StrokeAssociation, 2018).

As we age, the arteries become narrower, harder and more likely to be blocked. Some lifestyle choices and medical conditions could speed up this process and increase the risk of having a stroke (StrokeAssociation, 2018). Stroke injury is commonly recognized as a highly heterogeneous disease and characteristics of the lesion site are known to depend on a number of parameter such as duration of occlusion, severity and type of injury (Werner and Engelhard, 2007). Excitotoxicity is thought to be responsible for primary injury, whereas inflammation is thought to be the major contributor of secondary injury. In terms of brain repair, glial scarring, low cell replacement and inhibitory molecules at the lesion site limit regeneration and plasticity (Tam et al., 2014).

1.2 Types of stroke

1.2.1 Ischaemic

Ischaemic stroke is the most ubiquitous sub-class of stroke (about 85% of strokes) and result from a blockage in cerebral blood vessels (Stonesifer et al., 2017). There are two types of blockage due to fatty deposit: thrombotic and embolic. Cerebral thrombosis is when the blood flow is blocked by clot and obstructs the cerebral vessels. For example, a plaque forms and the intima are roughened along the injured vessels. Then platelets adhere and aggregate in the endothelial injury and the coagulation process is activated leading to formation of a thrombus at the plaque location. Cerebral embolism results from a segment of a blood clot formed elsewhere in the body that

enters the cerebral blood circulation and lodges in a smaller cerebral vessel to block it (Stonesifer et al., 2017). An example is in atrial fibrillation where a blood clot forms in the heart, breaks up and escapes to blood vessels that supply the brain and cause occlusion. Other risk factors for ischaemic stroke include heart valve disease, coronary heart diseases, excessive alcohol intake, an overactive thyroid gland (hyperthyroidism) and lung disease (NHS, 2017). Currently, ischaemic stroke patients suffer from limited options of treatment. Mechanical thrombolysis or a thrombolytic agent, tissue plasminogen activator (tPA), can only be administered during the acute early hours onset of stroke incident, and this limited therapeutic window means the majority of patients are not eligible for thrombolysis. Other than rehabilitation therapy, there is no current treatment for patients to improve functional recovery (Dailey et al., 2013, Zhang et al., 2015).

On the other hand, stem cell therapy could target the subacute and chronic stages of ischaemic stroke, and thereby could provide the patients a potential solution to the management of chronic symptoms that are associated with cerebral ischaemia (Jin et al., 2013).

1.2.1.1 The ischaemic cascade

The ischaemic cascade following stroke can be divided into three phases, acute phase, subacute and chronic phase. The acute phase occurs directly after few hours of occlusion. In this phase, lack of blood flow to the area of stroke makes a region vulnerable to excitotoxicity and oxidative stress

(Yilmaz and Granger, 2010). Reactive oxygen species (ROS) are formed that damage the tissue, mediate microvascular hyperpermeability and contribute to the vasogenic oedema that forms in this area due to water movement into intracellular space, primarily driven by interruption of ionic homeostasis. Na^{+} and Ca^{++} ions accumulate in the cell leading to cell death due to loss of ionic homeostasis and overactivation of Ca^{++} dependent processes (Iadecola and Anrather, 2011).

The subacute phase occurs directly after the acute phase and lasts for few days after stroke onset. During this phase, neuroinflammation is upregulated, with the release of chemokines, cellular adhesion molecules (CAMs), cytokines and matrix metalloproteases (MMPs) from astrocytes, microglia and injured neurons (Acosta et al., 2015, Iadecola and Anrather, 2011).

The third phase involves chronic inflammation that continues after the subacute phase and is driven primarily by astrocytes and activated microglia. These endemic brain cells secrete chemokines, cytokines and CAMs, which recruit more macrophages and neutrophils through the blood brain barrier (BBB). Chronic inflammation could lead to neural death and cerebral oedema. The chronic phase will result in the formation of a cavity in the brain (Iadecola and Anrather, 2011).

1.2.2 Haemorrhagic stroke

About 15% of stroke cases are accounted for by haemorrhagic stroke, which results from damage or malformation in cerebral vessels leading to rupture

and bleeding in the brain. The blood accumulates and condenses in tissues surrounding (subarachnoid haemorrhagic) or in (intracerebral haemorrhagic) the brain (Stonesifer et al., 2017). For example, an intracerebral haemorrhage occurs when there is an artery in the brain parenchyma that bursts leading to blood leaking into surrounding tissue and if not treated will lead to the development of haematoma. Usually preceded by a cerebral aneurysm, subarachnoid haemorrhage occurs when the blood vessels damaged on the superficial layer of the brain diverts the blood into subarachnoid space. This could increase the fluid pressure in the brain leading to swelling, vasospasm and hydrocephalus (Stonesifer et al., 2017).

There are two types of weakened blood vessels that usually lead to haemorrhagic stroke: arteriovenous malformations and aneurysms. Arteriovenous malformation is a group of abnormally formed blood vessels; one of these vessels can rupture causing bleeding in the brain. Aneurysm is swelling in weakened blood vessels. When this swelling is not treated it will ultimately lead to rupture, causing bleeding into the brain. Given that the majority of strokes are ischaemic strokes, the present thesis will focus on ischaemic stroke (Stonesifer et al., 2017).

1.2.3 Transient ischaemic attack

A transient ischaemic attack (TIA) (also called a mini stroke) happens when there is temporary blockage in the blood supply to the brain. It lasts for a

short time and the symptoms pass within 24 hours. A TIA is a sign that a full stroke may occur in the near future (Faiz et al., 2018).

1.3 Current therapeutic strategies

As mentioned above, mechanical or pharmacological (tissue plasminogen activator) thrombolysis are the only approved treatments in stroke in acute phase of brain injury by promoting reperfusion include direct clot lysis (Nih et al., 2016). Endovascular stent retrievers show substantial clinical trial success and are approved (Nih et al., 2016). Currently there is no medical therapy that could provide recovery and repair after stroke. Rehabilitation methods, such as speech therapy and physical occupation, are used to aid recovery in patients but have limited therapeutic effects (Dobkin and Dorsch, 2013).

There are many preclinical and clinical studies to treat stroke which include stem cell therapy to regenerate the lost tissue. Progenitor and stem cell transplantation after stroke promote recovery in pre-clinical models but unfortunately success of these studies are limited due to poor survival of transplanted cell when administered as a suspension form due to immunological attack and abrupt withdrawal of growth factor and attachment support (Lemmens and Steinberg, 2013, Nih et al., 2016).

Some studies have focused on engineered injectable biomaterials such as hydrogels that could be injected directly into the stroke cavity. Hydrogels can

be designed to mimic the mechanical properties of the brain tissue by modulating the crosslinking density. In addition, hydrogels can operate as protective vehicles for both cells and trophic factors with distinct advantages compared with simple injection of either alone (Tam et al., 2014, Nih et al., 2016).

The overall idea of the use of biomaterials in *in situ* tissue regeneration is to implant a biomaterial such as a hydrogel at the site of damage, in order to generate a reparative niche that could support stem cells in tissue repair. Hydrogels show many benefits as a variety of mechanical, chemical and spatial cues can be incorporated to adapt to the brain tissue and to the encapsulated cells. Given the considerable clinical burden of stroke in disabled survivors and paucity of medical therapy that provide recovery, there is an opportunity within preclinical stroke research to reveal new approaches that encourage *in situ* tissue regeneration therapy to promote brain tissue repair after stroke. In the present thesis, we will explore the use of self-assembling silk hydrogels as a support matrix for stem cells after stroke.

1.4 Introduction to stem cells.

Alexander A. Maximov, a Russian histologist was the first to propose the term (stem cell) in 1908 at the annual Congress of the Haematologic Society in Berlin. He gave these cells this term based on the process by which the stem of a tree gives rise to many branches (Loya, 2014). Stem cells originate

from the zygote (fertilized egg); all other cells come from these cells. Stem cells are primitive cells found in all organisms and have the unique capacity for self-renewal or for differentiating into more specialised cells (Robert Passier, 2003).

Stem cells have been classified by their developmental potential as summarised in Table 1.1. Totipotent stem cells have the ability to differentiate to all embryonic and extra-embryonic cell types and have the capacity to form fully functional complete organisms such as the zygote. Pluripotent stem cells are able to differentiate into three germ layers such as endoderm, ectoderm and mesoderm and have the ability to form adult or foetal cell types. Multipotent stem cells mostly consist of progenitor cells and have the ability to give rise to a subset of cell lineages. Oligopotent stem cells have the ability to 6 to a few specific cell lineages. Finally, unipotent stem cells have the ability to differentiate into only one mature cell type (Loya, 2014, Tam et al., 2014).

Table 1.1 Characterisation of Stem Cells

CLASS	CHARAERSTIC	EXAMPLE
Totipotent	Ability differentiate into all cell type. Ability to form full functional organism	Zygote
Pluripotent	Ability to differentiate into all three germ layers. Ability to form foetal or adult cells	ES and foetal stem cells
Multipotent	Ability to differentiate into only a limited number of cells	Adult stem cell and cord blood cell
Oligopotent	Ability to differentiate into cells of a specific tissue	Adult lymphoid stem cells
Unipotent	Ability to differentiate into a single type of cells	Adult muscle stem cells

1.5 Stem cells are potential candidates for brain repair.

There are several properties of stem cells that lend them well to tissue repair and regeneration. Firstly, stem cells often have natural tropism to areas of injury, inflammation and chronic disease. They can therefore be targeted to disease or injury sites either by their chemical tropism or focused delivery

(Miljan and Sinden, 2009). Secondly, stem cells are topologically heterogeneous with the capacity to change quickly as a biological response to their microenvironment (Sinden and Muir, 2012). Thirdly, stem cells can be autologous, generated from the patient's own cells such as cells aspirated from bone marrow, or allogeneic generated from donor and treat thousands of different unrelated patients. Finally, stem cells can provide potencies and unique properties for therapy by genetic modification or by being modified in culture (Sinden and Muir, 2012) .

Regenerative medicine is a fast-developing field of research with the ultimate aim of achieving new cures for different diseases. Cell therapy is being considered as a solution for the maintenance and regeneration of the brain. Until the 1990s, it was commonly believed that the cells of the CNS were unable to self-renew. Recent advances in regenerative medicine have shown that endogenous and exogenous cell therapies can promote angiogenesis, neurogenesis and synaptogenesis in neural tissue (Stonesifer et al., 2017).

Previously, stem cells were thought to have the capacity to replace cells that were dead or that had lost their function in some neurological diseases such as stroke. The expected mechanism by which the cell transplantation could improve stroke deficits was that the cells could differentiate into neurons and astrocytes. However, more recently evidence exists that the prominent mechanisms of stem cells is to increase neovascularization, reduce cell death and recruitment of endogenous progenitors via the secretion of potent biofactors (Bhasin et al., 2013).

Some researchers have evaluated the opportunity of administration the stem cells in early phases of stroke. After brain injury, there is natural process of brain repair such as angiogenesis, neurogenesis, gliogenesis, oligodendrogenesis and synaptogenesis (Diez-Tejedor et al., 2014). The optimal route of administration of stem cells is still unclear. Intravenous administration has the benefit of being less invasive than intracerebral administration. However intracerebral administration has the benefit of exerting local effects without circulating stem cells locating into unwanted organs (Gutierrez-Fernandez et al., 2011). A major aim of stem cell research is to develop local intracerebral stem cell delivery systems that are biocompatible, biodegradable, injectable, and have the ability to retain viability of the stem cells.

1.6 Type of stem cells:

Stem cells used for transplantation include embryonic, neural, induced pluripotent stem cells and mesenchymal stem cell. Their advantages and disadvantages are detailed below and summarised in Table 1.2.

1.6.1 Embryonic stem cells.

Embryonic stem cells (ESCs) are pluripotent stem cells that are derived from inner cell mass of pre-implantation embryo. ESCs are formed during embryonic development from the cleavage of the zygote, which normally occurs before blastocyst formation. When they are reintroduced into the

blastocyst they can colonize cells of different lineages that include the germline. These cells have pluripotent potential *in vivo,* moreover they can maintain their ability to self-renew and differentiation *in vitro* (Loya, 2014).

From a clinical viewpoint, the ESC has a significant greater therapeutic value than their adult counterparts due to their potential to generate all specialized tissue including somatic cells and germ cells. However, using ESC in both clinical and academic environment is fraught with both ethical, technical and safety challenges (Stefan Przyborski, 2008).

1.6.1.1 Technical challenges of *in vitro* research

There are some technical challenges for several reasons when culturing ESC such as: it is difficult to maintain the ESC in an undifferentiated state because of their high capacity to differentiate spontaneously. In addition, presence of the protective layer of tissue surrounding the blastocyst known as trophoectoderm make the isolation of the cells from the inner cell mass technically challenging (Stojkovic et al., 2004) and requires a feeder layer of mitotically-inactive mouse embryonic fibroblasts (Stefan Przyborski, 2008).

However, disadvantages of ESCs are their risks of teratoma formation and malignant transformation plus ethical issues over their availability. Due to high incidence of malignant transformation, limited sources and ethical concerns, the application of using ESCs in stroke treatment are limited. These ethical and technical limitations/disadvantages of embryonic stem cell behaviour, have resulted in increased interest in adult stem cell biology, as

such cells exist as promising alternatives for potential therapeutic applications in the clinic (Hao et al., 2014).

1.6.2 Neural stem cells

Neural stem cell (NSC) are undifferentiated precursors, self-renewing cell populations that maintain the ability to differentiate to neuronal and glial cells (oligodendrocytes and astrocytes) (Liu et al., 2014). NSC are found in the developing and adult mammalian CNS (Aranha et al., 2011). Recent preclinical data show that NSC could serve as cell therapies for neurological disease such as Parkinson's disease, Huntington's disease, Alzheimer's disease, spinal cord injuries and stroke (Rossignol et al., 2014).

NSC could be harvested from the adult brain and proliferated *in vitro* after adding epidermal growth factor and Basic fibroblast growth factor (bFGF) (M. Cai, 2014). NSC will differentiate into three primary neural cell types, including astrocytes, neurons and oligodendrocytes after withdrawal of cytokines. Endogenous NSC have been indicated to encourage angiogenesis in the brain following ischaemic injury (Zhang et al., 2014).

Endogenous populations of NSCs are common to the subventricular zone and subgranular zone of the dentate gyrus. In stroke condition, there is an increase in cellular activities in these zones and NSCs actively travel to the site of ischaemic injury (Zhang et al., 2014). Exogenous NSC transplants also have been shown to encourage the proliferation of endogenous NSC

and their differentiation into mature neural cells and the angiogenesis in the ischaemic area (P. Zhang et al., 2011).

NSCs, similar to other highly potent stem cell types, also carry the risk of abnormal proliferation. Tumorigenicity should be studied together with the adherence to the mandate that NSC cell populations are purified and homogenous before transplantation. However, NSCs are difficult to harvest from the CNS and the autologous treatments may require invasive surgeries prior to therapy. Moreover the generation of allogenic grafts of NSCs would potentially necessitate the induction of the phenotype in an alternative cell source or use of foetal cell lines (Stonesifer et al., 2017).

1.6.3 Induced Pluripotent Stem Cells (iPS).

Yamanka was the first to derive iPS from somatic cells in 2006 by induction of pluripotency (Takahashi and Yamanaka, 2006). Embryonic or adult mice fibroblasts were initially reprogrammed by introduction of four factors: Oct4, Klf14, Sox2 and cMyc using retroviral vector construct adult human fibroblast can be reprogrammed by addition of four factors SOX2, LIN28, OCT4 and NANOG. Properties of these cells are similar to ESCs, in terms of their pluripotency, capacity for self-renewal and proliferative capacity (Padmanabhan, 2014).

Improved proliferative capabilities of precursor cells are one of the advantages of retrograde conversion compared to mature cells. Several

benefits have been observed in the transplantation of iPS after stroke in animal models, such as reduced infarct size, enhanced sensorimotor functions, increased anti-inflammatory cytokines and decreased pro-inflammatory cytokines (Jiang et al., 2011). There are some concerns regarding the use of iPS, such as cellular immunogenicity and tumorigenesis even if autologous. For example, it was found that iPS induced a tetratoma formation after transplanted into mice ischaemic brains and iPS have also been known to induce an immune response and eventual rejection even if they are autologous (Stonesifer et al., 2017).

1.6.4 Mesenchymal stem cells.

Mesenchymal stem cells (MSCs) are an adult stem cell population and derive their name from an intrinsic ability to differentiate into multiple cell lineages such as fat, cartilage and bone. MSCs have the ability to differentiate and self-renew. MSCs can be defined as multipotent, meaning they are capable of differentiating into closely- related cell types of the same germ layer (Stefan Przyborski, 2008). They have been successfully isolated from many tissues in mammals such as placenta, blood, menstrual blood, heart, pancreas, skeletal muscle, dental pulp, bone marrow, Wharton's jelly and adipose tissue (Allen et al., 2014).

Three criteria need to be fulfilled to identify human MSCs including plastic adherence of the isolated cells in culture. These are the lack of expression of markers including CD34, CD79a or CD19, CD14 or CD11b, CD45, HLA- DR

in more than 95% of the culture; expression of CD90, CD73 and CD105 in more than 95% of the culture; and they have the ability to differentiate to adipocytes, chondrocytes and osteoblasts in vitro (Hao et al., 2014).

There are four properties that make MSCs a good choice for the present investigations. MSCs provide a safe therapy and promote repair of neurovascular unit (Paul and Anisimov, 2013). Although they are multipotent, they have been proven to differentiate into different cell lineages such as neurons and glia. They have immunomodulatory functions when stimulated by presence of IFNγ and any of these three cytokines IL-1α, IL-1β and TNFα. Also they have pro regenerative effects and release soluble factors resulting in paracrine activity (Paul and Anisimov, 2013). MSCs can reduce the inflammation of injury and have the ability to induce neuro-recovery and promote endogenous neuronal growth (Huang et al., 2014), encourage synaptic connection from damaged neurons, and reduce demyelination and oxidative stress by reducing levels of free radicals. Finally, MSCs are appropriate for use in autologous transplantation as well as allogeneic transplantation (Paul and Anisimov, 2013).

Table 1.2 Stem cells advantages and disadvantages (Shi et al., 2016)

Cell type	Advantages	Disadvantages
Embryonic stem cell	• Help in angiogenesis • Neuroprotective effects • High rate proliferation • Therapeutic secrotome in hypoxia	• Risk of tumorigenesis • Ethical controversy
Neural Stem cell	• Multipotent • Anti-inflammatory effect in animal model • Endogenous NSC proliferation • Angiogenic and neurogenic potential in ischaemic brain	• Sometimes intolerant of inflammatory and hypoxia • Risk of tumorigenesis • Sometimes require induction from foetal line • Invasive surgery to harvest the cells
Induced Pluripotent stem cell	• Pluripotent • Anti-inflammatory properties *in vivo* • Enhance the angiogenesis and neurogenesis in ischaemic brain • Reduce infarct volume and improve functional recovery in stroke models • Differentiate into neurons, microglia and astrocytes in vitro • Potential to differentiate into immunoregulatory cell type	• Risk of immunogenicity • High chance of being rejected • High risk of tumorigenesis
Mesenchymal stem cell	• Multipotent • Multiple routes of administration • Support endogenous neurogenesis • Safe in animal and clinical trials • Harvested almost from any tissue • Neuroregenerative neuroprotective results *in vivo* model • Could be induced toward neural phenotypes • Suppressive effect on neuroinflammation • Promising results in in vitro ischemia models	• Tissue source can influence function • More studies should be done to determine tumorigenic risk or risk of differentiation into inappropriate phenotypes (e.g. chondrocytes in brain)

1.7 Overview of Cell-Based Treatment Strategies

Several strategies to support tissue regeneration after injury are currently being explored including delivery of antibodies, growth factors, bioactive molecules and cell-based therapy (Pakulska et al., 2012, Shoichet et al., 2008). Cell-based therapy aims to alter the local environment and replace or/and promote the survival of damaged cells to be more beneficial for regeneration. Previous clinical trials showed that MSC transplantation into stroke injury sites in human patients had no adverse effect (Wechsler, 2009). However, unfortunately, clinical efficacy has been limited by uncontrolled differentiated, ineffective integration into the host tissue, poor cell survival and cell diffusion widely (Tam et al., 2014).

Strategies aimed to improve the survival rate and develop better ways to deliver MSC to the ischaemic area are required. We need a good vehicle to retain the MSCs, enhance their survival and improve host-tissue integration after ischaemic stroke (Tam et al., 2014, Reis et al., 2017).

1.8 Introduction to biomaterials.

Biomaterials can be either synthesized in the laboratory or derived from nature. Biomaterials span a broad range of material categories, including but not limited to metals, ceramics, composite materials or polymers. They are usually used or adapted for a medical application in order to be a part of, or the whole, living structure or replace a natural function (Kaplan, 2007).

Designing biomaterials is a significant task for tissue engineering. One of these tasks includes incorporating chemical, physical and biological cues to orchestrate cells into functional tissue via cell migration, adhesion, proliferation, differentiation to (ultimately) yield function. Typically the aim is to replace lost tissue. One strategy includes that the biomaterial degrades at the rate which is matched by new tissue formation to permit tissue regeneration and deposition of new extracellular matrix (ECM). During this time biomaterials should provide mechanical support suitable to the level of functional tissue development. Generally, biomaterials need to be biocompatible; this includes their ability to induce minimal immune response (Kaplan, 2007).

Using biomaterials has presented a new approach to increase the chance of successful treatment of many human diseases in which degeneration constitutes and/or cell death is a common factor (Burdick et al., 2013, Thurber et al., 2015). Biomaterials when combined with cells should create an adequate microenvironment, which could support retention, growth and function of engrafted cells as well as ECM component production and other soluble factors to promote functional integration of the cells in the host tissue (Fernandez-Garcia et al., 2016).

1.9 Other hydrogel and previous work

Many hydrogels presently being explored as carriers for cell therapies (Tam et al., 2014, Nih et al., 2016) are derived from a broad spectrum of materials,

including tissue-derived ECM, synthetic polymers, biopolymers, peptides and hybrid materials (reviewed in (Gasperini et al., 2014, Nguyen and Alsberg, 2014)). Examples include heparin (Freudenberg et al., 2009) or hyaluronic acid(Li et al., 2017) polyethylene glycol hybrid hydrogels, self-assembling $RADA_{16}$ peptides functionalised with a laminin-derived IKVAV motif (Cheng et al., 2013), alginate hydrogels (Emerich et al., 2010) and self-healing chitosan hydrogels (Tseng et al., 2015). Other materials include extracted ECM from Engelbreth-Holm-Swarm mouse sarcoma (i.e. Matrigel) or collagen from bovine or rodent tissues (Thonhoff et al., 2008). More recently, basement membrane and tunica propria ECM isolated from porcine urinary bladder is emerging as an interesting alternative to existing ECM preparations (Ghuman et al., 2017, Massensini et al., 2015).

All these systems have shown promise for CNS, but these materials continue to show limitations. Emerging evidence suggests that ECM tissue specificity is important for obtaining the desired treatment outcome (Prewitz et al., 2013), so ECM extracts from tumours or tissues that are unrelated to the brain are likely to require further optimisation. Single ECM component systems, such as collagen-based hydrogels, have been used extensively (reviewed in (Gasperini et al., 2014)), but these hydrogels have poor mechanical properties, limited resistance to biodegradation (or ability to fine tune this) and a marked tissue response (Gorgieva and Kokol, 2011). Collagen is also predominantly of bovine origin, so its use in the nervous system raises theoretical risks of introducing prions directly into the brain. The development of biomimetic hydrogels (e.g. peptides, peptoids) and

biohybrid hydrogel systems is promising, although these systems still require significant research efforts to yield self-assembling hydrogels with sufficiently robust mechanical properties, *in vivo* biocompatibility and the desired performance (Nguyen and Alsberg, 2014, Seliktar, 2012).

1.10 Introduction to Silk.

Silks are natural macromolecules proteins that are spun by silkworms or spiders into fibres. Silkworm, unlike spider silk, can be farmed in sericulture. The domesticated silkworm *Bombyx mori (B.mori)* produces excellent yields of high quality silk. Silk protein is usually synthesized in specialized epithelial cells that line the paired silk gland (Seib, 2018). Silk is an ecological and environmental friendly biopolymer that could be synthetic from renewable resources. For example cultivation of mulberry trees that are used to rear the worms contribute in reduction of CO_2 in the atmosphere. Typically, to reach 10,000 fold increase in body weight, a silk worm needs 30g of fresh leaves. Then it spends 72 hours spinning continuously to form its cocoon. The cocoon is made of a single thread that could be up to 1500 m long and 10-20 µm thick. The unique hierarchical structure of the fibre makes the silk have good properties, such as elasticity, mechanical strength and toughness (Seib, 2017). Silk fibroin molecules consist of a light chain ~35 kDa and a heavy chain ~390 kDa which are linked by a single disulphide bond (Figure 1.1).

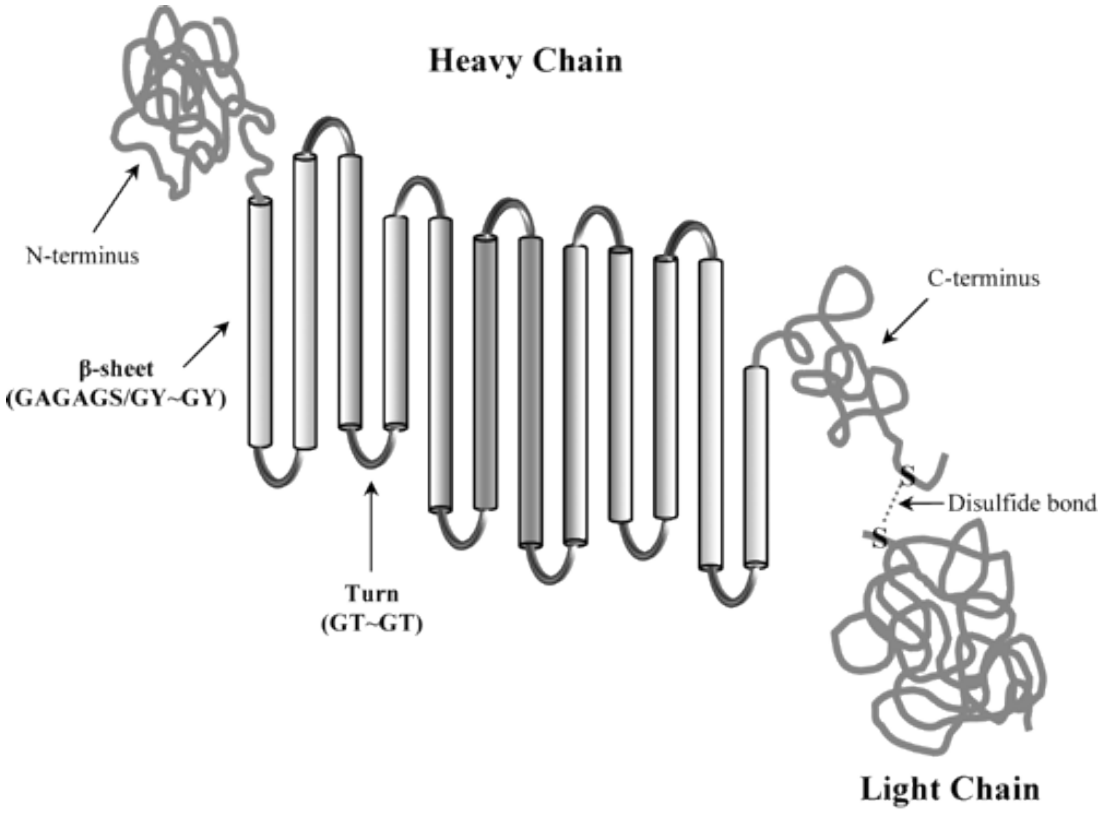

Figure 1.1 Schematic of silk structure, heavy and light chain. Adapted from (Ha et al., 2005).

The predominant amino acids in the primary structure of the silk heavy chain are, 45.9% glycine, 30.3% alanine, 12.1% serine, 5.3% tyrosine, 1.8% valine and 4.6% of the other 15 amino acid types. The silk light chain has completely non-repeating amino acid sequences, indicating that this subunit adopts a globular confirmation (Seib, 2017). During cocoon spinning, the silkworm generates two silk filaments from its paired silk gland; these filaments are merged and coated with sericin before the single silk thread emerges from the spinneret located in the head of the silkworm. The silk filament is responsible for the mechanical properties of the fibres while sericin, which is a water-soluble glue-like protein, binds the silk filaments together (Seib, 2018). Sericin also aids with the cocoon construction by "gluing" the silk fibres together. Sericin must be removed when silk is used in medical application because sericin in combination with silk is known to induce an inflammatory response both *in vitro* and *in vivo* (Seib, 2013).

Apart from the primary sequence, the secondary structure and hierarchical organization of silk as well as the carefully orchestrated self-assembly control many of silk biomaterial properties. The 12 hydrophobic blocks of the silk heavy chain contain highly repetitive glycine-X repeats, where X is alanine (65%), serine (23%) or tyrosine sequence that are assembled into nano-crystals β-sheet (Seib, 2017). The hydrophilic links between these hydrophobic crystallisable blocks include polar side chains. These 11 blocks of the silk heavy chain are amorphous. Silk elasticity is due to the random coil conformation present in the amorphous blocks of the silk heavy chain. In contrast, the mechanical strength of silk is due to the presence of nano-

crystals β-sheets in the hydrophobic blocks. (Kundu et al., 2013). Hydrophobic blocks could be categorised into three motif: 1) a highly repetitive GAGAGS sequence create the bulk of the crystalline regions and usually found at the beginning of each block; 2) a less repetitive sequence including hydrophobic and/or aromatic residues GAGAGV, GAGAGY and GAGAGVGY, creation the semicrystalline regions; 3) sequences very similar to (1) except for the presence of an AAS motif, that is typically found at the C-terminal end of each subdomain and could form a sheet-breaking motif (Seib, 2017).

There are two distinct structures of *B.mori*: silk I illustrates the structure before spinning during storage in the posterior silk gland; silk II illustrates the structure that occurs after spinning into silk fibre (Hu et al., 2006). Spherical micellar structures form from a block copolymer arrangement that contains a hydrophobic core of crystalline/amorphous domains and a hydrophilic shell of the terminal domains (Figure 1.2). These micelles remain loosely until they trigger by external factors such as shearing, change solution concentration, change the pH or ionic strength that leads to increase in β-sheet content and forms networks through a self-assembly process (Seib, 2018) (Figure 1.2).

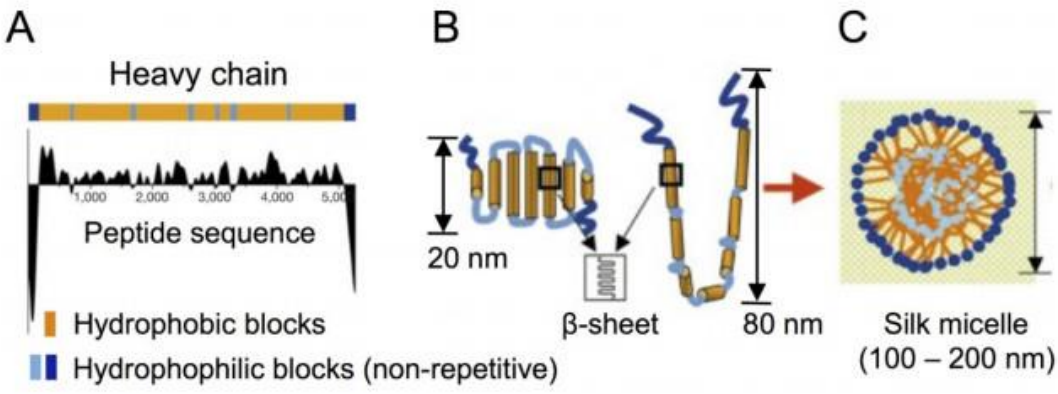

Figure 1.2 Solution conformation of B. mori silk. (A) Hydrophobicity pattern of the heavy chain with (B) possible chain folding and (C) micelle assembly of silk in water, adapted from (Jin and Kaplan, 2003).

1.11 Self- assembling silk hydrogel in biomedical applications

Many studies and researches are exploring silk-based materials for biomedical applications (S. Kapoor and S. C. Kundu, 2016). Silk has been used in a wide range of biomaterials. Silk has been successfully used in medical suture for centuries and artificial ligaments, breast implant coatings, bone and cartilage tissue engineering or recently in clinical trials for the reconstruction of the tympanic membrane (Fernandez-Garcia et al., 2016). Silk can be processed into different morphologies, such as hydrogels, microspheres, nanofibers, nanoparticles, sponge and films. The adaptability of silk proteins in terms of processing involves aqueous silk solutions, strong mechanical properties (Porter, 2009), controllable biodegradation, biocompatibility, absent or minimal immunogenicity, ability to protect the payloads and limited bacterial adhesion (Seib, 2018). (Gotoh et al., 1998, Inouye et al., 1998) found human and animal cell lines grew and attached very well on films that prepared from regenerated silk.

Silk has many advantages over other protein-based biomaterials that are derived from tissue of allogeneic or xenogeneic origin, such as the high risk of infection of those materials. These materials are expensive to process due to the purification and protein isolation processes. On the other hand, silk is already used in textile fibre and more than 1,000 metric tons of silk are produced and processed yearly.

Comparing silk with other biomaterials, such as polylactic acid or collagen, silk induces a lower inflammatory response. Although silk has never been used in preclinical models of the brain repair, silk has been successfully used for regeneration of peripheral nerves in rats as nanoparticles or in fibrillar structures and anti-epileptic drug carriers (Fernandez-Garcia et al., 2016).

1.12 Silk hydrogel

The reverse engineered silk solution converts to a silk hydrogel via solution-gel (sol-gel) transition through the aggregation of silk molecules into cross-linking and β-sheets to form an interconnected network (Leng-Duei Koh, 2015). Gelation occurs due to formation of inter and intra–molecular interaction amongst protein chains, including hydrogen bonding and hydrophobic interaction. There are important factors in gelation including Ca^{++}, silk polymer concentration, pH and temperature (Kaplan, 2007). Silk concentration can control the hydrogel pore size. When the concentration of silk is increased, the compressive strength and modulus of hydrogel is increased as a result of the decreased pore size (Leng-Duei Koh, 2015, Kaplan, 2007). Silk hydrogels are 3D biopolymer networks that are physically durable. Sonication of silk solution lead to formation of silk hydrogel and β-sheets formation (Kaplan, 2007). While early materials for brain repair used implantable materials, recent studies have focused on engineered injectable hydrogels, which could be transplanted directly within the stroke cavity with a minimal invasive procedure. By modulating the cross-linking density of the hydrogel it is possible to match the normal brain mechanical properties to

allow the hydrogel to function as a local drug or cell delivery (Nih et al., 2016). The silk fibre can be completely reverse engineered into an aqueous silk solution (Rockwood et al., 2011), which can then be processed into many different formats, including physically cross-linked hydrogels. It also has the ability to self-assemble in response to environmental triggers, making it particularly appealing for cell delivery applications, reviewed in (Seib, 2018). Silk hydrogel biomaterial plays an important role in delivery of cells and cytokines. Furthermore, silk is able to support cell growth and cell differentiation of various stem cells, including pluripotent (Sun et al., 2016a), neural (Bai et al., 2014, Sun et al., 2017) and MSC types (Wang et al., 2008). Silk has therefore been investigated in a range of regenerative medicine applications; however, at present, no studies have investigated the use of self-assembling silk hydrogels for MSC delivery to the stroke brain.

1.13 Sterilisability

An advantageous feature of silk as a biomaterial, comparing with other materials such as collagen, is the flexibility of option for sterilization (Sugihara et al., 2000). Silk can be sterilized by autoclave without changing the morphology or *β*-sheet structure with high temperature (120**°C**) whereas collagen denatures at these temperature. Silk can also sterilized using ethyle oxide, *γ*-radiation, 70% ethanol and by using filter (Li et al., 2006, Kaplan, 2007).

1.14 Biocompatibility.

Silk has been shown to be highly biocompatible due to its chemical composition and structure (Cao and Wang, 2009). In 1995 silk was assessed as biomaterial fibroblast cells showing good attachment and growth on *B.mori* silk matrices (Minoura et al., 1995). After many years, a negligible inflammatory response and good biocompatibility with blood have been demonstrated (Meinel et al., 2005). In 1993 silk was recognized as a biomaterial by US food and drug administration (FDA) and used as suture material widely (Horan et al., 2005). By now, there are different silk-based medical devices that have been approved by FDA for example SeriACL™, a silk fibroin based ligament graft and long term bioresorbable surgical mesh *Seriscaffold*® (Melke et al., 2016).

The main feature that differentiates between biomaterials and any other material is their ability to be present within the tissues in the human body without any unacceptable amount of harm to the patient (Georges et al., 2006). Silk used in *in vitro* studies demonstrates significant absence of macrophage spreading, minimal inflammatory potential, good infiltration of fibroblasts and satisfactory degree of biocompatibility (Nih et al., 2016).

1.15 Biodegradation.

Degradation plays an important role for biomaterials that are used in healthcare. Silk biodegradation can be achieved by enzyme catalysed

hydrolysis reaction and proteases resulting in peptide fragments and amino acids, which are easily metabolized and excreted (Seib and Kaplan, 2013). *In vitro* studies stated that silk degradation accounts for about 4% mass loss over seven days for scaffolds whereas the same value was lost over 4 weeks for silk hydrogels, implying different degradation rates for different formulations. Proteases XIV are good enzymes to determine the degradation properties of different silk formulations *in vitro*, but they are not mammalian enzymes, therefore different degradation properties are involved *in vivo*. Chymotrypsin, another enzyme used in silk degradation, is a mammalian enzyme and can degrade 2% w/v silk hydrogel within 28 days. There are some factors that accelerate degradation of silk *in vivo* which are, high porosity, low silk content and large pore sizes (Seib and Kaplan, 2013).

Silk degradation showed no significant cytotoxicity to neural cells in *in vitro* tests. Silk degradation can be influenced by the content of water-soluble silk I structure and water insoluble silk II, the former being induced during physical crosslinking (and β-sheet formation). When the amount of β-sheet structures increased the degradation time increased too (Melke et al., 2016).

Silk degradation has been found to be slower compared to many natural polymers. It may takes many days or weeks to degrade silk *in vivo* due to high crystallinity and the rate of absorption depending on some factors such as concentration of the silk, site of implantation and mechanical environment.

Biodegradation is an important property of silk to give transplanted cells the chance to spread within the silk hydrogel and form a network before the silk degrades as the cells and migrate to the ischaemic area to ultimately improve functional recovery (Nih et al., 2016). Due to controllable degradation rate, silk-based biomaterials provide suitable materials that could support neo-forming tissue for long duration (Sonia Kapoor and Subhas Kundu, 2016).

1.16 Silk hydrogel in stroke therapy

Stroke disability is one of the major diseases that has no effective treatment. Lack of medical therapy that promotes repair means that stroke results in substantial clinical burden in disabled survivors. However, this in turn requires the need to explore novel treatment strategies including the use of biomaterials to promote brain recovery after (ischaemic) stroke. For example a hydrogel could be injected into the chronic stroke cavity in its liquid form and solidify *in situ* to form a hydrogel matrix, so we reduce the shearing effect on cells during injection and thus protect the cells and the injection is minimally invasive. This matrix can be fine-tuned to mimic the ECM, including the brain mechanical properties (Nih et al., 2016). Many studies report hydrogels that contain either covalent or physical bonds to form a supra-molecular network. The crosslinking can be classified into covalent and physical crosslinks. Covalent cross-linked hydrogels, which often have long lasting mechanical properties. In contrast physically cross-linked hydrogels have bonds that can be broken (i.e. are dynamic) and thus reform as the cells infiltrate. Hydrogels with covalent crosslinks are widely studied for stem

cell transplantation into the stroke cavity; these hydrogel-cell construct have shown to promote angiogenesis and improve stem cells survival without the need to deliver angiogenic factors (Jianjun Zhang et al., 2011).

Similar to drug delivery, cell transplantation has potential to fail. For example, cell delivery not directed to the site of the injury but administered systemically can result in poor survival due to the lack of mechanical and biochemical cues (Adil et al., 2017, Quertainmont et al., 2012). Biomaterials can be used as a cell delivery and provide physical support for the cells to ensure their retention and distribution at the site of transplantation (Tam et al., 2014).

One perceived advantages of using silk hydrogel is to avoid cell loss in the brain, and to inject the cells directly to the exact location to support the trophic effects. Associated with stem cells that will be injected, silk has excellent mechanical properties and water-based processing. Furthermore, silk provides unique platform to bioengineer pro-repair environments directly at the stroke site and effectively bypass the BBB (Fernandez-Garcia et al., 2016). However, because access to the skull and the brain needs invasive delivery, the direct delivery of silk hydrogel encapsulated with cells into the brain after stroke should be controlled so the tissues surrounded to the infarct is not damaged. Silk hydrogel delivered to the brain should not swell significantly to avoid extra damage to the brain (Nih et al., 2016).

1.17 Hypothesis and objectives

The hypothesis to be tested in this thesis is that self-assembling silk hydrogels are a promising stem cell delivery platform for central nervous system diseases, especially stroke.

The following objectives were met to investigate the potential of self-assembling silk hydrogels as a mesenchymal stem cell (MSC)-support matrix for stroke.

(i) Establish the behaviour of self-assembling silk hydrogels, in terms of their secondary structure, how quickly they convert during the sol-gel transition, their swelling characteristics, their optimum stiffness to mimic brain tissue mechanics and find the optimum time and power output to prepare the silk hydrogels for subsequent cell encapsulation and intracerebral injections.

(ii) Assess the capacity and optimum concentration of self-assembling silk hydrogels for MSC expansion, distribution and survival with and without injection through needles *in vitro*.

(iii) Characterise self-assembling silk hydrogels and MSC encapsulation *in vivo* in terms of space conformity and cell distribution after intracerebral delivery after stroke

CHAPTER 2. MATERIALS AND METHODS

2.1 Materials:

Table 2.1 List of materials

Name	Company
Lithium bromide	Acros Organics, Geel, Belgium.
Sodium carbonate anhydrous	Thermo Fisher Scientific, Waltham, MA, USA.
Phosphate Buffered Saline	Sigma - Aldrich, MO, USA.
Gibco® Cell Culture Media	Thermo, Waltham, MA, USA.
Trypsin	Sigma Aldrich, MO, USA.
Trypan blue solution	Thermo, MA, USA.
Dimethyl sulfoxide	Thermo, MA, USA.
Bombyx mori silk cocoons	Tajima Shoji, Kanagawa, Japan.
Embedding Matrix	Thermo, MA, USA.
Superfrost plus Glass slides	Thermo, MA, USA
Light Microscope	Nikon Eclipse 50i, UK
96 well plate for cell culture	Sigma-Aldrich, MO, USA.
Electronic pipetting, Easypet	Eppendorf, Hamburg, Germany.
Micropipette and tips	Eppendorf, Hamburg, Germany.

Multipipette.	Eppendorf, Hamburg, Germany.
Slide-A-Lyzer Dialysis cassettes, 3.5K MWCO, 15 ml	ThermoScientific, MA, USA
Falcon tube 15 & 50 ml	Corning, MA, USA.
Flasks 75 cm^2	Corning, MA, USA.
5 ml Syringe	Terumo, Tokyo, Japan.
Needles	BD, New Jersey, USA.
Syringe Filter, 22μm	Millipore, Darmstadt, Germany.
6-0 Silk Thread	Henry Schein, Nitside, UK
Scarvenger aldosorber	Shirley Alder&Co, Cardiff, UK
Heat Mat	Harvard Apparatus, UK
Electro coagulated	Eschmann Equipment, Lancing, UK
Monofilament	Doccol Corporation, Sharon, USA
Sterile Saline	Henry Schein, Nitside, UK

2.2 Methods

2.2.1 *In vitro* approach

2.2.1.1 Cell Culture

Mouse C3H10T0.5 mesenchymal stem cells (American Type Culture Collection) passage 8, were grown on tissue culture treated polystyrene flasks (Corning, UK) and cultured in Roswell Park Memorial Institute medium 1640 containing 4.5 g GlutaMAX, supplemented with 10% v/v foetal bovine serum and penicillin and streptomycin (each with 100 units/ml) (Thermo Fisher Scientific). Cells were maintained in a humidified atmosphere of 5% CO_2 at 37°C, and subconfluent cultures were routinely subcultured with trypsin/EDTA (0.25%), every 2 to 3 days up to passage 40. To split the cells, the culture medium was aspirated with a Pasteur pipette (Fisher, UK), cells were washed with 10 ml of phosphate buffer solution (PBS) (Sigma, UK) and 2 ml of trypsin-EDTA was added to the flask (Corning, UK) and incubated for 2 minutes. Next, cell attachment was verified by microscopy and cells were collected in a falcon tube (Corning, UK) in 8 ml of medium and pelleted by centrifuged for 4 minutes at 347 x g relative centrifugal force (RCF). Next, the supernatant was aspirated, then cells were dislodged. A 10 ml of the medium was added to the tube (Corning, UK), cells were resuspended and 2 ml of the cell suspension was added to the flask plus 8 ml of culture medium. The flask was checked microscopically before incubation in 37°C and 5% CO_2.

2.2.1.2 Cells counting

Cells were trypsinised and 100 µl of trypan blue (Sigma, UK) was added to an equal volume of cell suspension. Next, an improved Neubauer haemocytometer was loaded and viable cells were counted in four corner squares. The average cell number was determined, multiplied by the dilution factor and scaling factor of the haemocytometer to determine the total number of cells.

2.2.1.3 Extraction and purification of silk solution

B.mori silkworm cocoons were obtained from (Tajima Shoji, Kanagawa, Japan). The silkworm cocoons were cut into pieces and added to a boiling aqueous 0.02M Na_2CO_3 (Fisher, UK) solution to remove the sericin protein. After 60 minutes, the silk was washed thoroughly in ddH_2O. The silk was air dried overnight and then dissolved in 9.3M LiBr (Acros, UK) solution and placed in a 60°C oven for 2-4 hours. The silk-LiBr solution was then inserted into dialysis cassettes (3500 Molecular Weight Cut Off) (Thermo, UK) and dialyzed against ddH_2O. The water was changed 6 times over 3 days. The aqueous silk solution was centrifuged at 8150 x g (RCF) at 4°C for 20 minutes twice to remove any impurities. The prepared aqueous solution of silk (4-7% w/v) is stable for several months at 4°C and for weeks at room temperature Figure 2.1 (Seib, 2018).

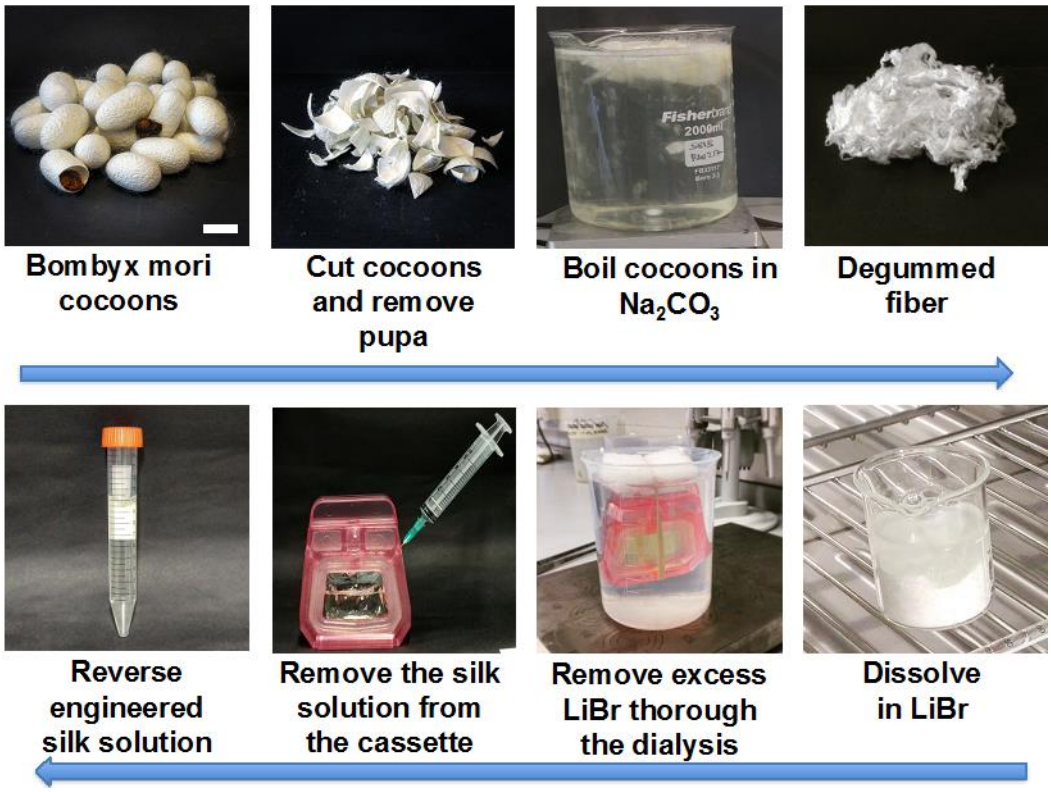

Figure 2.1 Extraction and purification silk of fibroin solution. Silk cocoon were cut to into dime-size 25 mm^2 pieces and boiled in 0.02M Na_2CO_3 for 60 minutes. Then the silk fibres were dried overnight and dissolved in LiBr for 2-4 hours then dialyzed against ddH_2O for 3 days and centrifuged twice and collected. Scale bar 10 mm.

2.2.1.4 Silk solution sterilisation and sol-gel transition

Silk solution was filtered using a 0.22 μm filter Polyethersulfone (PES) membrane (Millex, UK) (Kaplan, 2007). Then, the sol-gel transition was induced by sonicating the silk solution using an ultrasound sonicator (homogenisers Status, Germany) at 30% amplitude for two times sonication cycles on ice (one cycle consisted of 30 seconds on and 30 seconds off) to induce the solution-gel transition (Figure 2.2).

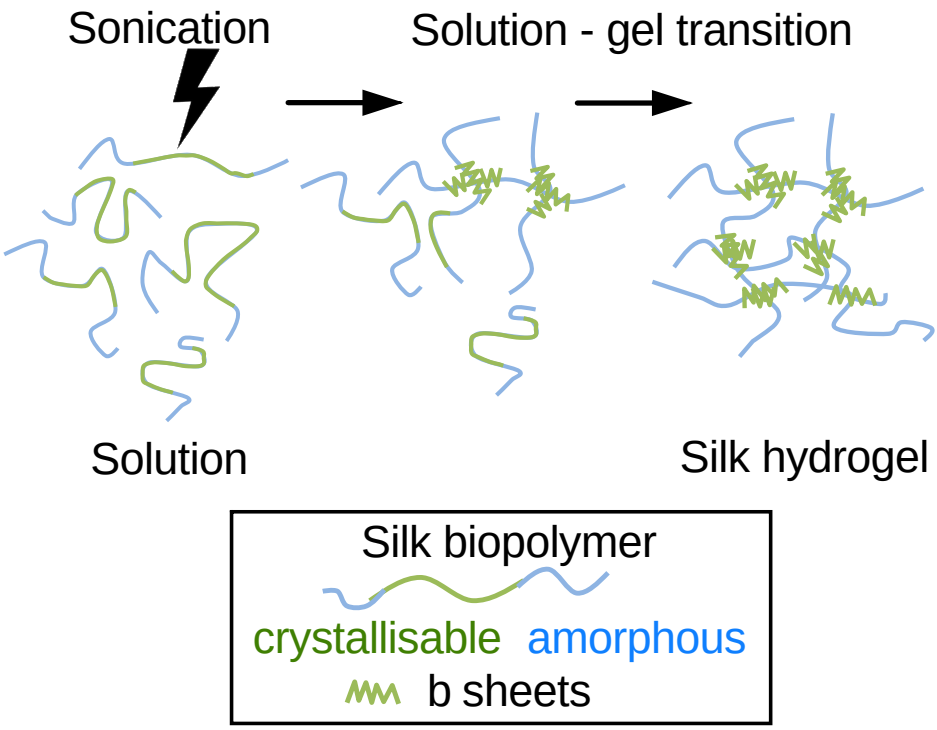

Figure 2.2. Self-assembling silk hydrogel manufacture and structural characteristics. Schematic illustration of the manufacture of silk hydrogels from reverse engineered silk.

2.2.1.5 Kinetic of sol-gel transition using light scattering

Aqueous silk solutions were diluted with ddH_2O to generate stocks with 1, 2, 3, 4 and 5% w/v then the absorbance was measured at 570 nm. Next, samples were sonicated for 30 seconds twice at 30% amplitude on ice, and the first measurement was taken within 2 minutes. Next, the instrument (SpectraMax M5, USA) was programmed to measure the absorbance every 10 minutes for 3 hours and a final measurement at 24 hours at 570nm. The plate was covered by polyolefin transparent film (StarLab, UK) to avoid any evaporation and dryness.

2.2.1.6 Visual inspection of self-assembling silk hydrogels

To find the optimum stiffness that is visually similar to the brain, 5 concentrations of silk hydrogels were examined 1, 2, 3, 4 and 5% w/v. 1ml silk solution was pipetted into 24-transwell (Corning, UK) plate and allowed to complete the sol-gel transition. Samples were removed from the transwell and placed on spatula to visualise the stiffness. In addition, to visually assess the solidity, 1 ml of 1, 3 and 5% w/v silk solution was placed in tubes and turned upside down 1 hour after sonication to assess the difference between the samples.

2.2.1.7 Measuring the elasticity of self-assembling silk hydrogels (Rheology)

Silk hydrogels 2-5% w/v 0.2 ml were prepared in 96 transwell and covered with PBS after the completion of the sol-gel transition and left overnight then subjected to rheological characterisation (Kinexus Pro+, UK) using a 20 mm diameter plate at 25°C, covered to control the temperature and reduce the evaporation during the test. The gap was determined by measuring the thickness with a micrometre. Strain stress was measured first from 0.1 to 100 % with a frequency 1.0 Hz then the frequency sweep was measured.

2.2.1.8 Swelling test for self-assembling silk hydrogels

To determine the extent of swelling of silk hydrogels, 300µl of sonicated silk solution 2-5% w/v were added to pre-weighed Eppendorf tubes (Corning, UK). Once gelled (1-2 hours), PBS (300 µl) was added carefully on top of the silk hydrogel, the Eppendorfs were re-weighed then left for 24 hours before complete removal of PBS and a final weight taken. In addition, the swelling ratio calculated by using this equation,

$$Swelling\ ration = (Wr - Wi)/Wi \qquad \text{Equation 2.1}$$

Wr: sample weight after removal of PB.

Wi: initial sample weight before adding PBS.

2.2.1.9 Circular Dichroism (CD)

The CD spectra were used to monitor the macromolecule conformational transformation in silk solution during the sol–gel transition. CD kinetic measurement (Chirascan plus instrument, UK) of silk β-sheets formation was monitored by assessing silk's secondary structure. A 5 mL aliquot of 2, 3 and 5% w/v silk solution was sonicated until sol-gel at 30% amplitude and immediately loaded to a 0.01 mm path length measuring cell. The temperature was kept constant at 25°C and sampling every 10 minutes or 10 seconds for over the 190 to 250 nm spectrum with a 1 nm resolution. CD measurements were taken 3 times per scan for 24 hours.

2.2.1.10 Fourier transform infrared spectroscopy (FTIR)

To reserve the secondary structure of the silk hydrogels, samples were immediately quenched in liquid nitrogen after treatment by high pressure CO_2 and subsequently lyophilized for 48 hours to get the dry samples for characterisation. Then, silk hydrogel samples 1-5% w/v, were run for 128 scans at $4cm^{-1}$ resolutions over the wavenumber range 400-4000 cm^{-1} using a TENSOR II FTIR spectrometer (Bruker Optik GmbH, Ettlingen, Germany). Baseline and peak fit were corrected by OriginPro 9.2 software at amide I region (1595-1705). The amide I region was identified and deconvoluted: 1605−1615 cm^{-1} as side chain/aggregated strands, 1616−1637 cm^{-1} and 1697−1703 cm^{-1} as β-sheet structure, 1638−1655 cm^{-1} as random coil structure, 1656−1662 cm^{-1} as α-helical bands, and 1663−1696 cm^{-1} as β-turns.

2.2.1.11 Scanning electron microscope (SEM)

For scanning electron microscopy (SEM), silk hydrogel 2-5% w/v were left to gel overnight (room temperature), then moved to -80°C freezer followed by freeze drying. Silk hydrogels were cross-linked with glutaraldehyde and progressively dehydrated in a graded series of ethanol (10%, 30%, 60%, 80%, 90% and twice in 100%, 20 min at each concentration. Then, samples were subsequently dried by critical point drying with a liquid CO_2 dryer. Samples were moved to a desiccator and sputter coated by Carbon using a vacuum coater (Polaron Division E6100, Bio-Rad, Birmingham, UK), then run on a FE-SEM SU6600 (Hitachi High Technologies, Krefeld, Germany) using 5 kV and images were analysed using ImageJ v1.50i (National Institutes of Health, Bethesda, MD, USA).

2.2.1.12 *In vitro* Conformity test

To test space conformity *in vitro*, silk hydrogel 2, 3 and 4% w/v samples were either (i) left in the syringe to complete the solution-gel transition and subsequently transferred to a cuvette, or (ii) immediately transferred from the syringe to the cuvette (i.e. still in its liquid form) and allowed to gel in the cuvette. In both conditions, the cuvettes were filled with the silk hydrogel samples up to the 1 ml mark. The cuvettes were then weighed and the conformity was calculated.

2.2.1.13 Cell encapsulation in self assembling silk hydrogels

Silk hydrogel solutions 2-4 % w/v were sonicated 3-6 times at 30% for 30 seconds on ice then allowed to gel (eye-test) at 28-32°C. MSCs C3H10T0.5 (1600-200k/50 µl) were added to the silk prior to gelling (number of cells as indicated later). 50 µl of the silk hydrogel and MSCs mixture were added to 96 well plate and left in the incubator for 10-30 minutes to solidify. 200 µl of medium (same medium used in 2.1.1) was added on the top of the mixture and changed every 3 days.

2.2.1.14 Measuring cells proliferation in self assembling silk hydrogels using 3-(4, 5-dimethylthiazol-2-YL)-2, 5-diphenyltetrazolium bromide (MTT)

Metabolically active cells reduce the yellow tetrazolium MTT in part by the action of dehydrogenase enzymes, to generate reducing equivalents such as NADH and NADPH. The resulting soluble purple formazan produced is directly proportional to the number of living cells. Solubilisation solution usually Dimethyl Sulfoxide (DMSO) is added to dissolve the formazan product into a coloured solution. The absorbance of this coloured solution can be quantified by measuring at a certain wavelength at 570 nm by a spectrophotometer (Sylvester, 2011).

Cells were encapsulated in self-assembling silk hydrogels as described in section (2.1.13). A 20 µl of 5g/ml MTT (Thermo, UK) was added to the

medium and incubated for 5 hours at 37°C. Then, the medium was removed and the plates were incubated at 60°C overnight to evaporate the water. Next, 200 µl of DMSO was added on the dried silk hydrogel and incubated at 37°C for 10 minutes to dissolve the formazan crystals. DMSO was then removed and placed into a 1.5 ml Eppendorf tube and centrifuged for 10 minutes and 10391 RCF. Finally, 100 µl were transferred to reading plate and absorbance was measured over 7 days. The controls used in this experiment were self-assembling silk hydrogels only and cells only.

2.2.1.15 Measuring cells proliferation by using AlamarBlue (Resazurin)

AlamarBlue (AB) is an indicator for viability and metabolic cell function that uses the reducing power of living cells to convert resazurin to the fluorescent molecule which is resorufin. Resazurin is used as an oxidation-reduction (REDOX) indicator that undergoes colorimetric change. This redox reaction is resulting in change in colour of the culture medium from blue to fluorescent pink, which can be easily measured by fluorometric reading. AlamarBlue is stable and, importantly, non-toxic to the cells and continuous monitoring of cultures over time is possible (Al-Nasiry et al., 2007).

Cells were encapsulated in self-assembling silk hydrogels as described in section (2.1.13). AlamarBlue 10% of (medium + silk) were added to the medium in each well and incubated for 4 hours at 37°C and 5% CO_2. Next, 100 µl were collected from the supernatant and transferred to black plate to

measure the florescence at EX 560 nm and EM 590 nm and low photomultiplier tube PMT.

2.2.1.16 Gelatine coated slides for histology

Microscope slides (Super Premium Microscope Slides, VWR, UK), were coated with gelatine to improve adherence of frozen cerebral tissue sections. 0.5% gelatine solution was prepared fresh by dissolving gelatine powder bovine serum albumin, type B (Sigma, UK) in dH_2O, which was cooled and 0.05% chromium potassium sulphate ($CrK(SO_4)$) (Sigma, UK) was added. Slides were then immersed for twenty minutes in acid alcohol 96% ethanol: 3% HCl 12% (Sigma, UK), followed by two dips in dH_2O. Finally the slides were dipped three times in 0.5% gelatine solution and left to dry overnight in wrapped in foil to prevent dehydration and protect them from the dust. The slides were stored in at 4°C in their original boxes for a maximum of three months to prevent dehydration or fungus.

2.2.1.17 Distribution of cells encapsulated in self-assembling silk hydrogels

The distribution of encapsulated MSCs in silk hydrogel was assessed histologically after the sample was gelled in either 10 minutes or 60 minutes. 200µl of the silk hydrogel/MSCs were placed in 96 transwell plate and completely solidified in either 10 minutes or 60 minutes depending on the sonication process, then removed from the transwell gently prior to fixation in

4% paraformaldehyde for 30 minutes. Samples were then sucrose sunk in 30% sucrose (Sigma, UK) overnight at 4°C and frozen in isopentane/dry ice -42°C for 2 minutes then stored at -20°C until used. Then, samples were cryosectioned (20 µm) then stained with haematoxylin and eosin (H&E) as described below.

2.2.1.18 Cells viability in self- self-assembling silk hydrogels after injection through different needle sizes

In this experiment 2, 3 and 4% w/v) silk hydrogels were tested for cell viability post injection through needle gauge sizes 21, 25 and 30 G. Silk solution was sonicated 150-240 seconds at 30% amplitude and the temperature 28-32°C then mixed with cells, and before the gelation occurs the pre gelled samples were injected in 96 well plate 100 µl. For post gelled samples, silk hydrogel with cells were left in the needle for 1 hour until complete solidify. Next, the silk hydrogel were injected after the gelation occurred through the needle. After that, 200 µl of medium was added on the top of the silk hydrogel and 10% of AB was added and incubated for 4 hours to check the difference in the viability.

2.2.1.19 Cell labelling to track the cells in the brain

The stock powder CM-Dil (Invitrogen, UK) 1 mg was reconstituted in 1 ml DMSO. Then the stock was diluted in cell culture medium 3 µg/ml. Next, 5 µl/ml of labelling solution were added to flasks and incubated for 5 minutes in

37°C then at 4°C for 15 minutes. Finally the cells were collected as previous described (section 2.1.2). Numbers of cells were manually counted under a light microscope (Nikon Eclipse 50i, UK) within a fixed field of view in predetermined layers (levels 1-4) to give 2 dimensional distributions of cells throughout the gel

2.2.1.20 Haematoxylin and Eosin (H&E) staining

H&E staining is one of the most commonly used histological stains and was used herein to assess the distribution of cells encapsulated in self-assembling silk hydrogels (section 2.1.18) and the conformity of self-assembling silk hydrogels in brain after stroke. Haematoxylin stains cell nuclei blue and eosin stains the cell cytoplasm pink. The fixed cryosectioned samples of hydrogel-cell constructs, rehydrated on descending alcohol 100-90-70%. Slides then washed by water then immersed in Haematoxylin stain (Sigma, UK) for 3 minutes followed by a water wash. Then, the slides were differentiated in acid alcohol (1% v/v HCL in absolute ethanol) (Sigma, UK) followed by water wash and Scott's tap water for 1 minute then washed by water again. Next, the slides were immersed in Eosin Y (1% w/v aqueous) (Sigma, UK) for 1 minute prior washing by water until the water clear. The sections were dehydrated in ascending alcohol solution 70%, 90%, 100% for four minutes each before clearing with histoclear for two minutes twice. Finally, the slides were mounted with coverslip with DPX (Sigma, UK) and examined under the light microscope (Nikon Eclipse 50i, UK).

2.2.2 *In vivo* approach

2.2.2.1 Animal source

In order to establish translation of space conformity in the stroke cavity, self-assembling silk hydrogels were injected post-middle cerebral artery occlusion (MCAO). Experiments were conducted on adult male C57BL/6 mice aged 10-12 weeks and weighing 25-30 g. prior to surgery animals were group housed in a temperature-regulated environment for 12 hours light dark cycle with food and water provided *ad libitum.* Animals found to be moribund through excessive weight loss (>20% of start weight) or those unable to move and/or correct gait were terminated and excluded. The regulations, as specified by the Animals (Scientific Procedures) Act (1986) where strictly adhered to throughout and were carried out under local ethical approval and the appropriate Home Office licence (Project Licence No. PPL 60/4469; Personal licence 60/11900). All surgical procedures were carried out by Dr Craig McKittrick.

2.2.2.2 Animal preparation for surgery

Animals were exposed to anaesthesia (3% isoflurane/1000ml/min oxygen (O_2)) by inhalation for approximately 2-3 minutes in an induction chamber. Then, the mouse was moved to a facemask and the anaesthesia was reduced to 2% isoflurane/1000ml/min O_2 and maintained for 20 minutes and then reduced to 1.5% isoflurane/1000ml/min O_2 for the rest of the procedure. A scavenger aldosorber unit (Shirley Alder & Co, Cardiff, UK) was used to remove the excess isoflurane. Body temperature was monitored using a

rectal probe and maintained at 37 ± 0.5°C with an automatic heat mat (Harvard Apparatus, UK).

2.2.2.3 Electrocoagulation model of permanent MCAO (pMCAO)

Skin between the left ear and eye was depilated and cleaned with betadine using a sterile cotton bud. The mouse was covered with a sterile drape and an incision around 1 cm long was made between the left eye and ear to expose the temporalis muscle. Saline was applied to the site and a small opening between the muscle and the skull was made. Muscle was detached using bipolar McPherson forceps (0.45mm). Using a dental drill, the skull was thinned over the MCA, and the skull removed to expose the MCA. Using the bipolar McPherson forceps (0.45mm) the MCA was coagulated distal to the bifurcation of the MCA. The wound was closed with 5-0 suture and the mouse injected i.p. with 500 µl saline and allowed to recover before it was returned to its home cage and given soft diet and water and monitored three times daily. .

2.2.2.4 ILT model of transient MCAO (tMCAO)

Before making an incision in the midline neck, lidocaine (5% w/v), a topical local anaesthetic, was applied to the neck area of the mouse. Rounded blunt scissors was used to open the incision further to fully expose the submandibular gland. Then the submandibular gland was dissected and retracted onto a sterile gauze and kept moist with sterile saline all the time

during the procedure. The left common carotid artery (LCCA) and its bifurcation to the left external carotid artery (LECA) and left internal carotid artery (LICA) were exposed by blunt dissection of the overlaying connective tissue using tweezers and Tri-swabs (Royem Scientific, Luton, UK). Next, a branch of the ECA called left superior thyroid artery was electro-coagulated using a diathermy probe (Eschmann Equipment, Lancing, UK) and dissected. The left occipital artery, lying across the LICA was also electro-coagulated with great care so as not to upset the adjacent vagus nerve.

A 6-0 silk thread (ligature) (Henry Schein, Nitside, UK) was placed below the LECA by dissecting the underlying connective tissue with 90˚ tweezers and passing the thread through with tweezers. The ligature was double knotted distally from the bifurcation of LCCA. A second thread was placed below the LICA by first passing a thread under LCCA and then passing the trailing end under the LECA. This thread was left untied and taped to the operating surface. A third thread was placed below the LECA and loosely tied at the LCCA-LECA bifurcation point, and a final thread was placed under the LCCA, distal from the bifurcation point and was left untied.

The segment of vessel distal to the first ligature on the LECA was electrocoagulated then followed by the placement of a 13 mm microaneurysm clip on the LCCA, distal to its bifurcation point. To cease blood flow along the LICA, tension was applied to the thread around the LICA then the tense thread was taped down to the operating surface. Then, a 0.01 mm incision was made on the abluminal surface of the LECA, and a silicon-

rubber coated monofilament (20 mm length of which 9 mm is coated with silicone giving an overall diameter of 0.23 ± 0.01 mm) (Doccol Corporation, Sharon, USA) inserted approximately 9 mm until its tip reached the bifurcation with the LCCA and LICA. The filament was held in place by tightening the loosely tied thread on the LECA. The coagulated area distal to the ligature on the LECA was cut and pulled to give an angle into the LICA. Tension on the thread around the LICA was freed and the filament was inserted until resistance was noticed, indicating the filament had reached the origin of the middle cerebral artery. Then the filament was tied in place and stayed for 45 minutes. The filament was then carefully removed and the insertion incision electro-coagulated and the microaneurysm clip removed. The submandibular gland was returned to its original position and the wound sutured with 5-0 suture. Finally the isoflurane was switched off and the mouse received 100% O_2 for 2 minutes until recovery and injected intraperitoneally with 500 µl sterile saline (Henry Schein, Nitside, UK). Following recovery animals were returned to their home cage, given soft diet and water and they were monitored three times daily.

2.2.2.5 Stereotaxic surgery

At a pre-determined time after MCAO, either self-assembling silk hydrogels or, in a separate series of experiments, self-assembling silk hydrogel/MSC constructs or MSCs alone were injected intracerebroventricularly or into the stroke cavity as detailed in the relevant results section by stereotaxic injection. Unless otherwise stated, the following protocol was used. A sterile

drape was placed over the heat mat. Two drapes were placed on either side. Anaesthesia was induced by inhalation of 3% isoflurane/1000ml/min oxygen (O_2) for approximately 2-3 minutes in induction chamber. Mice were transferred to a facemask and anaesthesia was reduced to 2% isoflurane/1000ml/min O_2, which was maintained for 20 minutes and subsequently reduced to 1.5% isoflurane/1000ml/min O_2 for the remainder of the procedure. Hair removal cream was used to remove the hair from scalp between the ears and left for 1 minute then removed by a sterile cotton bud before applying lidocaine 5%. Next, the mouse was covered by a sterile drape and ensuring it was sufficiently anaesthetised by testing pedal reflex and viscotears was applied to the eyes. After that, an incision was made around 1 cm long between the ears and the skull was exposed. Then, the bregma was identified on the surface of the skull and the needle was moved to the appropriate stereotaxic coordinates (+1.5mm anterior/posterior, +2.5mm medial/lateral unless otherwise stated) above the skull. A dental drill was used to make a burr hole then the dura matter was broken. Next, either 3% w/v or 4% w/v silk hydrogel was prepared and sonicated for 30 seconds and 30% amplitude. Before the sol-gel transition a predetermined volume of either self-assembling silk hydrogel or self-assembling silk hydrogels encapsulated with C3H10T0/5 (as previously described in section 2.1.13) or C3H10T0/5 cells alone were injected into the brain at +1.5mm anterior/posterior, +2.5mm medial/lateral and 1mm ventral relative to Bregma, unless otherwise stated, with a 26-gauge needle attached to a Hamilton syringe for 5 minutes which was left in place for a further 5 minutes

prior to withdrawing slowly. Next, the wound was sutured and the mouse was injected i.p with 500 µl saline. After recovery, the mouse was returned to its home cage for a predetermined time before being terminated and the brain removed for histology.

2.2.2.6 Termination and tissue collection

At the end of the experiment mice were killed by inhalation of CO_2 followed by vertebral dislocation unless it was to undergo perfusion fixation (see section 2.2.8). Then, the brain was removed and placed in 4% PFA for 30 minutes then moved to 30% sucrose cryoprotection for overnight until the brain sink.

2.2.2.7 Tissue sample preparation and histology

After the brain was removed from the 30% sucrose, it was frozen in isopentane and dry ice at -42°C then stored at -20°C until used. Then, the brain was embedded in M-1 embedding matrix (Thermo, UK) and sliced by cryostat 20 µm sections with low profile microtome blades and mounted to superfrost plus glass slides (Thermo, UK). Coronal sections were collected at eight regions of interest (as described by Osborne et al., 1987 and adapted for the mouse) which were positioned at 6.02 mm, 4.48 mm, 3.94 mm, 3.34mm, 2.86 mm, 1.98 mm, 1.00 mm and -0.8 mm relative to the interaural (IA) line (Dong, 2008) and stored at -20°C until stained by H&E staining (section 2.1.19) and viewed by light microscopy (Nikon Eclipse 50i, UK).

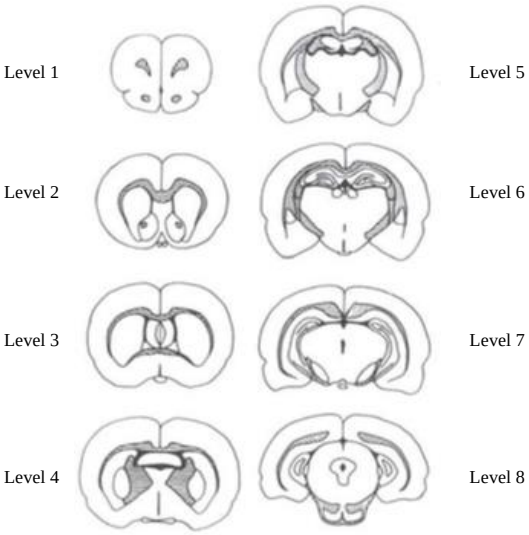

Level	1	2	3	4	5	6	7	8
Interaural distance(mm)	6.02	4.66	3.94	3.34	2.86	1.98	1.00	0.16

Figure 2.3 Line diagrams of 8 pre-determined coronal levels used for assessing conformity of self-assembling silk hydrogels. Brains sections were collected at these levels relative to the interaural line and using anatomical landmarks. Adapted from (Osborne et al.,1987).

2.2.2.8 Perfusion fixation

Chemical fixation is one of the common method that used to preserve tissues and brain biochemistry results in less alteration of the tissue compared to fresh freezing method. Fixation with paraformaldehyde produces tissue that is much more resilient and clear of blood which might interfere with visualising cell staining and gives good cellular definition of the tissue with fewer artifacts. Mice were placed in a supine position; an incision was made below the sternum to expose the rib cage. The diaphragm was cut away from the rib cage and the rib cage cut at either side to expose the heart. A 21-guage needle (Emoven, UK) attached to the perfusion apparatus was inserted into the heart and clamped in place. The right atrium was incised and a constant pressure applied using an infusion/withdrawal pump (Harvard Apparatus, UK) to allow the perfusion of about 20 ml heparinised saline. When the saline outflow from the atrium was bloodless, 30 ml fixative and 4% PFA at a rate of 5 ml per minute was perfused. Next, the brain was removed and immersed in 4% PFA for 30 minutes then moved to 30% sucrose solution for overnight until the brain sunk.

2.3 Statistical analysis

Data were analysed using GraphPad Prism 7.0 (GraphPad Software, La Jolla, CA, U.S.A.). Sample pairs were analysed with the Student's t-test. Multiple samples were evaluated by two-way analysis of variance (ANOVA), followed by Bonferroni or Tukey's multiple comparison post hoc test.

Asterisks were used to denote statistical significance as follows: *P < 0.05, **P < 0.01, ***P < 0.001. All data were presented as mean values ± standard deviation (SD). The number of independent experiments (n) is noted in each figure legend.

CHAPTER 3. Characterisation of self-assembling silk hydrogels to achieve optimum processing parameters for use in cell encapsulation and intracerebral injections.

3.1 Introduction:

Silk hydrogels are of interest for many biomedical applications due their excellent processability, compatibility, controlled biodegradability and mechanical properties. Silk proteins are characterised by highly repetitive primary sequence that leads to homogeneity significantly in the secondary structure, informing peculiar structural properties that is different to globular proteins which are less ordered and provide catalytic and molecular recognition function (Floren et al., 2016b). Silk biomaterials are known generally to have good oxygen and water vapour permeability, minimal inflammatory properties and high mechanical strength (Kundu et al., 2014, Krishna and Kiick, 2010). Though, control over mechanical properties, in particular stiffness, is essential for cell adhesion and viability and to recreate the appropriate tissue environment (Straley et al, 2010), stiffness properties of self-assembling silk hydrogels appropriate for brain tissue has not yet been studied. An ultrasonication based method was developed and used now to accelerate the sol-gel transition as previously, the gelation times took days to weeks. When there is alteration in hydrophobic hydration in the protein chains the physical β-sheet crosslinks created lead to rapid gelation and convey much resiliency of silk materials and strength. The gelation time is controllable and could be minutes to hours depending on sonication

parameters applied such as the amplitude (energy power), duration time, temperature, pH, salt concentration and silk concentration (Wang et al., 2008). Therefore the optimum parameters to control gelation time of self-assembling silk hydrogels need to be characterised and optimised.

3.2 Hypothesis and aims:

The aim of this chapter is to study the behaviour of self-assembling silk hydrogels, in terms of their secondary structure, how quickly they convert during the sol-gel transition, their swelling characteristics, their optimum stiffness to mimic brain tissue mechanics and to find the optimum time and power output to prepare the silk hydrogels for subsequent cell encapsulation. These studies were performed to establish the optimum properties of the self-assembling silk hydrogels as a prelude to introduce cells into the hydrogels (Chapter 4) and as a prelude to exploring the behaviour of the hydrogels *in vivo* (Chapter 5).

3.3 Protocol:

All experiments were carried out on *B.mori* silk cocoons to prepare the silk solution (as described in 2.1.3). Next, to transfer the silk solution to the silk hydrogel, sonication was applied (as described in section 2.1.4) and self-assembling silk hydrogels underwent testing for structural and mechanical properties as described in sections (2.1.5 - 2.1.12).

3.4 Results:

3.4.1 Light scattering increased over time after sonication and with increasing silk hydrogel percentages

5 ml silk aqueous solutions at concentrations of 1, 2, 3, 4 and 5% (w/v) were sonicated for 30 seconds (at 30% amplitude power output (unless stated otherwise in the figure legend) on ice. It was found that light scattering always increased with time as shown in (Figures 3.1 to 3.4), due to physically cross-linked silk hydrogels developing nanocrystalline regions that scatter light. Light scattering increased in a linear fashion; at 24 hours, the silk hydrogels showed the highest light scattering properties. The extent of light scattering depended on the amount of silk present: the highest scattering values were observed for the 5% w/v hydrogels gels and lowest for 2% w/v hydrogels. Though 1% w/v hydrogels didn't gel, they still scattered the light due to their opaqueness.

However, the starting point was 45 seconds of sonication and 30% amplitude power. It was found that the sonication process became unreliable and produced inconsistent results (Figure 3.1) and took time to gel. Therefore, the next step was to reduce time of sonication process to 30 seconds but increase the amplitude power to 60% however, again, we produced unreliable and inconsistent results (Figure 3.2). Moreover the sample gelled very quickly using these parameters, which is undesirable for our studies of cell encapsulation and intracerebral injection. Therefore, sonication time was

kept at 30 seconds and power was reduced back to 30%, the results for which were reliable and the gelation time reasonable and manageable for future cell encapsulation and intracerebral injection studies (between 5-60 minutes) (Figures 3.3 and 3.4). Therefore we concluded that 30 sec and 30% power are the optimum parameters for sonication. However, when the power output exceeded 30% amplitude or the volume used was less than 2 ml, the sonication generated foams and the silk didn't gel in homogeneous manners. Therefore the use 4 ml as a minimum volume of self-assembling silk hydrogels and an exact amplitude of 30% are required for future experiments.

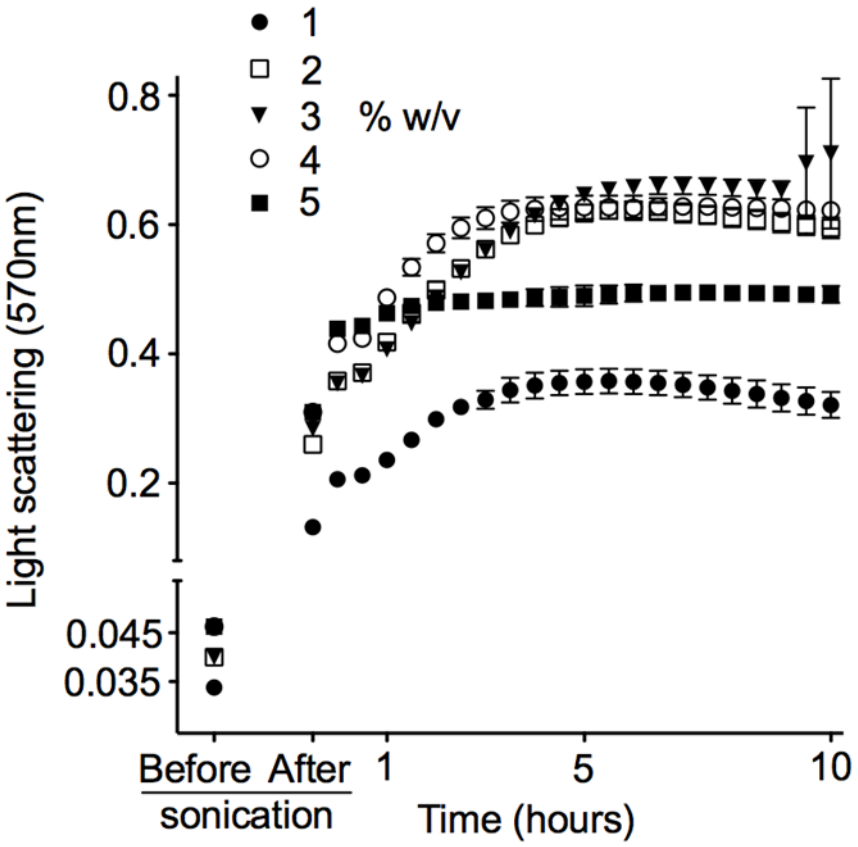

Figure 3.1 Sol-gel kinetic study for 1-5% w/v by monitoring gelation induced light scattering, sonication process for 45 seconds and 30% amplitude. Measuring the sol-gel kinetic of 1-5% w/v before sonication and after sonication for upto 10 hours. The light scatter increased sharply after the sonication process, continue to increase until sample gelled and give steady measurements. Values are average ± standard deviation of n=3.

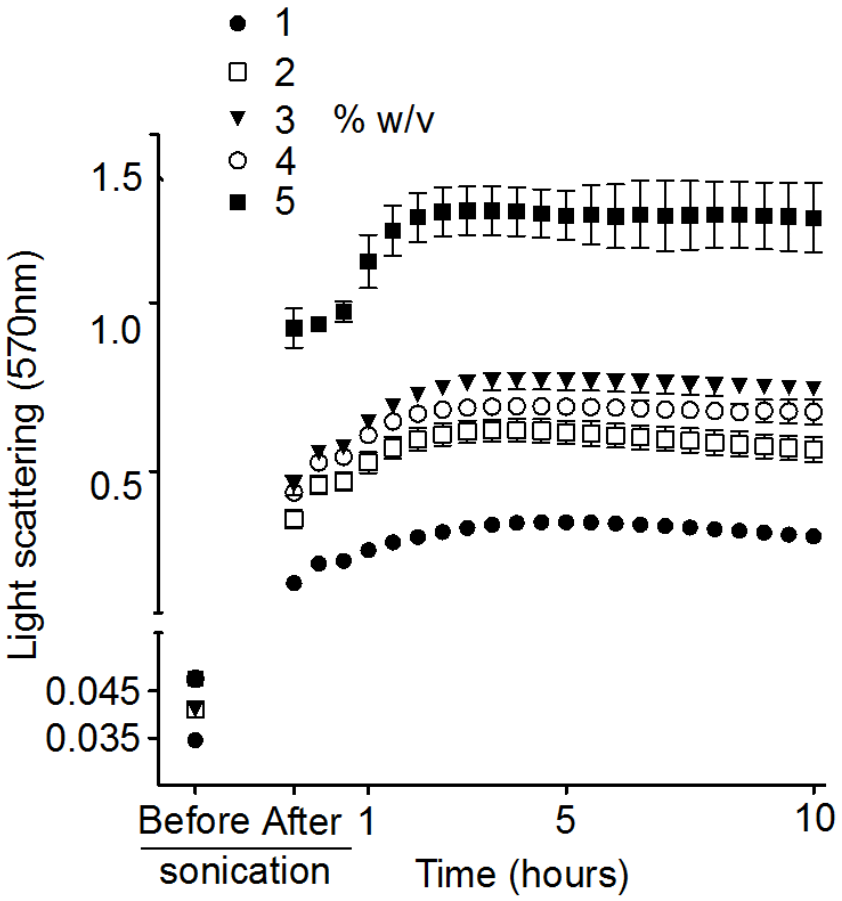

Figure 3.2 Sol-gel kinetic study for 1-5% w/v by monitoring gelation induced light scattering, sonication process for 30 seconds and 60% amplitude. Measuring the sol-gel kinetic of 1-5% w/v before sonication and after sonication for upto 10 hours. The light scatter increased sharply after the sonication process, continue to increase until sample gelled and give steady measurements. Values are average ± standard deviation of n= 3.

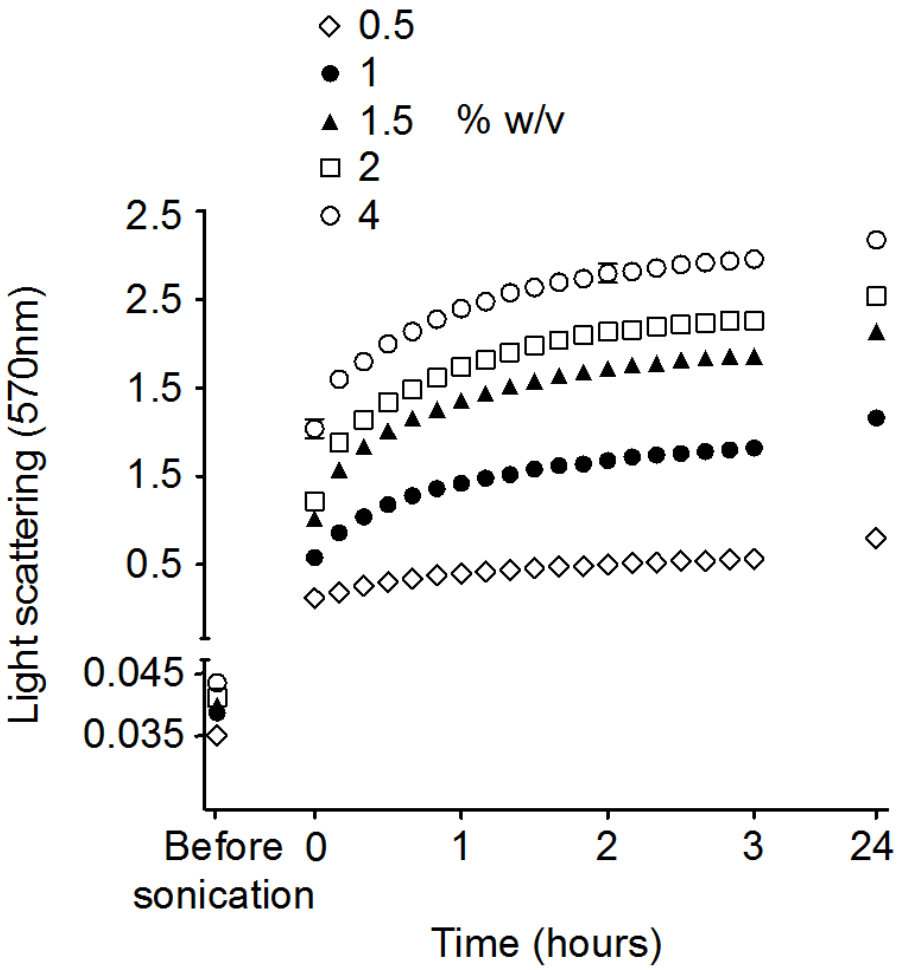

Figure 3.3 Sol-gel kinetic study for 0.5, 1, 1.5, 2 and 4% w/v by monitoring gelation induced light scattering, sonication process for 30 seconds and 30% amplitude. Measuring the sol-gel kinetic of 0.5, 1, 1.5, 2 and 4% w/v before sonication and after sonication for three hours and then at 24 hours. The light scatter increased sharply after the sonication process, continue to increase until sample gelled and give steady measurements. Values are average ± standard deviation of n=3.

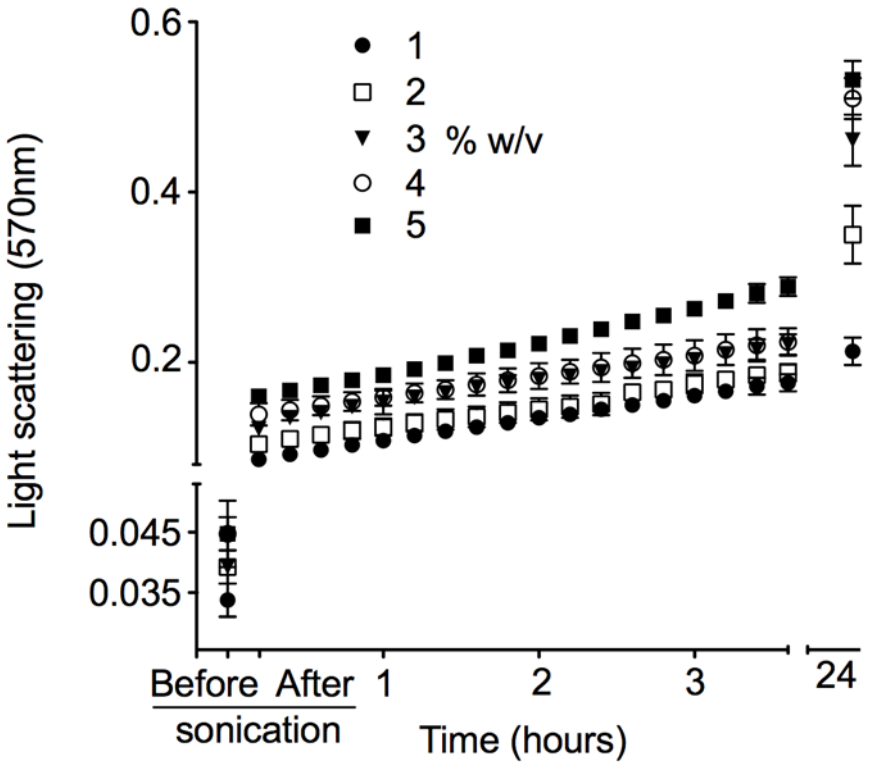

Figure 3.4 Sol-gel kinetic study for 1-5% w/v by monitoring gelation induced light scattering, sonication process for 30 seconds and 30% amplitude. Measuring the sol-gel kinetic of 1-5% w/v before sonication and after sonication for three hours and then at 24 hours. The light scatter increased sharply after the sonication process, continue to increase until sample gelled and give steady measurements. Values are average ± standard deviation of n=3.

3.4.2 Stiffness of self-assembling silk hydrogels

Structure properties of self-assembling silk hydrogels (1-5% w/v) were examined on a spatula to visualise the optimum stiffness that is similar to the brain. After sonication the silk samples were kept in a 24-transwell plate to complete the sol-gel transition. A 24 transwell plate made it possible to remove the gels from the wells and 5% w/v samples were collected after 1 hour, whereas 2, 3 and 4% samples were collected after 4 hours and 1% w/v samples were collected after 24 hours then placed on spatula. Time differences of collection were due to the samples not gelling at the same time, as higher concentration gelled in less time. It was found that 5% was solid and was easily removed from transwell whereas 2, 3 and 4% w/v were removed with some difficulties due to the softness and 1% w/v was not solidified even after 24 hours. As seen in (Figure 3.5), we observed that 2 and 3% w/v were soft and more similar to the brain stiffness and elasticity. The solidity test was done on 1, 3 and 5% w/v. After 1 hour, the 5% w/v remain in the bottom of the tube whereas 3% w/v was semi-gelled and moved a little bit but 1% w/v was liquid and didn’t gel (Figure 3.6).

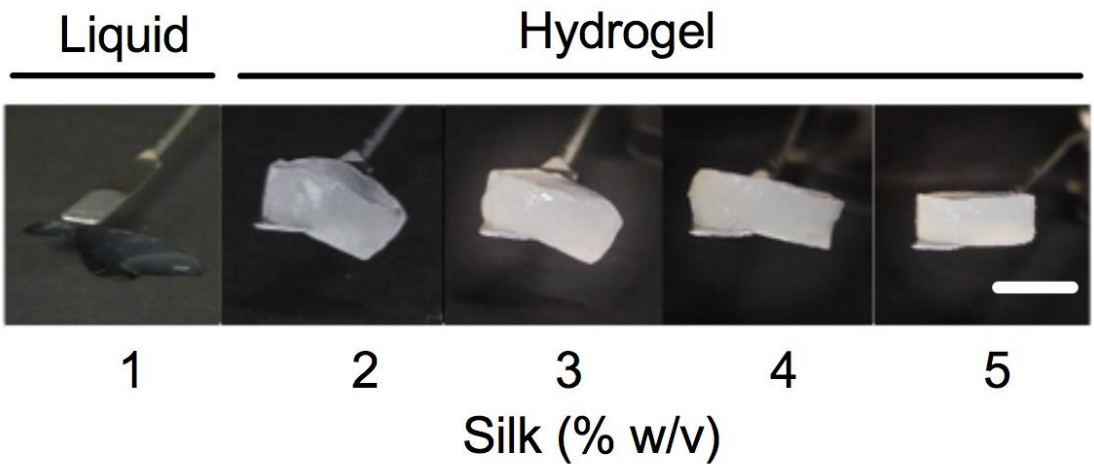

Figure 3.5 Structure properties of silk hydrogels. Silk hydrogel prepared on transwell at various percentages (1-5% w/v) then placed on a spatula to visualise theirs stiffness. Scale bar = 10 mm.

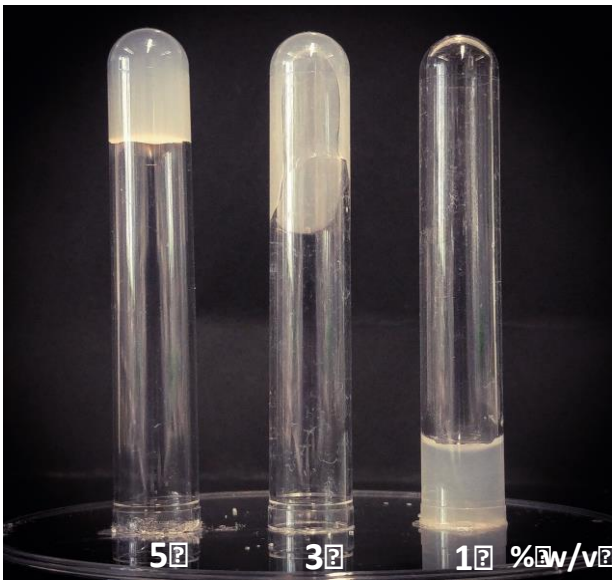

Figure 3.6 Hydrogel formation of 1, 3 and 5% w/v silk. After the samples were sonicated, they were placed in the tubes and left for 1 hour before they were turned upside down.

3.4.3 Elasticity measurement of 2-5% (w/v) self-assembling silk hydrogels using rheology

To confirm whether 2 and 3% w/v exhibit similar stiffness to the brain, we performed rheology experiments to compare the elasticity of the different concentrations with that cited in the literature for brain. Stiffness, as measured by rheology, of self-assembling silk hydrogels increased with increasing concentrations of silk (2-5% w/v) with matrix elasticity similar to that of brain tissue (0.1 - 1 kPa (Engler et al., 2006) Figure 3.7) for 2 and 3% w/v silk hydrogels (Figure 3.8). These rheology results were also confirmed manually using a finger press test, where 5% w/v was too hard compared to brain tissue press test by finger, 4% w/v was closer but 2 and 3% w/v were very close to the brain elasticity as tested by finger press.

Figure 3.7 Solid tissues exhibit a range of stiffness, as measured by the elastic modulus. (Engler et al., 2006)

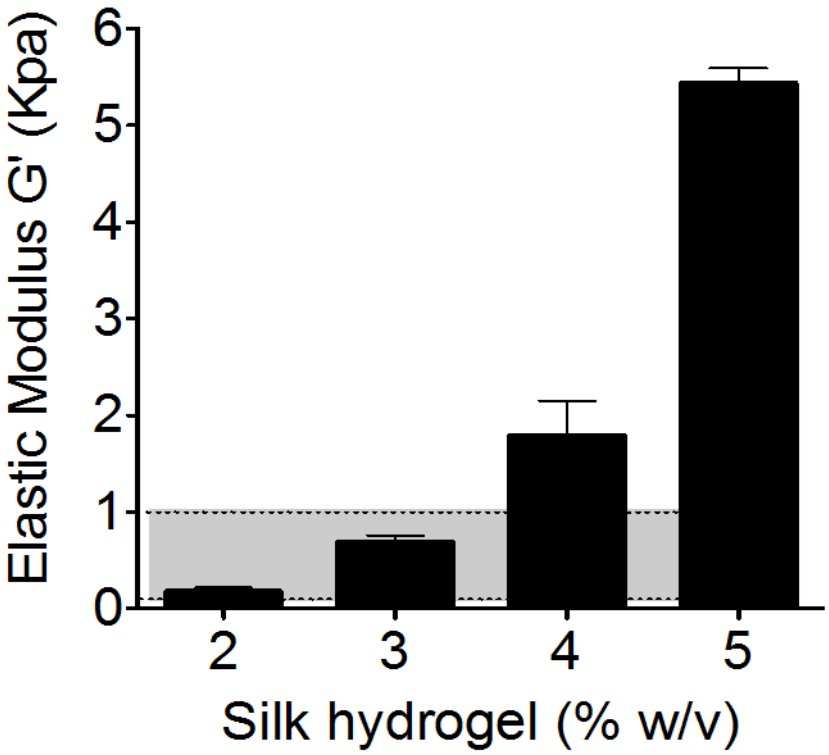

Figure 3.8 Silk hydrogel stiffness measurement. The dotted lines and shaded area show the stiffness range of brain tissue 0.1-1 kPa. Values are average ± standard deviation n=3.

3.4.4 There was no swelling of silk hydrogel *in vitro*

Given that hydrogels delivered intracerebrally must not swell significantly to avoid compression on surrounding cellular components which may induce further injury, *in vitro* swelling was calculated by adding 300 µl PBS on the top of pre-weighed silk hydrogels 2-5% w/v for 24 hours before completely removing the PBS and reweighing. We found that there was no difference between the initial sample weight and the rehydrated sample in any of the percentages tests 2-5% w/v (Figure 3.9). In addition, the swelling ratio was calculated as follows and was found to be zero for every sample.

$$Swelling\ ratio\ =\ (Wr - Wi)/Wi$$

Wr: sample weight after removal of PBS.

Wi: initial sample weight before adding PBS.

Therefore, given there was no significant increase in weight after removal of PBS and given that the swelling ratio was zero for all samples this indicates that there was no swelling *in vitro* of the self-assembling silk hydrogels at all concentrations tested.

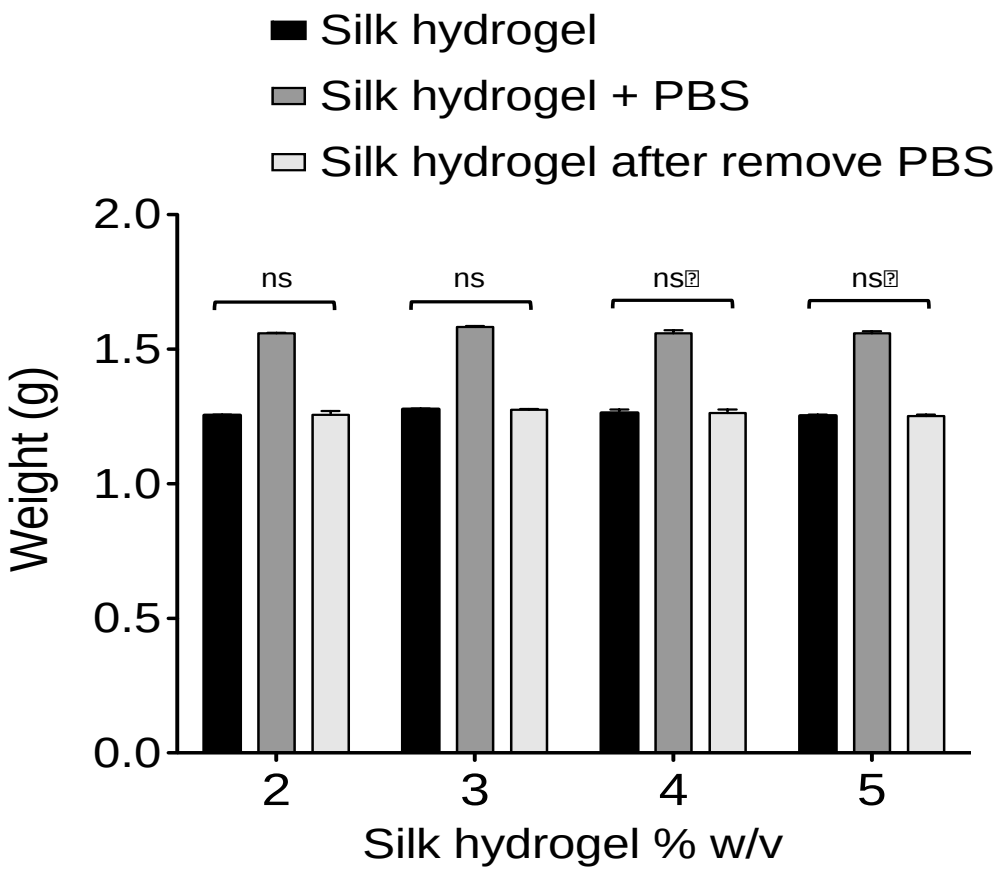

Figure 3.9. Assessment of swelling of self-assembling silk hydrogels. The respective hydrogel weights before, during and after incubation with phosphate buffered saline. Values are average ± standard deviation of n=6.

3.4.5 Self-assembling silk hydrogels exhibited increased β-sheet formation after sonication for all concentrations tested.

The alteration in hydrophobic interaction and the subsequent physical crosslinks lead to β-sheet formation, which is an important parameter to yield mechanically robust hydrogels. To assess the extent of β-sheet formation, Circular Dichroism (CD) was used. In the first run, the sampling was every 10 minutes for 24 hours, however the curves produced were too coarse and difficult to interpret (Figure 3.10a showing 4% w/v and 3.10b showing 5% w/v). Therefore the setting was changed to every 10 seconds producing smoother curves that could be interpreted (Figure 3.11a showing 2% w/v, 3.11b showing 3% w/v and 3.11c showing 5% w/v, plotted at 1, 3, 6 and 24 hours). CD measurement showed a rapid formation of β-sheets structure after sonication, indicated by the increase in ellipticity at 217nm (β-sheet structure peak) (Figures 3.11). The gelation of silk hydrogel happened at the transition point, when the early rapid formation of β-sheets slowed down.

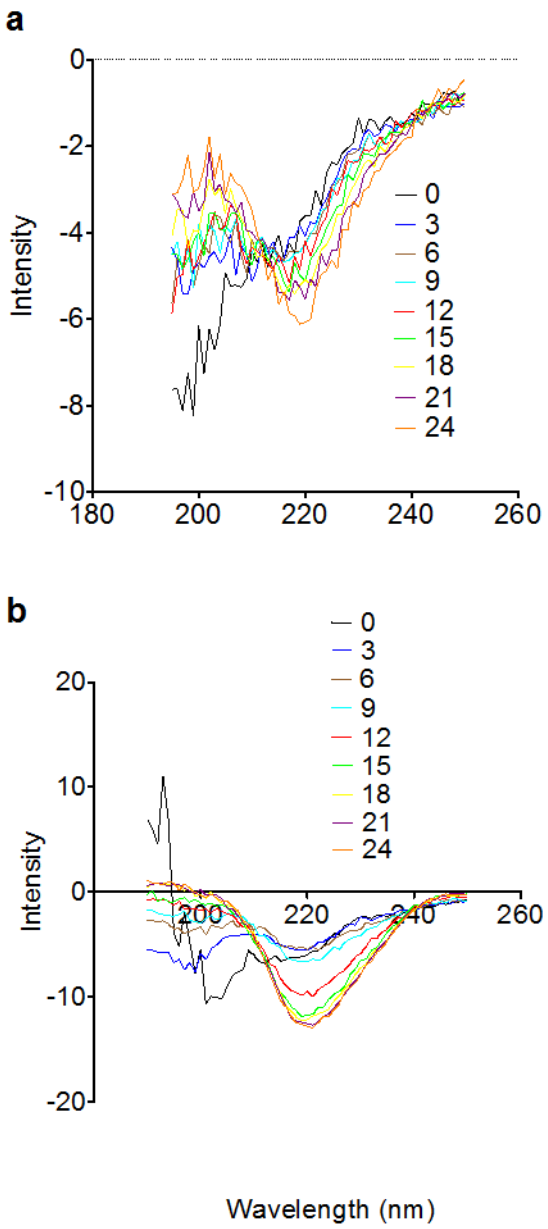

Figure 3.10 Secondary structure of self-assembling silk hydrogels, wavelength scanned every 10 minutes. Circular dichroism measurements of a silk solution undergoing solution-gel transition for a) 4% w/v and b) 5% w/v following sonication energy input (note Ellipticity at 217 nm represents β-sheets).

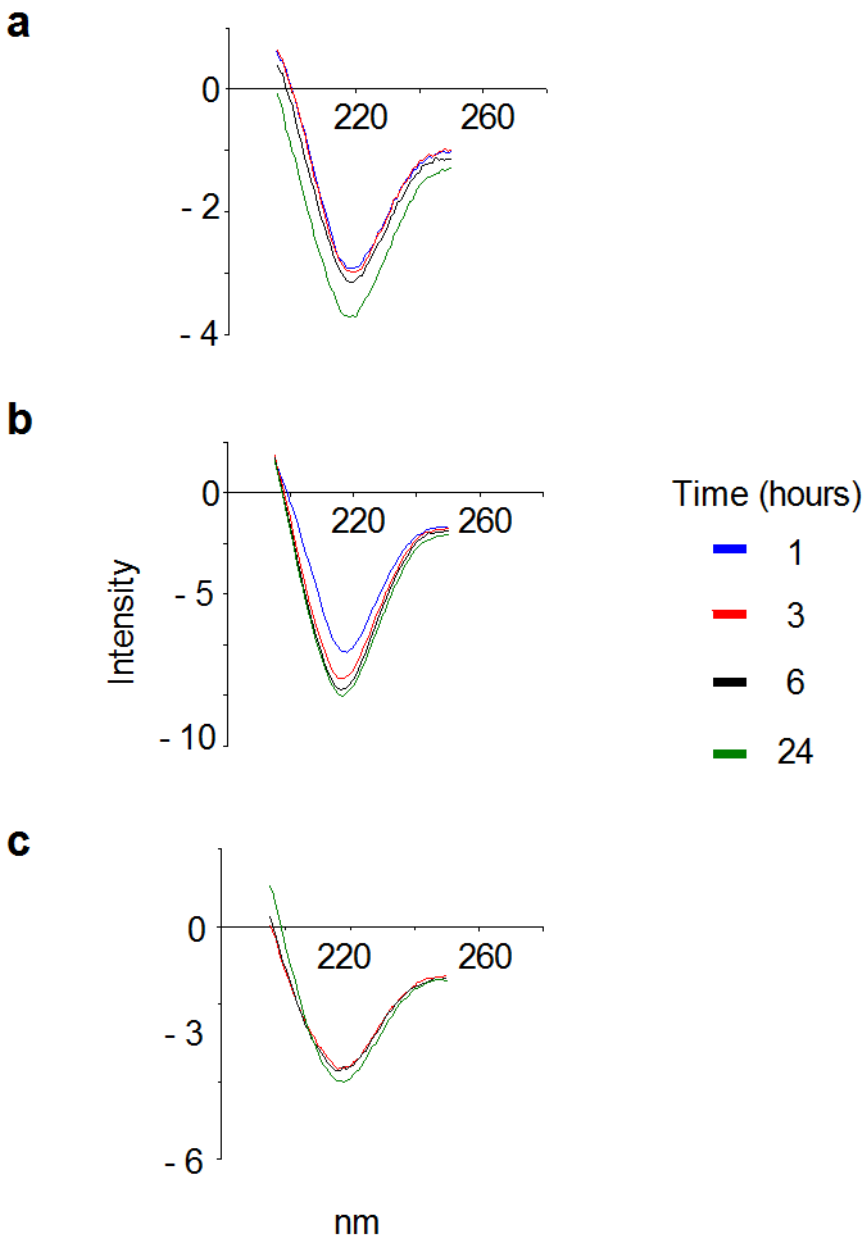

Figure 3.11 Secondary structure of self-assembling silk hydrogels, wavelength scanned every 10 seconds.

Circular dichroism measurements of a silk solution undergoing solution-gel transition for a) 2% w/v, b) 3% w/v and c) 5% w/v following sonication energy input (note Ellipticity at 217 nm represents β-sheets).

3.4.6 Validation of β-sheet formation in self assembling silk hydrogels by Fourier Transform Infrared Spectroscopy (FTIR)

The β-sheet formation was further validated across the different concentrations using FTIR. Figure 3.12 shows the original FTIR spectra in the amide I region for 5 samples of self-assembling silk hydrogels 1-5% w/v. The dotted light shows the absorption band at 1625 cm^{-1} indicating the presence of β-sheet and random coil band at 1655 cm^{-1}.

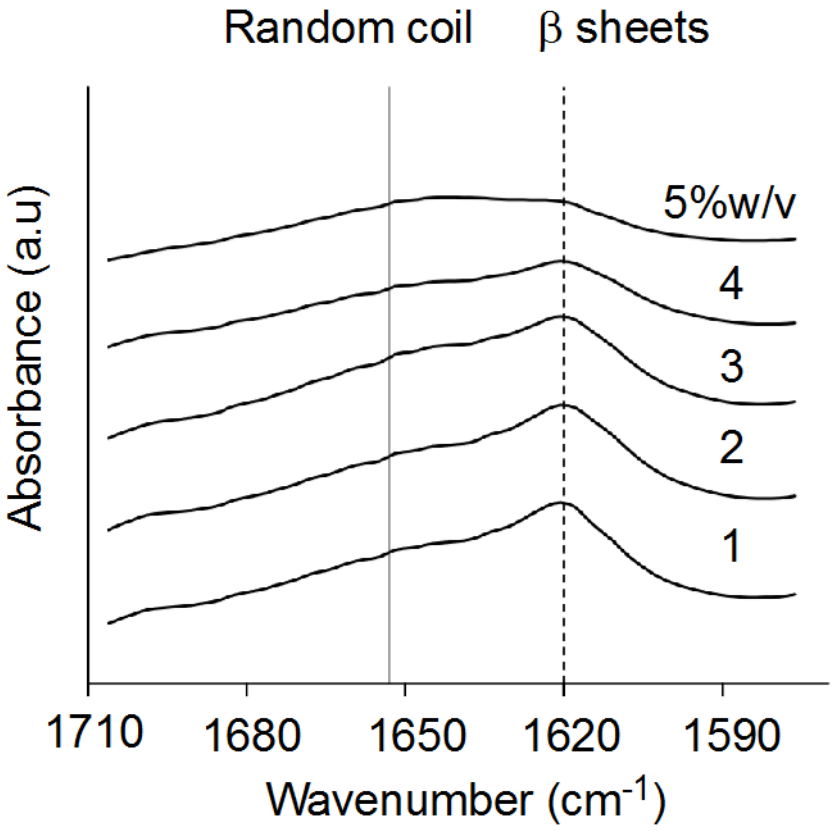

Figure 3.12 FTIR absorbance spectra in the amide I region vs wavenumber for self-assembling silk hydrogels 1-5% w/v.

3.4.7 Self-assembling silk hydrogels exhibited good porous 3-dimensional structure

Porosity is important to allow nutrient access and exchange of metabolic waste to ensure cell viability and growth. Therefore, the inner structures of silk hydrogel 2-5% w/v were examined by SEM in the freeze dried state. In 2% w/v the silk hydrogel formed like large flakes with lots of spaces compared with 3% w/v that formed porous and fibrous structures (Figure 3.13). Unfortunately, 4 and 5% w/v were not clear due to sample movement during image acquisition.

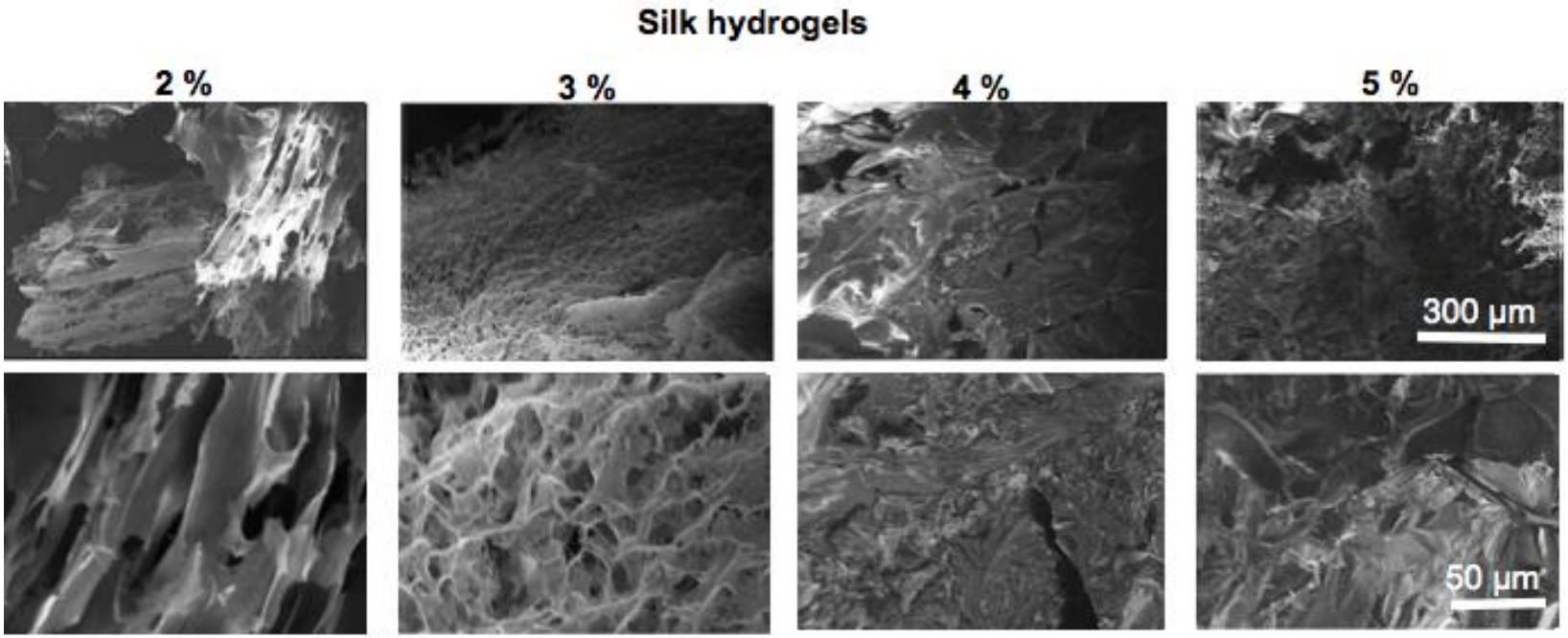

Figure 3.13 SEM images for freeze dried self-assembling silk hydrogels 2-5% w/v in 37°C.

3.4.8 Self- assembling silk hydrogels exhibited good *in vitro* space conformity if gelation was allowed to occur *in situ*

Space-conforming properties are important in order to fill the stroke cavity and therefore were tested *in vitro* prior to translation *in vivo*. The temperature of silk hydrogel was kept between 30-37°C to provide the optimum and safe environment for future studies involving cells and to be close to the brain temperature. In the *in vitro* conformity test, cuvettes were filled until the 1 ml graduation line with silk hydrogel injected from a 26-gauge needle under two conditions; pre and post gelled. In the pre gelled condition (silk solution was sonicated then loaded into the syringe and injected immediately into the cuvette) the entire amount was discharged from the syringe, and therefore the silk hydrogels reached the 1 ml line and gelled in the cuvette (Figure 3.14a). On the other hand in post gelled condition (silk solution was sonicated then loaded in the syringe and left until gelled before injecting into the cuvette). The gel exhibited a snake like space on injection, left spaces and cavities in the cuvette (Figure 3.14a) and was still present in the syringe after the cuvette was filled to the 1ml line (Figure 3.15). Though, no statistical difference was observed for 2% w/v silk samples, for 3% w/v and 4% w/v silk samples, significantly more silk could be applied to a fixed volume when silk was in the solution state rather than in the gelled state, showing good space conformity if gelation is allowed to occur *in situ*. This is important given that gelation of biomaterials could potentially block the lumen of the needle or disrupt the space conforming properties of the biomaterial post-injection.

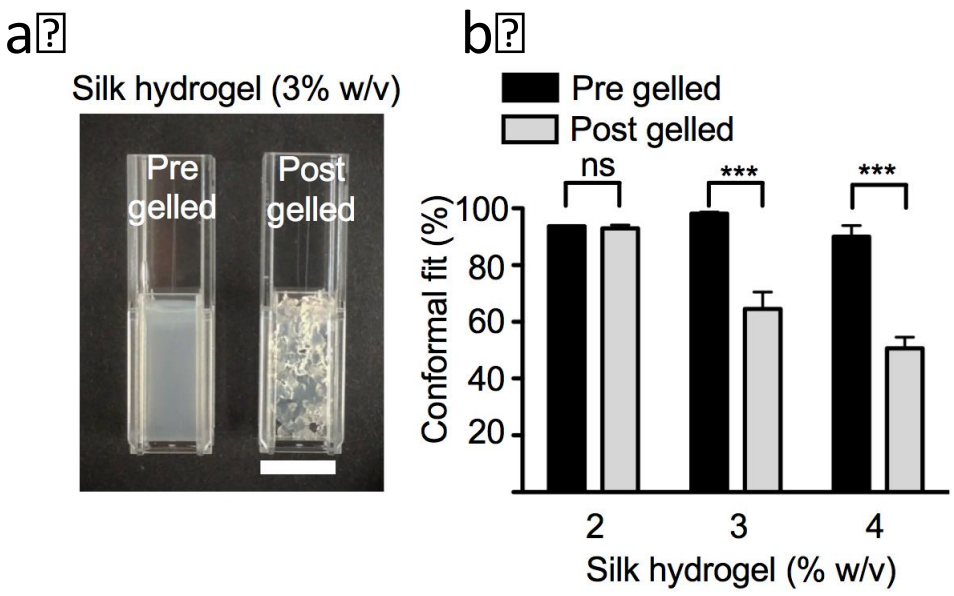

Figure 3.14. Space conformity of self-assembling silk hydrogels. (a) Qualitative images of 3% w/v silk samples added to a cuvette in the pre- and post-gelled state using a sample volume of 1 ml (scale bar 10 mm). (b) Quantitative assessment of space conformity of silk hydrogels. There is significant difference in 3 and 4% w/v between pre and post gelled silk hydrogel. ***P< 0.001 (Mean ± SD, error bars hidden in bars when not visible, n=3 to 6)

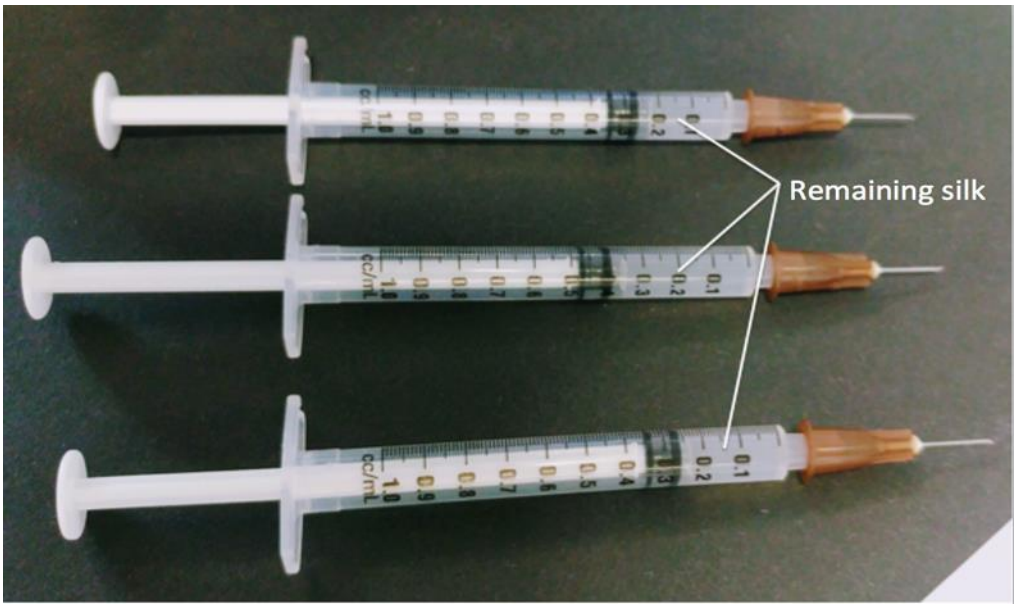

Figure 3.15 Conformity test for silk hydrogel *in vitro*. This picture shows the remaining post gelled silk hydrogel 3% w/v in the syringe after injection.

3.5 Discussion:

The key findings of the present chapter are that self-assembling silk hydrogels exhibited predictable and controllable solution-gel kinetics, elasticity and β-sheet formation and good space conformity in the absence of any silk hydrogel swelling.

3.5.1 Self-assembling silk hydrogels exhibited predictable and controllable solution-gel kinetics.

Regarding sol-gel transition, there are several ways to accelerate the conversion of the silk solution to silk hydrogel. These include chemical methods such as pH, chemical crosslinking, precipitants, high pressure CO_2 and change the ionic concentration by adding some salts like $CaCl_2$ or KCL and exposure to solvents, gases and surfactant such as sodium-lauroyl sacrosinate and sodium dodecyl sulphate (Ciocci et al., 2017). In addition, physical methods such as shear force, temperature, electric fields, removal of the bulk of water by osmotic stress and ultrasound. These physical stimuli lead to transfer of energy within the system, affecting the hydration and folded state of the protein that cause protein assembly and aggregation. Unfortunately most of these processes are harsh and not suitable for preparing hydrogels in the presence of stem cells (Floren et al., 2016b, Ciocci et al., 2017). Therefore sonication energy was used throughout this thesis and cells were added to the treated sample after sonication. This in turn enabled successful 3D cell culture in silk hydrogels (Chapter 4)

We used sonication physical crosslinking to generate the silk hydrogel due to the following advantages over the above-mentioned approaches. When the sonication (high frequency sound waves) is applied, the sound waves create locally expanded and compressed area within the medium leading to bubble formation and cavitation, these two lead to fluid accelerated and create molecular collisions that resulted in high temperature and pressure (Paulusse and Sijbesma, 2006). All of these effects contribute to local chain dehydration and encourage the macromolecular aggregation that resulted from increased exposure of hydrophobic domain (i.e. β-sheet formation) (Floren et al., 2016b, Paulusse and Sijbesma, 2006). The gelation time could be controlled from minutes to hours by adjusting the sonication parameters, namely time and power output as well as the silk solution concentration and temperature (Floren et al., 2016b).

In the present chapter, we performed studies on five different concentrations between 1-5% w/v hydrogels, the minimum concentration was 1% w/v to achieve stable network for self-assembly process. Silk solution without sonication showed almost zero light scattering as previously described (Seib et al., 2013). After sonication, as the silk hydrogels undergo sol-gel transition, they are observed to become stiffer and cloudier. To quantify the sol-gel transition using sonication and test its reliability, we assessed light scattering properties of the hydrogels. We found, using light scattering, that when the sonication time of 45 seconds and the power of 60% were used the sonication process became unreliable and produced inconsistent results. However, we found that using sonicator parameters of 30% amplitude and 30

seconds with a break for 30 seconds then another 30 seconds on ice to avoid the high temperature produced predictable and consistent sol-gel where light scattering always increased with time after sonication.

Light scattering increased sharply after the sonication and gradually increased over the time until the complete gelation occurred. The most likely process to explain these results is that energy input, using sonication, into a silk solution displaces solvating water molecules and exposes the hydrophobic silk domains, these rearrange and subsequently grow into nanocrystallites. These nanocrystallites are responsible for light scattering and result in the opaqueness of silk hydrogels (unlike chemically cross linked silk hydrogels which are transparent to visible light) (Seib, 2018). In addition, as expected, the overall solution-gel kinetics were concentration-dependent with higher silk concentrations forming mechanically stable hydrogels faster. The lower threshold for the formation of silk hydrogels was found to be 1% w/v; it is likely that at this concentration not sufficient silk is present to form a mechanically robust hydrogel network despite the formation of nanocrystallites.

Therefore we conclude that the optimum sonication parameters for sol-gel transition of self-assembling silk hydrogels are 30% amplitude for 30 seconds and overall, observation in relation to changes to solution-gel transition are in good agreement with previous studies (Vu et al., 2016, Sonia Kapoor and Subhas Kundu, 2016) when they used the same parameters.

3.5.2 Self-assembling silk hydrogels exhibited elasticity similar to brain tissue

Control over mechanical properties such as stiffness is essential for cell adhesion and viability and to recreate the tissue environment that any given cell type would grow and interact within the body (Straley et al, 2010). By observation using a spatula, the structural properties for the silk hydrogels were between liquid and stiff for 1% w/v and 5% w/v respectively, 2 and 3% w/v were soft gel and more similar to that observed for brain tissue. 1% w/v didn't gel even when it was left overnight so it was excluded from most of the experiments. On the other hand, 5% w/v was hard and too high compared to the brain elasticity. Using rheology we showed that, as the concentrations of silk hydrogels increased (2-5% w/v), the hydrogels became stiffer, due to the presence of nanocrystallites that provide mechanical strength. At 2 and 3% w/v these silk hydrogels exhibited matrix elasticity similar to that of brain tissue (0.1-1 kPa) (Engler et al, 2006), whereas 4 and 5% w/v out of the range.

3.5.3 Self-assembling silk hydrogels exhibited β-sheet formation.

In section 2.1.4 and 2.1.5 we showed that energy input by sonication into a silk solution resulted in increased light scattering probably as a result of the formation of nanocrystallites. In order to confirm that these nanocrystallites were β-sheets and thereby the points of physical crosslinking within the hydrogel, important parameters for generating a mechanically robust

hydrogel, we examined the secondary structure of self-assembling silk hydrogels by CD and FTIR. Two major time-dependent points were identified in the spectra at 199 nm for the random coil and 217 nm for β-sheets. As gelation continued the negative band at 217 nm became stronger and increased as more β-sheets formed. As gelation continued, the intensity at 199 nm increased, whereas the intensity at 217nm decreased, corresponding to decreased random coil content and increased β-sheet content, respectively. Therefore we have verified that, after sonication, the random coil changed to β-sheets based on an increase of ellipticity at 217 nm with interchain physical crosslink occurring leading to hydrogel formation. When the rapid formation of β-sheets slowed, the silk hydrogel formed at this point.

To further evaluate the secondary structural changes of silk during sol-gel transition, FTIR analysis was performed for different silk percentages 2-5% w/v. The deconvolution peak analysis was used to assess the fraction change of the β-sheets structure during the gelation process. All the solution concentration have approximately 20% content of β-sheets and this percentage remained until the degree of gelation reached 15-20% and thereafter increased (Matsumoto et al., 2006). There was no significant change in the fraction of β-sheets once the gelation occurred. Other laboratories have used 0.9% w/v of silk as the minimum concentration and the extent of β-sheet formation in the gel condition reached 50%. In those studies, there was no difference in the fractional change in β-sheets structure even when the samples gelled quicker when the temperature increased (Matsumoto et al., 2006). Previous studies have shown that when the

concentration increased, the β-sheets increased (Floren et al., 2016a). However in the present study we found the opposite, even though we tested our experiment twice, so we can see the 1% w/v had increased β-sheets compared to 5% w/v which was non-predictable while they found 5% w/v higher than 1% w/v. Finally, qualitative assessment of these hydrogels by scanning electron microscope showed a porous three-dimensional structure (Kim et al., 2004).

3.5.4 Self-assembling silk hydrogels exhibited good *in vitro* space conformity in the absence of any silk hydrogel swelling.

Hydrogels have limited interfacial tension, which make them suitable for good integration of payload with host tissue after *in vivo* administration, reducing the barrier for delivery of payload at the host tissue-hydrogel interface (Fon et al, 2010). We tested the conformity of silk hydrogel before gelled and after gelled *in vitro*. In the 'before gelled' (pre gelled) condition the samples were injected into the cuvette after the sonication but before the sample was gelled so it was injected completely and filled the cuvette (until 1 ml mark) then gelled in the cuvette after couple of minutes. On the other hand, for the after gelation (post gelled) condition, the samples were left in the syringe after sonication for 4 hours until they complete gelation had occurred before injecting to the cuvette. In this condition the silk hydrogel reach the line of 1ml but in reality it was not 1 ml injected due to the empty spaces and cavities that resulted from injection of silk hydrogel in the post gelled condition. Therefore the pre gelled condition of self-assembling silk hydrogels would be

superior for translation *in vivo*, where self-assembling silk hydrogels injected into the stroke cavity would be expected to fill the cavity and then gel in situ (see chapter 5).

In addition, for clinical translation of hydrogels for intracerebral administration, good space-conforming properties without swelling are required to avoid compressing against adjacent tissue which may expand cellular injury (Massensini et al 2015). The present chapter showed that there was no swelling in silk hydrogel after covering with PBS for 24 hours for 2-5% w/v, in agreement with other laboratories (Kim et al., 2004, Seib, 2018).

In summary, an ideal scaffold should mimic the ECM by providing signals that help in cellular morphogenesis and development. In the present chapter we have shown the potential of self-assembling in terms of having the appropriate physical cues such as substrate elasticity and surface topography. This chapter shows that 3% w/v self-assembling silk hydrogels, using sonication of 30% amplitude for 30 seconds, injected in the pre gelled state to allow good conformity, were identified as the optimum concentration and conditions for testing for cell encapsulation (chapter 4) and intracerebral delivery (chapter 5).

CHAPTER 4. Characterisation of MSC encapsulation in self-assembling silk hydrogels.

4.1 Introduction

Tissue engineering and regenerative medicine advancement are dependent on the development of biocompatible, biodegradable and inexpensive biomaterials that are easily prepared and are able to match the durability, resilience and mechanical properties of native tissue (Bouten et al., 2011).

In the previous chapter, we showed that 3% w/v self-assembling silk hydrogels, produced using sonication of 30% amplitude for 30 seconds, were identified as the optimum concentration and conditions without cell encapsulation. Therefore the next step was to establish the optimum concentration of silk hydrogels for MSC encapsulation in terms of viability, distribution throughout the hydrogel and injectability. MSCs have clinical advantages because these cells can be derived from an autologous cell source and they have proven capacity to promote the repair of neurovascular units and exert potent immunomodulatory functions that result in neurorestoration in experimental models (Wang et al., 2014). However, one key issue hindering the translation of cell therapies to the clinic is the lack of suitable cell delivery technologies that allow an even distribution of cells and that can support cell survival even after injection through needles required for intracerebral injection. These initial concepts need to be proven before establishing whether the behaviour of these hydrogels in vivo.

The support of stem cell survival and distribution in the *in vivo* environment is normally provided by cueing functions from the ECM, which is critical for the storage and presentation of growth and signalling factors and the provision of cell adhesion sites to guide and promote proliferation and survival. Physical cues, such as substrate elasticity and surface topography (as explored in Chapter 3), also direct stem cell lineage commitment (Vining and Mooney, 2017, Dalby et al., 2014). Therefore, the ECM represents a critical signalling hub that allows (stem) cells to respond to their environment. The ECM can be mimicked quite effectively by engineered hydrogels (Prewitz et al., 2012, Darnell and Mooney, 2017). Interactions of cells with the local microenvironment are known to be critical for many important biological events including cell adhesion, differentiation, growth and apoptosis (Discher et al., 2009, Kuraitis et al., 2012). Specially, substrate biophysical properties such as geometry, soluble factor (Narita et al., 2008), rigidity (Engler et al., 2006), biological ligand (Suzuki et al., 2010) or a combination thereof have been explored to support MSC properties and function (Suzuki et al., 2010). As a result, neural tissue engineering relied on combining potent regenerative cells such as mesenchymal stem cells with a delivery matrix for transplantation to support their viability, proliferation and function (Cheng et al., 2013).

In this study the C3H10T1/2 cell line has been chosen because it is recognized as a model for MSCs, because of its multi-lineage differentiation potential (Jian et al., 2015). This cell line was established in 1973 and

derived from 14-17 day old C3H mouse embryo by (Reznikoff et al., 1973). C3H10T0.5 cells have some features that are MSC-like, including the ability to secrete paracrine factors to promote tissue regeneration and mediate interactions with endothelial cells to increase and participate in blood vessel formation. Moreover, these cells are easily cultured and provide consistent performance and avoid issues with no donor variability (Sharma et al., 2015).

Silk hydrogels have the potential to act as scaffolds for cell encapsulation and deliver bioactive molecules and cells such as cell therapeutic applications and tissue engineering due to their high water content (Park and Lakes, 2007). Kaplan and Jiang demonstrated marked cytocompatibility of the silk hydrogel encapsulated with stem cells (Ding et al., 2017). Silk hydrogels are a good candidate materials for cell delivery because they can mimic the ECM (Ciocci et al., 2017). Based on the evidence that the silk hydrogels have good biocompatibility, excellent mechanical properties and controllable degradation, scientists have been used different cell lines have been used with silk in different formats such as fibers, hydrogel, nano particles, films or porous scaffolds (Bellas et al., 2015, Ding et al., 2017). Between all those forms silk hydrogel is an ideal cell carrier because it can faithfully recapitulate the ECM. Moreover, during silk hydrogel processing it is possible to include cells before gelation, which is critical for minimally invasive application into the stroke cavity. To encapsulate the cells and deliver them successfully, the hydrogel should be formed without any damage to the cells, including after injection through a needle, allowing even

cell distribution while protecting their viability and proliferative capacity (Ding et al., 2017).

In the present chapter, cell viability and biocompatibility assessment in silk hydrogels were carried out using MTT, AlamarBlue and live dead stain. Cellular distribution in self-assembling silk hydrogels of different concentrations was also assessed by histological examination when the samples gelled in a short (10 minutes) or a long (60 minutes) time. In addition, we examined the injectability of self-assembling silk hydrogels encapsulated with cells and the impact on cell viability.

4.2 Hypothesis and aim

The aim of this chapter was to assess the capacity and optimum concentration of self-assembling silk hydrogels for MSC expansion, self-renewal, survival and distribution as a step towards determining if self-assembling silk hydrogels can act as a MSC support matrix for stroke treatment.

4.3 Protocol

Cells were collected from the flask as previously described in section 2.1.1. Silk solution was sonicated as previously described in section 2.1.4 and maintained at a temperature between 30-37°C before C3H10T0.5 MSCs were encapsulated as detailed in section 2.1.13. The cell number used is

indicated in each section. Samples were loaded into 96 wells plate or into a 1 ml syringe.

4.4 Results

4.4.1 MTT assay produced unreliable results for assessing the cytocompatibilty of MSCs encapsulated in self-assembling silk hydrogel

The MTT assay is widely used to examine cell viability by monitoring the metabolic activity of mitochondria. Using NAD(P)H-dependent cellular oxidoreductase enzymes as an indicator of cell viability the tetrazolium substrate is converted into the water insoluble formazan (crystals) with a strong absorbance between 500 to 600 nm.

In the present study, MTT was added to the silk hydrogels, incubated for 5 hours and the excess media was subsequently removed and the silk hydrogels were left at 60°C overnight to dry. However, we found results using MTT to be unreliable as shown in Figure 4.1. These experiments were repeated another two times (n=3 each) and were also found to be equally unreliable, as some wells dried up after incubation at 60°C, while some wells needed more time at 60°C to evaporate the water. However when the plate was left longer, the silk hydrogels became ruined. Therefore our results using MTT were conflicting and lacking in accuracy.

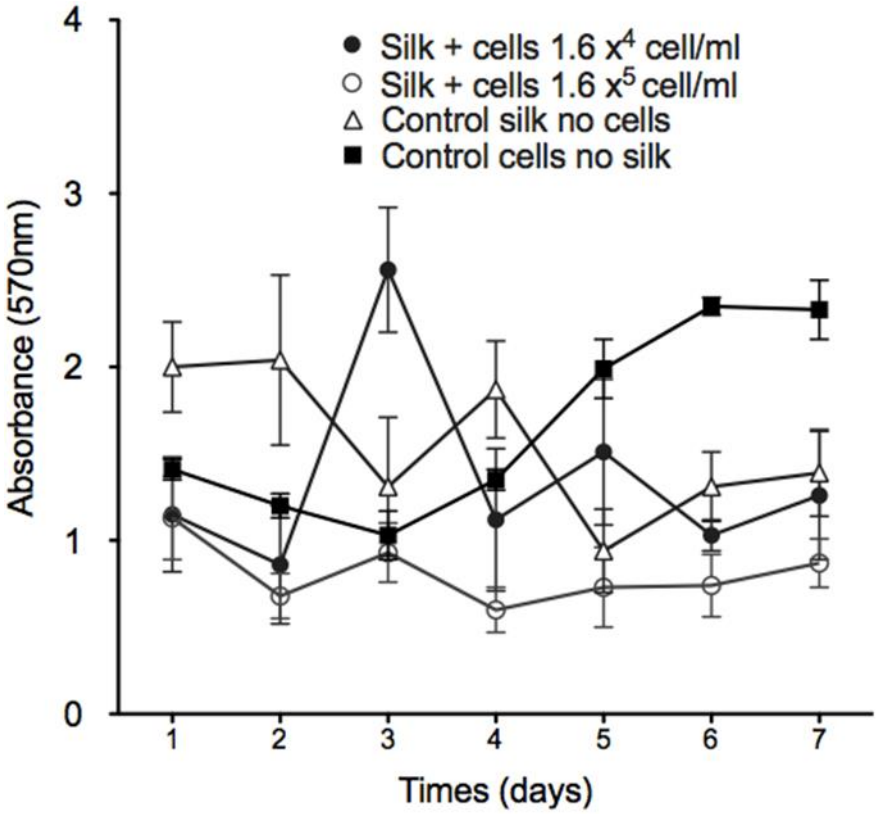

Figure 4.1 Viability of C3H10T0.5 cells encapsulated in 4% (w/v) silk hydrogel over 7 days using MTT. 16X10^3 cell/ml for low density and 16X10^4 cell/ml for high density and thickness of the mixture is 100 µl of the mixture (silk hydrogel encapsulated with MSC). Each value represents the mean ± SD, n=3

4.4.2 Self-assembling silk hydrogels exhibited excellent MSC cytocompatibility using AlamarBlue

After the unsatisfying results using MTT, we used AlamarBlue assay to quantify the cell viability and proliferation. AlamarBlue assay, unlike MTT, is direct with no need to remove the water, non toxic, slightly more sensitive than the MTT, easy and less time consuming (Hamid et al., 2004).

Another advantage of this assay against MTT, is that both cells and biomaterials can be conserved allowing multiple readings in the same sample at multiple time-points. We used $2X10^3$ cells/ml, $2X10^4$ cells/ml (Figure 4.2) and $5x10^5$ cells/ml (Figure 4.3) encapsulated in 100 µl of silk hydrogel. However there was no difference in fluorescence compared with the background fluorescence in the control silk only (no cells). Increasing the cell number to $4X10^6$ cells/ml (Figure 4.4) and reducing the silk volume (silk encapsulated with cells) to 50 µl allowed a difference to be observed between the fluorescence observed from the silk hydrogels with cells and the background fluorescence observed from control silk for the first 3 days after encapsulation (Figure 4.4).

By extending the time of encapsulation over 10 days, we observed that the viability of MSCs significantly decreased ($p<0.001$) in the first 4 days of encapsulation in silk hydrogels for all percentages. Thereafter MSC viability started to increase (Figure 4.5). Therefore monitoring time was extended over ~14 days and tested for the range of silk concentrations (2-4% w/v) and

again, observed a significant decrease ($p<0.001$) in the viability of MSCs in the first 3 days of encapsulation in silk hydrogels. Again, after 3 days, MSC viability significantly increased ($p<0.001$), showing good proliferation from day 3 (Figure 4.6) with the lower (2% w/v) concentration of silk hydrogel providing significantly better growth than the higher percentage. Therefore using $4X10^6$ cells/ml MSC in 50 µl, self-assembling silk hydrogels exhibited excellent MSC cytocompatibility over ~14 days, especially for 2% w/v silk concentration.

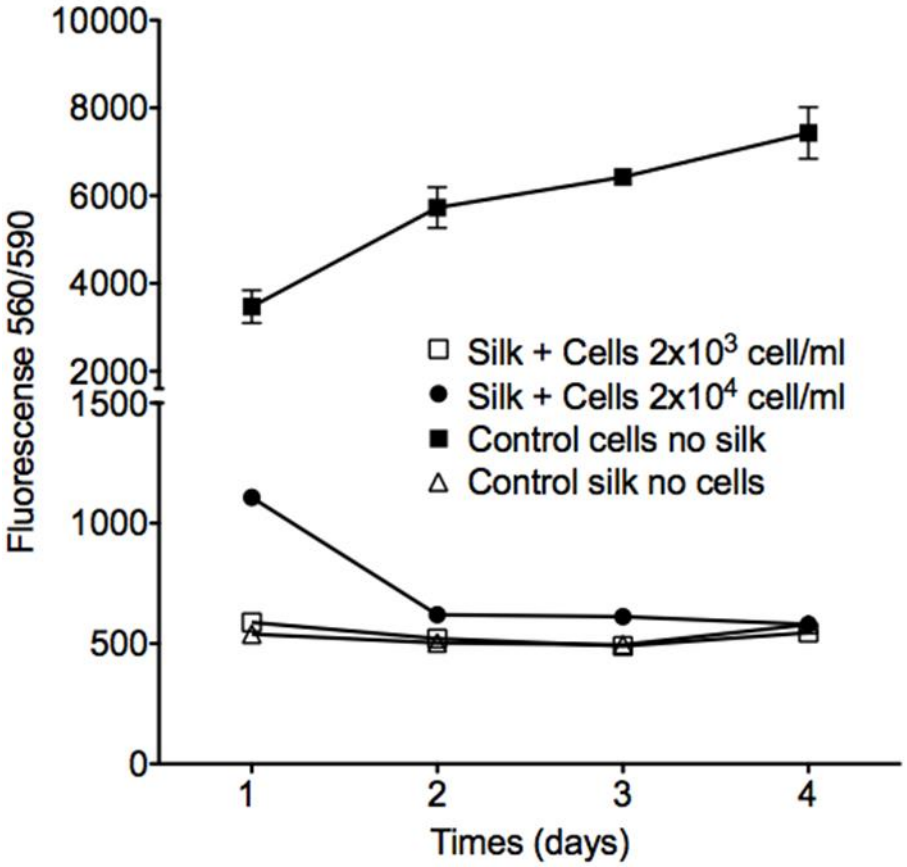

Figure 4.2 Viability of C3H10T0.5 cells encapsulated in 4% w/v silk hydrogel over 4 days using AlamarBlue. $2X10^3$ cell/ml for low density and $2X10^4$ cell/ml for high density and thickness of the mixture is 100 µl. Each value represents the mean ± SD, n=3

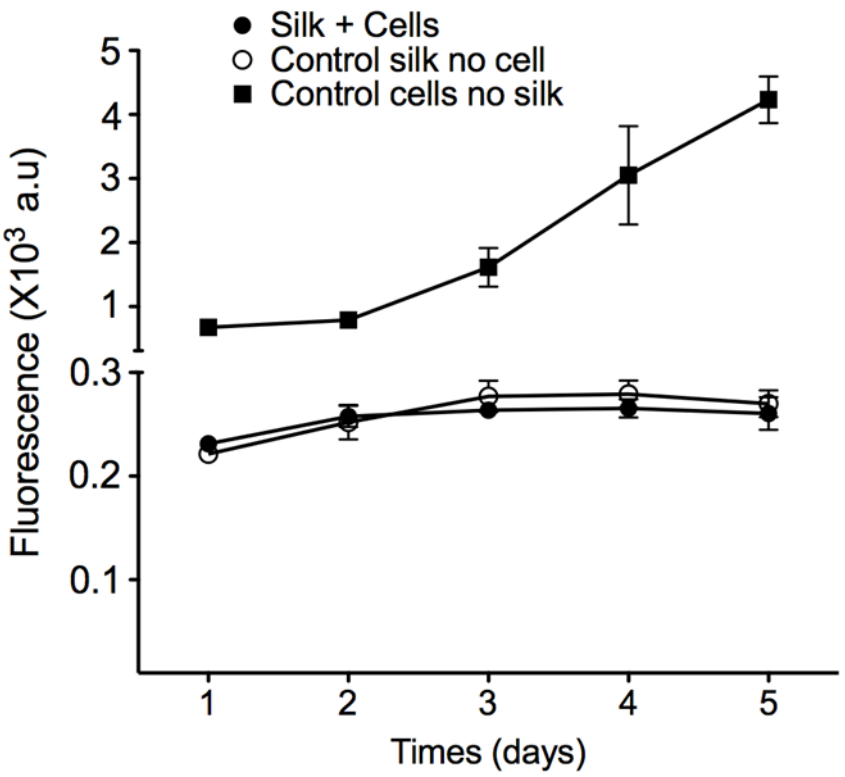

Figure 4.3 Viability of C3H10T0.5 cells encapsulated in 4% w/v silk hydrogel over 5 days using AlamarBlue. Cells density used was $5x10^3$ cell/ml and thickness of the mixture is 100 µl. There was no different between silk encapsulated with cells and control only silk which indicate there was no cells present in the silk. Each value represents the mean ± SD, n=3

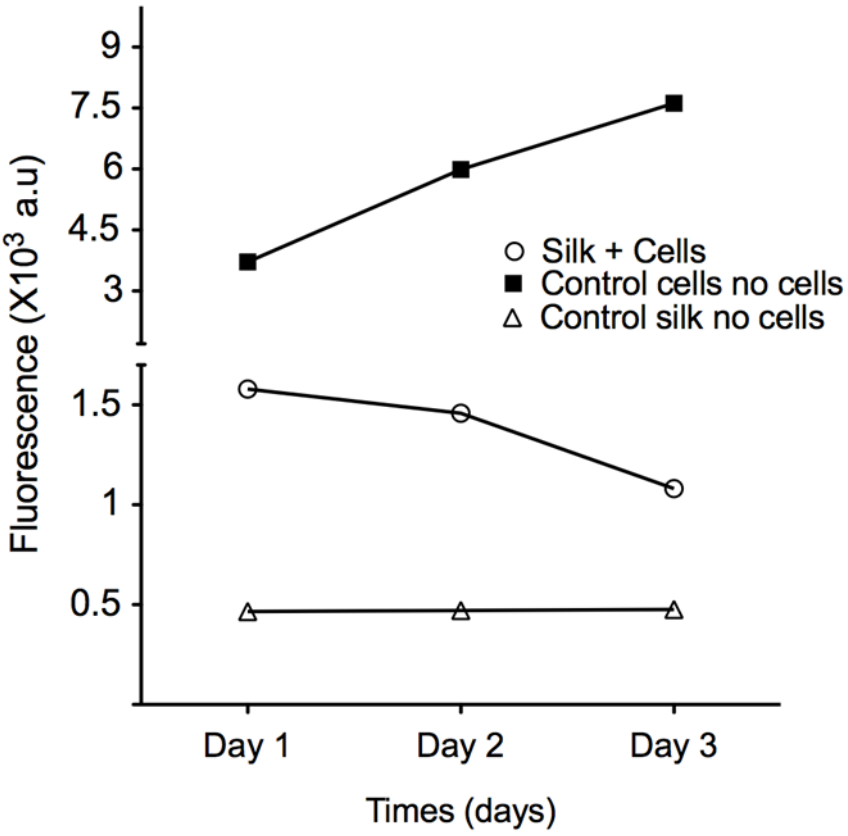

Figure 4.4 Viability of C3H10T0.5 cells encapsulated in 4% w/v silk hydrogel over 3 days using AlamarBlue. Cells density used was 4X10^6 cell/ml and thickness of the mixture is 50 µl. Each value represents the mean ± SD, n=3

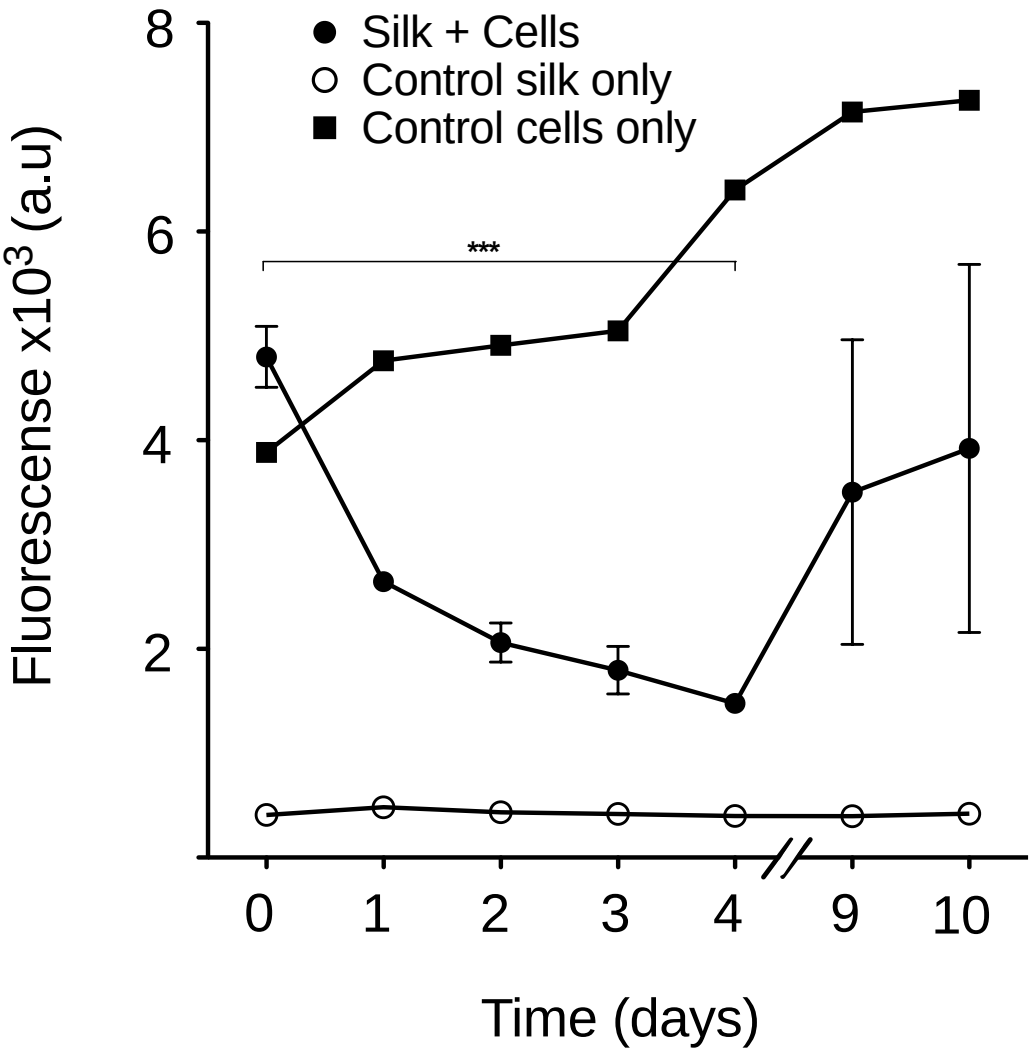

Figure 4.5 Viability of C3H10T0.5 cells encapsulated in 4% (w/v) silk hydrogel over 4 days then day 9 and 10, using AlamarBlue. Cells density used 4X10^6 cell/ml and thickness of the mixture is 50 µl. ***P< 0.001 Each value represents the mean ± SD, n=3

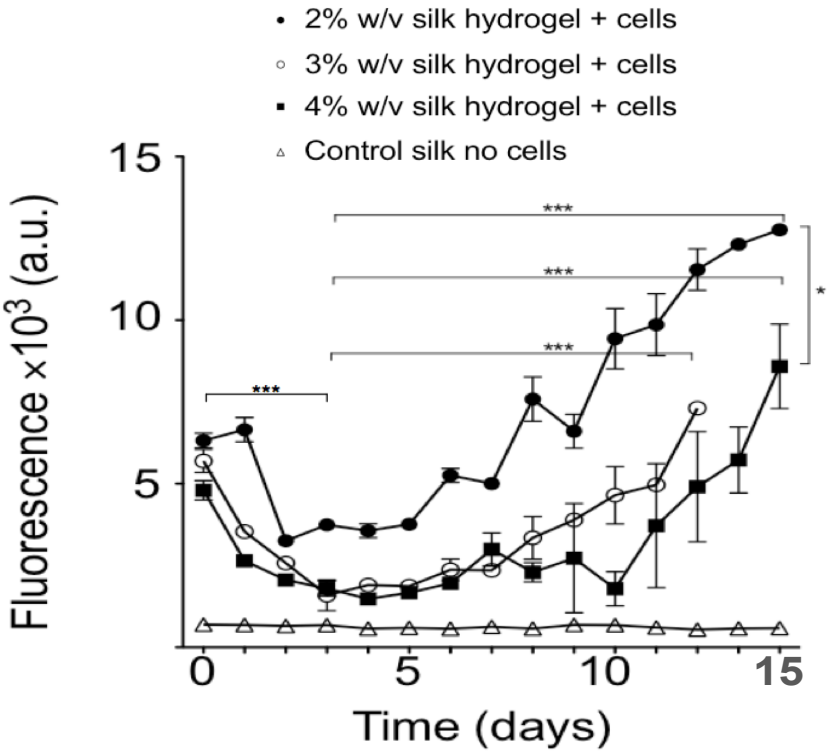

Figure 4.6 Viability of C3H10T0.5 4X10^6 cell/ml encapsulated in 2, 3 and 4% w/v silk hydrogel over 12-14 days using AlamarBlue. Cells density used was 4X10^6 cell/min 50 µl. *P< 0.05, ***P< 0.001 Each value represents the mean ± SD, n=3

4.4.3 Cell viability of MSCs in self-assembling silk hydrogels when injected in pre-gelled condition was better than post-gelled condition

For clinical translation, stereotaxic injections requires the smallest needle size possible to limit the damage to surrounding tissue. In the previous chapter, we showed that self-assembling silk hydrogels can be injected through 26-gauge needles in the pre gelled condition with good space conformity. The next step was to establish if cells encapsulated in the silk hydrogels would be damaged by injection through a needle due to shearing forces. By passing cells through a needle cells experience several of mechanical forces such as shear forces and extensional forces during injection, which could result in cell damage (Lam et al., 2014). In the present study we therefore studied the viability of cells when MSC/silk hydrogel constructs were injected through needle gauge size 21, 25 and 30, for 2-4% w/v silk hydrogels. We found that the viability of MSCs was significantly better when the MSC/silk hydrogel construct was injected in the pre gelled condition compared to post-gelled condition for 4% w/v silk hydrogels for all needle sizes (Figure 4.10). MSC viability was significantly better when the MSC/silk hydrogel construct was injected in the pre gelled condition compared to post gelled condition for 3% w/v silk hydrogels for 25 and 30 gauge needles. Finally, MSC viability was not significantly better when the MSC/silk hydrogel construct was injected in the pre gelled condition compared to post-gelled condition for 2% w/v silk hydrogels for any needle sizes though there was a trend for 30-gauge needle size only (Figure 4.10).

Therefore injection of MSC/silk hydrogel constructs in the pre gelled condition is better for cell viability than the post gelled condition.

The viability of cells injected through larges size of needle gauge demonstrated more cell viability compared to smaller sizes. In addition the viability of the cells when injected in the pre gelled condition was higher than the post gelled condition. Moreover, although not tested statistically, when the percentage of silk hydrogel deceased (2% w/v) the viability of cells was observed to be higher than higher percentages (4% w/v) possibly due to the elasticity and less stiff material which was confirmed in the experiment measuring the viability of the cells encapsulated in silk hydrogel using AlamarBlue.

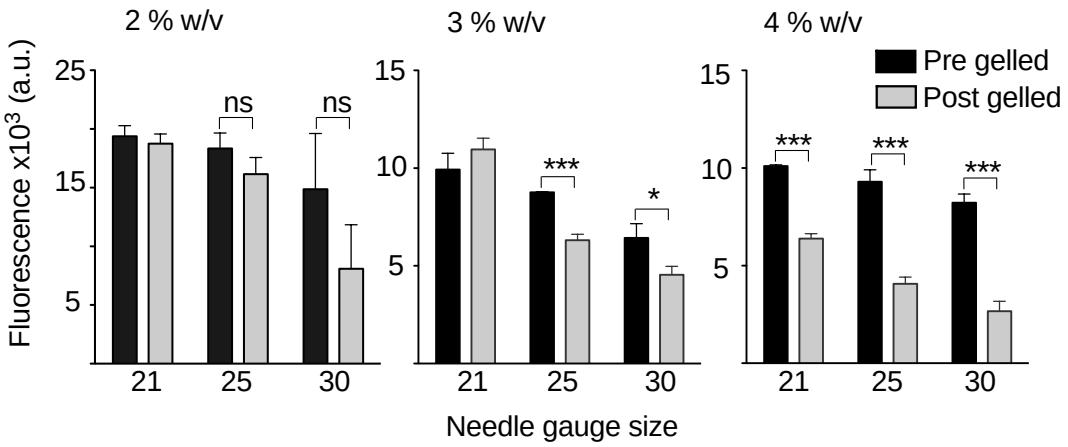

Figure 4.7 Pre gelled and post gelled 2, 3 and 4% w/v silk hydrogel encapsulated with MSCs. Viability of MSCs encapsulated in pre-gelled or post-gelled silk hydrogels and injected through 21, 25 and 30 gauge needles. Values represents the mean ± SD, n=3..

4.4.4 MSC distribution in self-assembling silk hydrogels was better if gelation occurred in less than 10 minutes.

Delivery of cells from the injected biomaterial requires even distribution of cells throughout the hydrogel. Therefore, the distribution of MSCs encapsulated in hydrogels were assessed using haematoxylin and eosin staining.

A more even number of cells at each level throughout the gel was observed in samples that gelled in less than 10 minutes after cell addition than in samples that gelled in 60 minutes after cells addition (Figure 4.11, left panel). In samples that gelled in less than 10 minutes there was no significant difference in the number of MSCs amongst the levels examined at all concentrations of silk hydrogel whereas, in samples that gelled in 60 minutes, a significantly greater number of cells were observed at the bottom of the gel (level 4) compared to the top of the gel (level 1) for all concentrations tested (Figure 4.11, right panel). Therefore 2-4% w/v self-assembling silk hydrogels supported even distribution within hydrogel samples that gelled in less than 10 minutes but not in 60 minutes for all concentrations tested.

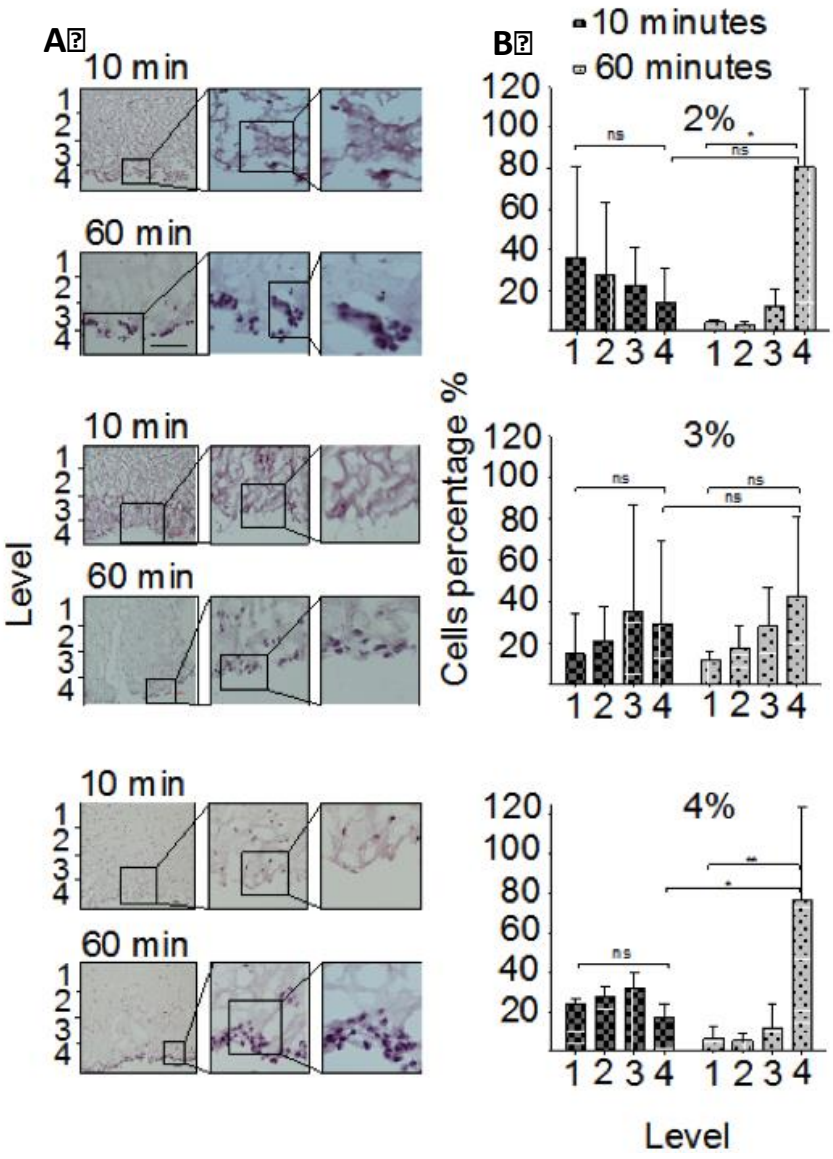

Figure 4.8 Impact of the solution-gel transition on cell distribution in self-assembling silk hydrogels. Cells were added at 10 minutes or 60 minutes before the completion of the solution-gel transition. (A) Histology images of MSCs encapsulated in silk hydrogels stained *in vitro* with H&E. (B) Images were segmented into 4 regions and the cell distribution was quantified. Note that for the 60 minute samples most of the cells had descended by gravity to the bottom of the hydrogel (level 4) (Values are average ± SD, n=3).

4.5 Discussion

The key findings of the present chapter are that it is possible to achieve uniform distribution and viability of MSCs in self-assembling silk hydrogels when gelled within 10 minutes of MSC encapsulation and when injected in the pre-gelled state. To reach this insight it was necessary to optimise and select a suitable assay to monitor cell viability. Therefore, in the first set of experiments, it was critical to establish the optimum number of MSCs for encapsulation. For these particular studies we opted to use 4% w/v silk hydrogel due to its quick completion of the solution-gel transition.

To track cell viability and proliferation, the MTT assay was selected initially. However, in our hands, the MTT assay was unreliable and inconsistent for our 3D hydrogel system. Because formazan is water insoluble there is the need to use DMSO to solubilise this metabolite to transfer the dissolved formazan to a measuring plate. However, residual water in the hydrogel sample as well as the presence of silk *per se* made it not possible, in our hands, to obtain reliable and quantitative data sets. In contrast AlamarBlue is a cell viability reagent that allows quantitative measurement of cell proliferation, without the need for DMSO due to its water solubility. Therefore, we tested many conditions and permutations to optimize the measurement of MSC proliferation in self-assembling silk hydrogels. We found that cell densities ranging $2 \times 10^3 - 2 \times 10^4$ cells/ml in 100 µl of self-assembling silk hydrogels were too few and may be associated with low fluorescent reading equivalent to background readings and/or the silk hydrogels were too thick

(100 µl), impeding the transfer of non-reduced forms of AlamarBlue reaching the cells as well as the transfer of reduced forms of AlamarBlue for detection. Furthermore, there were concerns regarding reading mass transport of nutrients to the cells (detailed above). We found that the optimal conditions to allow quantification of cell survival and proliferation were $4X10^6$/ml MSCs encapsulated in 50 µl of self-assembling silk hydrogel. This is in agreement with (Sun et al., 2016b).

The present results showed good cytocompatability of MSCs with self-assembling silk hydrogels. This is in agreement with other studies showing that silk exhibits good biocompatibility. Kaplan and colleagues, who showed that human bone marrow derived mesenchymal stem cells (hMSCs) were successfully incorporated into these silk fibroin hydrogels after sonication, followed by rapid gelation and sustained cell function (Wang et al., 2008). The ability of silk hydrogels to support cell survival and proliferation likely comes from the tunable, soft, and elastomeric properties of silk hydrogels (as shown in chapter 3). In addition, the high resilience and wide range of properties of silk hydrogels suggest that they could be useful for numerous of *in vitro* and *in vivo* applications

The cell survival after encapsulation was robust and capable of long-term (tested up to 14 days) proliferation and survival despite some cells losses during early incorporation. The reason for the initial decrease in cell viability up to day 5 is unclear. Silk hydrogels have a permeability that allows, in principle, the transfer of nutrients to feed the encapsulated cells and preserve

the viability after encapsulation. However, it is likely that a limited mass transport of nutrients and oxygen inside the hydrogels may be responsible for the initial decreased survival. This is supported by the observation that a reduction of the hydrogel volume from 100 µl to 50 µl improved cell viability as detailed above. Growth factors and other factors may be secreted by the MSCs (Partlow et al., 2014) over time after encapsulation in self-assembling silk hydrogels. This in turn may adapt the silk hydrogel to the needs of MSCs and thus providing a possible explanation for the increased viability and proliferation of encapsulated cells from day 5 onwards. An alternative approach may be the incorporation of exogenous growth factors or ECM proteins to promote cell adhesion and viability at earlier time points (e.g. at day 0). Further experiments would be required to establish if such an approach prevents the initial decrease in cell viability that we observed during the first 3 days of encapsulation.

Uniform cell distribution is critical for the delivery of cellular payloads from the injected biomaterial. Therefore, we evaluated the distribution of C3H10T0.5 in different percentages of silk hydrogels at different time point of gelation. In general, the cells encapsulated in silk hydrogel that gelled quickly (i.e. within 10 minutes) produced a uniform cell distribution. In contrast, the cells sank to the bottom of the gel when gelation time was prolonged for all concentrations of self-assembling silk hydrogels tested. Taken together with our previous experiment (conformity test section 3.4.8), we can conclude that the pre gelled condition is ideal to achieve excellent conformal fit however gelling within 10 minutes is ideal to achieve uniform cell addition; prerequisites to

translate these observations to a stroke cavity *in vivo*.

The present chapter showed the importance of careful consideration and optimisation of the administration protocol of cell suspensions according to cellular response and nature of the cells after injection. Several studies have been carried out to measure the effects of the injection process on cell functionality and viability during and after the injection through the needles (Amer et al., 2015). However, during the process of cell death, cells release cytotoxic agents that could affect viability of host cells or delivered cells. Hence, the viability of cells after transplantation is important (Agashi, 2010). Cells experience an increase in linear velocity when they pass through the needle because the inner diameter of the syringe is larger than that of the needle. This could lead to cell injury during the injection from the extensional force from the injection exposing the cells to shear stress (Amer et al., 2015).

In the present study, cells had greater viability when injected in the pre gelled condition versus post gelled condition. Therefore, if the cells remain in the syringe until gelation is completed, there is extensive cell loss after injection. Percentage of viable cells delivered decreased during the cell injection because of the shear stress, so, it was hypothesised that injection cells prior to the completion of the solution-gel transition will improve cell viability. Taken together with our previous results on space conformity and cell distribution, our results indicated that injections should be performed with self-assembling silk hydrogels in the pre gelled condition with the gelation occurring within 10 minutes after cell encapsulation.

In summary our results for the cell adhesion and proliferation indicate that either 2 or 3% w/v self-assembling silk hydrogels are optimum concentrations. However, in our previous chapter we found long solution-gel transition times for 2% w/v silk concentration precluding its use *in vivo*. Therefore, 3% w/v self-assembling silk hydrogels, that gelled within 10 min of MSC encapsulation and that were injected in the pre-gelled state were identified as optimal for MSC viability and distribution and as a promising cell delivery platform for CNS diseases.

CHAPTER 5. Characterisation of self-assembling silk hydrogels and MSC encapsulation in self-assembling silk hydrogels: space conforming and cell delivery and distribution *in vivo* after intracerebral delivery after stroke.

5.1 Introduction

Stem cells transplantation after stroke was shown to support recovery in pre-clinical models (Lemmens and Steinberg, 2013). However, translating cellular therapeutics to the clinic is hindered by loss of transplanted cells after the delivery. The success of cell therapy relies on the reliable and effective of viable cells to damaged area so they can generate the desired therapeutic effects. However, due to immunological attack and adhesive support that lead to poor survival of the cells when administered to the brain as a suspended form, one strategy is to use cells encapsulated in hydrogels that protect the transplanted cells from the mechanical forces experienced during syringe needle flow to increase the viability of the cells (Aguado et al., 2011, Nih et al., 2016).

Therefore, tissue engineering applications for brain repair is a promising strategy to aid repair of the injured brain. The hydrogel scaffolds function as an artificial environment to provide long-term support of endogenous and exogenous therapeutic cells seeded in the hydrogel and facilitate cell regeneration, attachment, growth, migration, differentiation and prevent

further damage to adjacent tissues (Howard et al., 2008). The three components: cells, carrier matrix (e.g. hydrogel) and signalling cues (physical properties) are usually combined for tissue engineering applications (Howard et al., 2008). For clinical translation of hydrogels for intracerebral administration, good space-conforming properties are required to avoid compressing against adjacent tissue which may exacerbate cellular injury (Massensini et al., 2015)**.** Our previous chapter (chapter 3) showed that self-assembling silk hydrogels exhibit good space conformity without swelling *in vitro*.

The present chapter study the translation of space conforming properties of self-assembling silk hydrogels *in vivo* after MCAO. Hydrogels have limited interfacial tension, which makes them suitable for good integration of payload after *in vivo* administration, reducing the barrier for delivery of payload at the host tissue-hydrogel interface (Fon et al, 2010). As mentioned above, cells injected into the brain, especially into a hostile environment such as the stroke cavity, can result in poor distribution of cells and poor survival after injection. Therefore, to achieve good retention and distribution within the stroke cavity, require structural support that may mimic their natural microenvironmental niche is required (Uludag et al., 2000). Silk hydrogels can be implanted to provide a temporary structure to support 3D formation, to facilitate cellular proliferation, and promote cell to cell interactions and cell migration (Ciocci et al., 2017). However, due to access to the skull and brain requiring invasive delivery, the direct delivery of cells encapsulated in silk hydrogel into the brain after stroke should be controlled to avoid any further

damage to the adjacent tissue (Lemmens and Steinberg, 2013). In chapter 4, we have shown the promising biocompatibility and injectability of self-assembling silk hydrogels that allow a uniform cell distribution *in vitro* when injected in the pre gelled condition. Therefore, this chapter aims to establish if self-assembling silk hydrogels provide a structure for good space conformity and uniform cell distribution *in vivo* after intracerebral delivery in stroke mice.

5.2 Aims

In this chapter, the aims were two-fold:

Study 1: to establish space conformity *in vivo* by injection of silk hydrogel into the brain after stroke.

Study 2: to establish if silk hydrogels support cell distribution *in vivo* by injection of silk hydrogel/MSC constructs into the brain after stroke.

5.3 Protocol

All experiments were carried out on 10-12 week old male C57BL/6 bred in-house, weighing 25–30 g and were prepared for surgery as described in sections 2.2.2 and 2.2.3. Mice underwent MCAO in two separate studies. In study 1, we investigated the conformity properties of silk hydrogels after MCAO using the electrocoagulation model (section 2.2.3). In study 2, we investigated whether silk hydrogels improve the distribution of cells injected after MCAO using the intraluminal thread model (section 2.2.4). All animals

underwent stereotaxic surgery for *in vivo* transplantation of C3H10T0.5 cells and/or silk hydrogels (section 2.2.5). The size of the needle bore should be as small as possible for intracerebral injection to minimise any damage to local tissue due to the needle tract (Bible et al., 2009). In our previous chapters we showed that self-assembling silk hydrogels can be injected through needles in the pre gelled condition (chapter 3), without significant loss of MSCs when injected in pre gelled state (chapter 4). Therefore, the present study injected self-assembling silk hydrogels in the pre gelled condition through a 26-gauge needle *in vivo*. Thereafter brains were sectioned and H&E stained (section 2.1.19).

5.4 Results:

5.4.1 Study 1: *in vivo* injection of silk hydrogel into the brain after stroke to establish space conformity

Given that the electrocoagulation model induces a stroke cavity in a consistent location relative to other MCAO models, this model was deemed most appropriate for assessing space conformity of silk hydrogels in the stroke cavity *in vivo*. For this experiment, approximately 1 month post-pMCAO, the animal underwent stereotaxic surgery using the stereotaxic coordinates +1.5 mm anterior/posterior, +2.5 mm medial/lateral and 1 mm ventral relative to bregma for injection of 4 µl of 4% w/v silk hydrogel and allowed to recover for 7 days before termination.

However, on injection, the silk hydrogel came back out of the needle tract. As can be observed from (figure 5.1), no silk hydrogel was observed at the site of injection. This was deemed to be due to the increase in intracranial pressure caused by injection of biomaterials causing material to seep out as described in previous studies (Massensini et al., 2015).

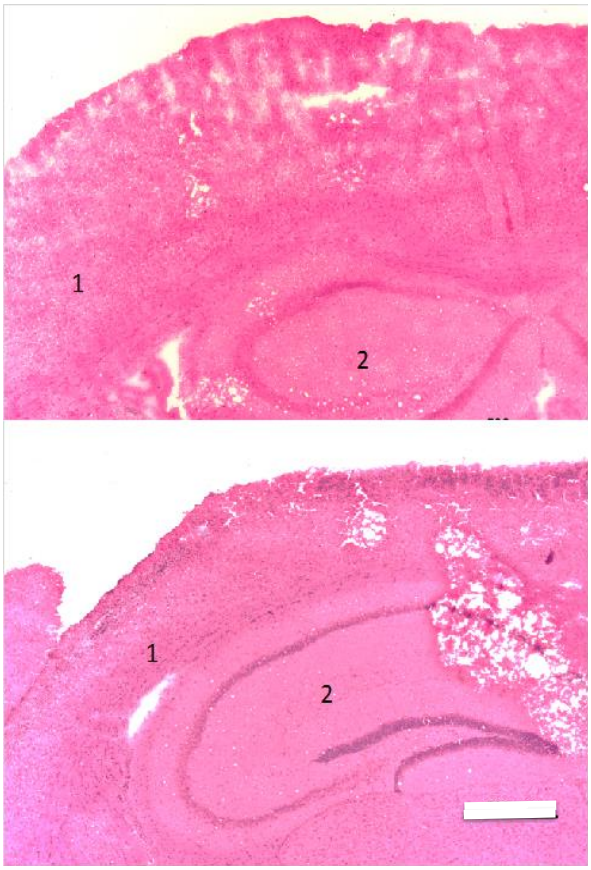

Figure 5.1 Space conformity of self-assembling silk hydrogels in the stroked mouse brain. Representative images of coronal H&E stained sections. 1) cortex and 2) hippocampus. No silk hydrogel present in the brain sections. Scale bar 500 µm.

In order to prevent an increase in intracranial pressure with the injection of the hydrogels, we adopted the approach described by (Massensini et al., 2015) of draining the extracellular fluid from the cavity prior to injection of the biomaterial. Approximately 2 months after pMCAO, under the same anaesthesia as the stereotaxic surgery, an additional burr hole was created at -0.5mm anterior/posterior, 2.5 mm medial/lateral relative to the Bregma with the intention of this acting to drain the extracellular fluid from the cavity. A 32-gauge needle was inserted into the burr hole at 1.5 mm ventral to the brain surface and, initially, no fluids were displaced. A second burr hole was created a further 1 mm posteriorally and a needle inserted. A small volume of fluid leaked from this hole upon insertion of the needle. Thereafter, 5 µl of 4% w/v self-assembling silk hydr^{o}gel was injected 1.5 mm ventrally over 5 minutes (Figure 5.2). The needle was left in place for a further 5 minutes before being retracted slowly. The mouse was left under anaesthesia for an additional 10 minutes before termination.

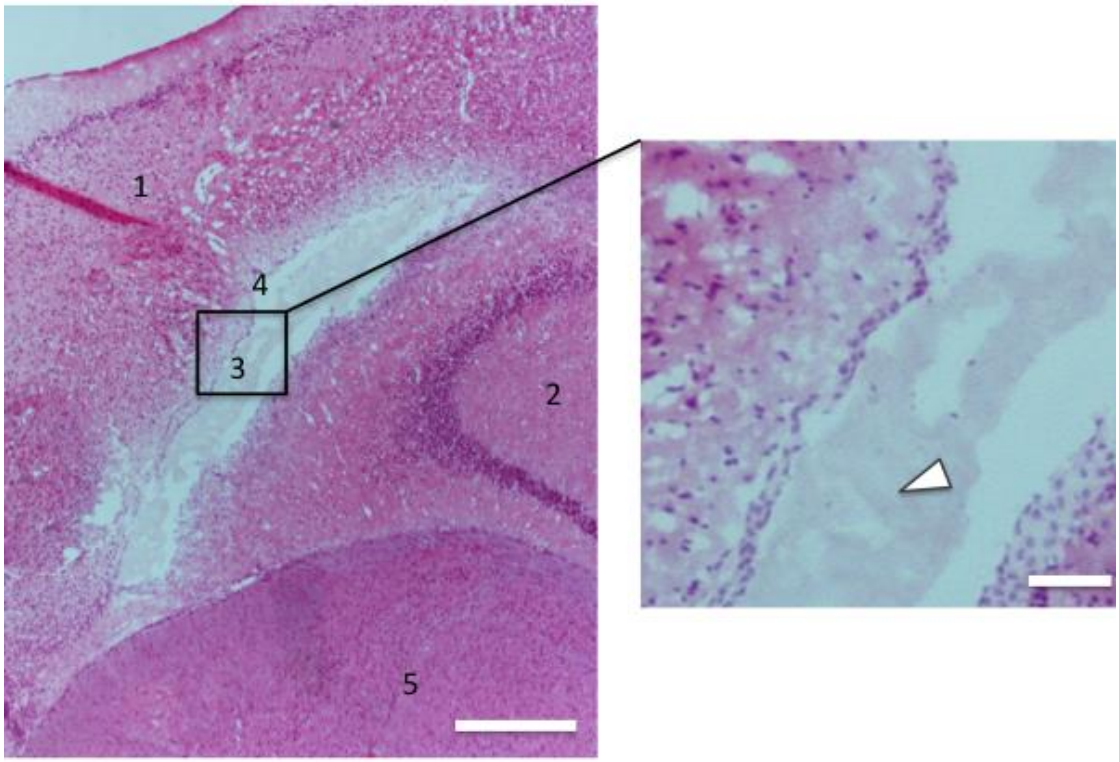

Figure 5.2 Space conformity of self-assembling silk hydrogels in the stroked mouse brain. Mice were subjected to MCAO and treated with 3% w/v self-assembling silk hydrogel. Mouse with a minor stroke (i.e. absence of stroke cavity) on the left hand panel: 1) cortex 2) hippocampus 3) self-assembling silk hydrogel (3% w/v) accumulated in the 4) lateral ventricle cavity 5) thalamus and on the right hand panel: the arrow showing silk hydrogel. Scale bar 500 μm for left panel and 100 μm for right panel.

The brain sections magnified in Figure 5.2 shows the presence and structure of the silk hydrogel graft (visualised by light pink eosin staining). However there was no indication of hydrogel in the stroke cavity, rather it appeared that the self-assembling silk hydrogels was present in the lateral ventricle cavity. The self-assembling silk hydrogel filled the ventricle and was evenly spread throughout the entire space. Whilst this result does indicate excellent space conformity *in vivo*, this experiment has not successfully allowed the assessment of space conformity in the stroke cavity, the objective of the present study.

Given that accurately targeting the stroke cavity of mouse brain by intracerebral injection of hydrogel, in our hands, was proven to be problematic, an alternative approach is to use magnetic resonance imaging (MRI) (Nicholls et al., 2016) to assess the presence, location, volume of damaged tissue, determine amount of silk hydrogel to be injected and prevent extra damage to additive tissue. However this approach is limited by the availability of specialised equipment and staff, and therefore we adopted the approach of applying silk directly to the brain surface at the location of the stroke cavity. Animals underwent MCAO by electrocoagulation (section 2.2.3) followed by topical application of self-assembling silk hydrogels. Approximately 4 months post-MCAO, as topical application was a new protocol not established in our lab, the mice (n=2) were terminated in advance of the rest of the procedure. After termination the mice were placed on a heat pad to maintain the temperature 37°C. Next, an incision was made around 1.5 cm long between the ears and the skull was exposed. A dental

drill was used to thin the skull above the stroke cavity which was then removed gently to avoid brain tissues damage. Next, the stroke cavity was clearly exposed. Then, 3% w/v silk hydrogel was sonicated for 30 seconds at 30% amplitude and before the sol-gel transition, 10 µl or 20 µl were applied topically onto the surface of the cavity and left for one hour to completely solidify. The brain was then removed and frozen with isopentane at -42°C and stained with H&E.

The brain sections (Figure 5.3) showed no presence of the silk hydrogel. This was deemed to be because the volume (10 µl) applied topically was too small. Therefore the procedure was repeated using 20 µl of silk hydrogel. From the images in Figure 5.4, silk hydrogel can be observed on the surface of the brain at the location of the MCAO cavity and as a layer to cover the stroke cavity. However the presence of the hydrogel did not seem stable, possibly due to removal or disintegration during processing of the tissue. Nevertheless, this approach of topical application of the silk hydrogel was not considered to be consistent enough for pursuing and therefore the approach of intracerebral injection of the silk hydrogels was adopted to the next study (study 2).

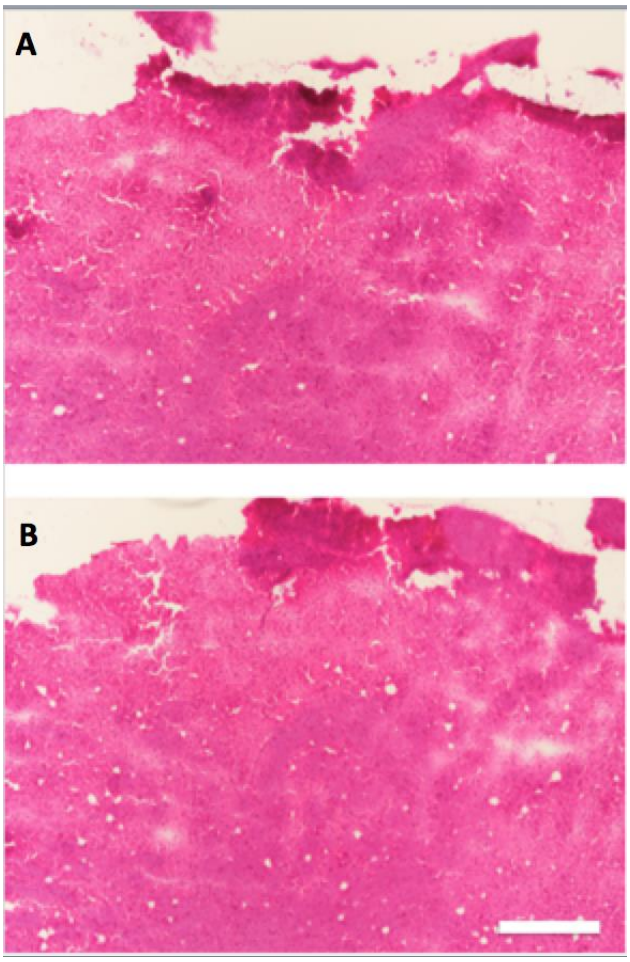

Figure 5.3 Self-assembling silk hydrogels in the stroked mouse brain. Mice were subjected to MCAO and treated with 3% w/v self-assembling silk hydrogel. Representative images of adjacent H&E stained sections (A and B) from an animal that received topical application of 10 µl of 3% w/v silk hydrogel to the MCAO cavity area, no presence of the silk hydrogel. Scale bar 500 µm.

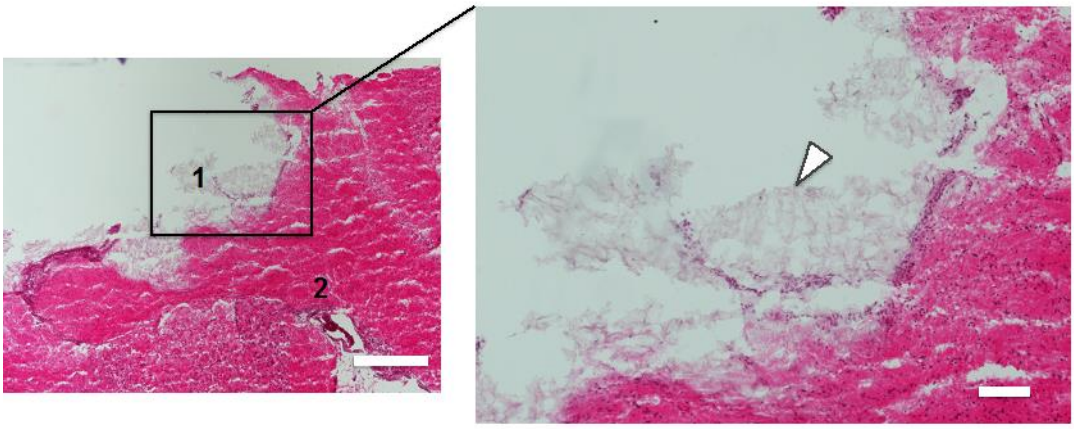

Figure 5.4 Self-assembling silk hydrogels in the stroked mouse brain. Mice were subjected to MCAO and treated with 3% w/v self-assembling silk hydrogel. Representative images of H&E stained section from an animal that received topical application of 20 µl of 3% w/v silk hydrogel to the MCAO cavity area. Boxed area zoom showing the tissue-silk hydrogel interface, the arrow indicating the presence of the silk hydrogel. Scale bar 500 µm for the left panel and 100 µm for the right panel.

5.4.2 Study 2: *in vivo* injection silk hydrogel/MSC constructs into the brain after stroke to establish if silk hydrogels support cell distribution

In this set of experiments, the cells were pre-labelled with CM-Dil cell tracker (see section 2.1.18) to enable tracking the cells in tissue sections using fluorescent microscopy, after mice underwent transient MCAO using ILT (section 2.2.4) Initially, animals were injected CM-Dil-labelled C3H10T0.5 cells alone (no hydrogels) and Figure 5.5 shows distribution of cells after injection throughout different coronal sections.

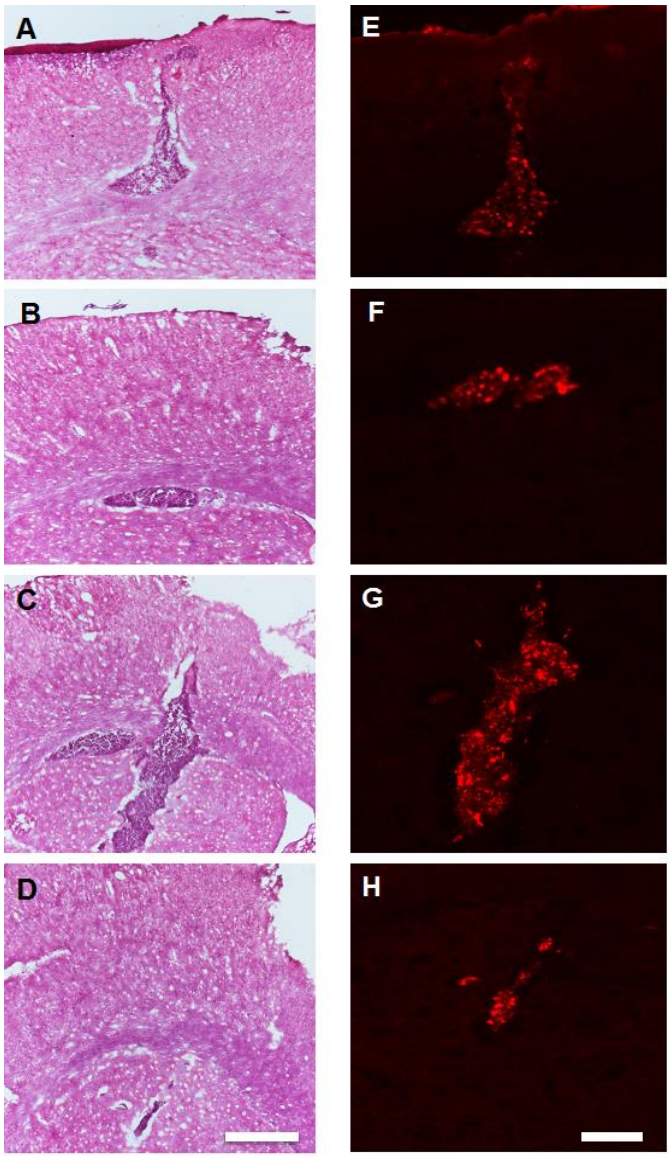

Figure 5.5 Microscopic images of distribution of MSCs delivered to the stroked mouse brain. Representative images of adjacent coronal H&E stained sections images (A-D) by light microscope and fluorescent images of CellTracker CM-DiI labelled MSCs (E-H) visualised by epi microscope. A 5 µl containing 20,000 cells, injected to the stroke brain. The cells look like randomly distributed not in consistent shape.Scale bars of H&E images 500 µm and 100 µm for fluorescent images by epi microscope.

In the next set of pilot experiments, animals were injected with self-assembling silk hydrogels loaded with CM-DiI-labelled C3H10T0.5 cells, resulting in a more even cell distribution at the injection site (Figure 5.6).

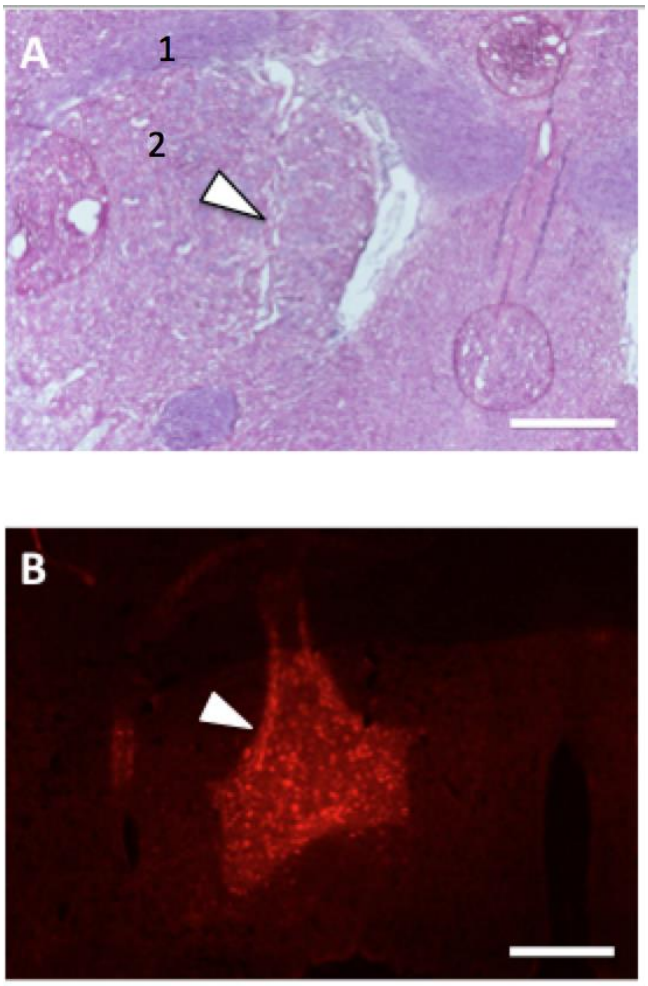

Figure 5.6 Microscopic images of C3H10T0.5 encapsulated in silk hydrogel 3% w/v. Cells were pre-labelled with cells tracker CM-Dil 5 µl contain 20,000 cells, injected to the stroke brain. (A) Representative image of H&E stained section with epi microscope, 1) corpus collasum 2) striatum and the arrow indicates to the needle tract and the presence of the hydrogel. (B) Representative image was taken by confocal microscope the arrow showing C3H10T0.5 encapsulated in silk hydrogel in consistent shape. Scale bar 500 µm for the top panel and 100 µm for the lower panel.

5.5 Discussion

MSC administration has been shown to support neurological functional recovery despite the side effects that occurred to some stroke patients such as seizures, subdural hematomas and syncopal events after injection of MSC (Fernandez-Garcia et al., 2016). The effective transplantation window of MSC for stroke patient's range from 30 minutes to 6 weeks since the cerebral infarction occurred (Zhang et al., 2017). For the therapeutic use of MSC in the stroke setting, previous studies showed that intravenously injected MSC are likely to lodge and arrest or primarily locate to the lung, spleen and liver with only 1% of the injected cells reaching the brain (Zhang et al., 2017). Therefore there is an urgent need to develop a hydrogel system, which is suitable for minimally invasive delivery via direct stereotactic injection into the brain. The material of such a system needs to be biocompatible, biodegradable and capable to deliver the MSC to the stroke cavity. We demonstrated in our previous chapters that the silk hydrogel are readily manufactured and can encapsulate cells *in vitro*. The key findings of the present chapter are that self-assembling silk hydrogels can be injected into the brain after stroke and pilot experiments indicate that they provide good space conformity; and that self-assembling silk hydrogels provide structure for uniform cell distribution *in vivo*.

In pilot experiments we tested three conditions. We started with injections of only silk hydrogel to the stroke brain in an attempt to fill the stroke cavity and thereby assess conformity and space filling capacities of self-assembling silk

hydrogels. After direct injection of the silk hydrogels, we found that some of the silk hydrogels seeped out. Therefore, we then used an injection-drainage approach to displace the extracellular fluid as previously described (Massensini et al., 2015). By this approach we avoided the increase in intracranial pressure and silk hydrogel and extracellular fluid mixing. This approach showed excellent space conforming capabilities of self-assembling silk hydrogels by filling the ventricle, however the target was to fill the stroke cavity. One solution was the use of targeting delivery to the cavity using MRI (Nicholls et al., 2016), requiring specialised staff and facilities and another approach was to topically apply the silk hydrogel to the cavity. The latter approach has the advantage of no needles being inserted into the brain and avoids any extra associated damage to the brain. In that set of experiments, however, unfortunately the silk hydrogel did not remain (intact) on the brain surface during sample manipulation. This could be due different reasons including inadequate adhesion to the brain tissue. This in turn directly impacted performance but also ease of sample preparation for histological analysis. For example, the steps of the brain removal and fixation may have caused the hydrogel to tear away from the rest of the brain. Therefore the approach of intracerebral injection was adopted for the injection of hydrogel/MSC scaffolds.

After the successful injection of silk hydrogel into the brain we first injected only C3H10T0.5 that was pre-labelled with cell tracker CM-Dill to monitor cells distribution. The injection process was successful with minimal damage to the brain but the cells were diffused randomly over a big area and regions

without being localised to the target site. Next, we injected silk hydrogel encapsulated with pre-labelled C3H10T0.5 into the brain. Our pilot results indicate that the cells remained within the silk hydrogel and exhibited an even distribution indicating that the silk hydrogels appeared to be provide a structural support for the retention of cells *in vivo.*

In summary the pilot experiments in this chapter indicate that self-assembling silk hydrogels have the potential to serve as a valuable local delivery platform of MSCs to the brain and provides the foundation for the development of silk-based hydrogels for stroke and brain regeneration.

CHAPTER 6. Conclusion and summary

Stroke is a leading cause of death and primary cause of disability in the majority of developed countries. Ischaemic stroke is the most predominant class of stroke that induces the acute neuroinflammation that leads to brain damage (Stonesifer et al., 2017). Stem cells are ideal candidates for potential clinical application in regenerative cellular-based therapies and tissue engineering strategies against a wide range of clinically important disorders. MSCs are garnering significant interest as they are broadly accessible and avoid the ethical concerns of the use of embryonic stem cells for example. The approach of using hydrogels particularly injectable hydrogel for MSC delivery to the CNS is rapidly expanding in regenerative medicine.

In the first part of this thesis, we studied the effects of sonication on silk solution and the physical gelation kinetics was evaluated by monitoring light scattering. There were many ways to sol-gel transition but we used the sonication due to many advantages such as: it is controllable and has minimum harmful environment on the cells. The stiffness was assessed to mimic the brain stiffness and for cell proliferation and viability. Moreover, silk swelling was tested and there was no swelling in the presence of liquid, which is desired to avoid compression against adjacent tissues. The overall solution-gel kinetics were concentration dependent, higher silk concentration form hydrogels faster and mechanically stable. Secondary structure analysis by FTIR and CD showed that these nanocrystallites were β-sheets and thus represented the points of physical crosslinking within the hydrogel. The

observed changes in secondary structure and the solution-gel transition were in good agreement with those reported in previous studies. Self-assembling silk hydrogels can be fine-tuned to achieve uniform distribution and space conformity *in vivo and in vitro* when it is injected in pre gelled condition.

In the second part, C3H10T0.5 were encapsulated in silk hydrogel to evaluate the suitability of these gels as an *in vitro* cell culture platform. Cells were encapsulated in silk hydrogel pre gelled for two weeks. The viability in the first 3 days was decreased but subsequently the cells started to proliferate up to day 14. Delivery of the cells requires a sustained cell viability and efficient cell distribution. We found that C3H10T0.5 encapsulated in silk hydrogels that gelled within 10 minutes showed excellent cell distribution throughout the gel, when compared to longer solution-gel transition times where gravity resulted in C3H10T0.5 settling. Shear stress also affected on cells viability, as expected, cell viability was higher following injection from wider needles than from narrower needles.

In the third part, silk was injected into the post-stroke brain, trying to fill the stroke cavity and assess the performance and conformity. Then, only tracked cells were injected and the cells diffused randomly in a large area and to multiple regions. Lastly, C3H10T0.5 encapsulated in silk hydrogel and were injected into the brain. The cells remained in a confined area and distributed very well within the silk hydrogel. In summary, the present chapter has proven that self-assembling silk hydrogels have potential to serve as a valuable local delivery platform of C3H10T0.5 to the brain and provides the

foundation for the development of silk-based hydrogels for stroke and brain regeneration. The unique structure, biocompatibility, controllable degradation, ease of sterilization, diversity in morphologies, thermal stability and options for genetic engineering, all make it extremely promising for many clinical and biomedical functions.

Future plan

Studies in this investigation have examined several aspects of the ability of self-assembling silk hydrogel to encapsulate C3H10T0.5, In particular we found good distribution, the ability to proliferate and amenability to intracerebral injection. The next step, outwith the scope of this thesis, would be to establish if self-assembling silk hydrogels provide transplanted cells with the necessary cues to perform their intended restorative functions such as trophic factor production (Lindvall and Kokaia, 2010, Wang et al., 2014). There is an indication that self-assembling silk hydrogels would promote beneficial secretions from MSCs through our data showing increased proliferation after day 3 of encapsulation. Future studies should be performed to explore the secretory behaviour of MSCs encapsulated in self-assembling silk hydrogels that leads to the initial decrease in viability observed in the first three days after encapsulation. This should then be extended to monitor the subsequent cellular proliferation beyond this time point. Given that the aqueous processing of the silk hydrogel enables the inclusion of biological molecules (e.g. growth factors) during the hydrogel manufacture, knowing the biofactors secreted from MSCs during the proliferative stage would all us to

incorporate these biofactors to promote cell adhesion and viability at earlier time points (e.g. at day 0). It would also be of interest to establish when the proliferation would stop and when the silk hydrogel starts to degrade and how this compares to secretions and degradation in the *in vivo* stroke environment.

Several additional areas would also be important to study, such as using MRI to determine the exact location of the lesion to allow precise injection into the lesion cavity. Thereafter, further studies should determine the best time of administration after stroke and the optimum volume and dose of silk and cells. In addition, given that substrate elasticity and surface topography (explored in Chapter 3) also direct stem cell lineage commitment (Vining and Mooney, 2017, Dalby et al., 2014), future studies are required to establish differentiation phenotypes of MSCs encapsulated in hydrogels over time *in vitro* as well as in the *in vivo* stroke brain. The next step towards proving the potential use of self-assembling silk hydrogels for improving cell-based therapy for stroke would be to establish if self-assembling silk hydrogels provide functional support for the MSCs by improving their capacity to promote brain repair.

Although much of the data generated throughout this study is promising, further verification of certain aspects and continued investigation, as detailed above, would add significant impetus to these findings and facilitate the generation of novel cell delivery.

REFERENCES

Acosta, S. A., Tajiri, N., Hoover, J., Kaneko, Y. & Borlongan, C. V. 2015. Intravenous Bone Marrow Stem Cell Grafts Preferentially Migrate to Spleen and Abrogate Chronic Inflammation in Stroke. *Stroke,* 46**,** 2616-27.

Adil, M. M., Vazin, T., Ananthanarayanan, B., Rodrigues, G. M., Rao, A. T., Kulkarni, R. U., Miller, E. W., Kumar, S. & Schaffer, D. V. 2017. Engineered hydrogels increase the post-transplantation survival of encapsulated hESC-derived midbrain dopaminergic neurons. *Biomaterials,* 136**,** 1-11.

Agashi, K. 2010. *The analysis of cell fate post-ejection through parenteral devices and the development of systems that aid the transportation of cell therapy products.* University of Nottingham.

Aguado, B. A., Mulyasasmita, W., Su, J., Lampe, K. J. & Heilshorn, S. C. 2011. Improving viability of stem cells during syringe needle flow through the design of hydrogel cell carriers. *Tissue Engineering Part A,* 18**,** 806-815.

Al-Nasiry, S., Geusens, N., Hanssens, M., Luyten, C. & Pijnenborg, R. 2007. The use of AlamarBlue assay for quantitative analysis of viability, migration and invasion of choriocarcinoma cells. *Human reproduction,* 22**,** 1304-1309.

Allen, A. B., Gazit, Z., Su, S., Stevens, H. Y. & Guldberg, R. E. 2014. In vivo bioluminescent tracking of mesenchymal stem cells within large hydrogel constructs. *Tissue Eng Part C Methods,* 20**,** 806-16.

Amer, M. H., White, L. J. & Shakesheff, K. M. 2015. The effect of injection using narrow-bore needles on mammalian cells: administration and formulation considerations for cell therapies. *Journal of Pharmacy and Pharmacology,* 67**,** 640-650.

Aranha, M. M., Santos, D. M., Sola, S., Steer, C. J. & Rodrigues, C. M. 2011. miR-34a regulates mouse neural stem cell differentiation. *PLoS One,* 6**,** e21396.

Bai, S., Zhang, W., Lu, Q., Ma, Q., Kaplan, D. L. & Zhu, H. 2014. Silk Nanofiber Hydrogels with Tunable Modulus to Regulate Nerve Stem Cell Fate. *J Mater Chem B,* 2**,** 6590-6600.

Bellas, E., Lo, T. J., Fournier, E. P., Brown, J. E., Abbott, R. D., Gil, E. S., Marra, K. G., Rubin, J. P., Leisk, G. G. & Kaplan, D. L. 2015. Injectable silk foams for soft tissue regeneration. *Advanced healthcare materials,* 4**,** 452-459.

Bhasin, A., Srivastava, M. V., Mohanty, S., Bhatia, R., Kumaran, S. S. & Bose, S. 2013. Stem cell therapy: a clinical trial of stroke. *Clin Neurol Neurosurg,* 115**,** 1003-8.

Bible, E., Chau, D. Y., Alexander, M. R., Price, J., Shakesheff, K. M. & Modo, M. 2009. Attachment of stem cells to scaffold particles for intra-cerebral transplantation. *Nature protocols,* 4**,** 1440.

Bouten, C., Dankers, P., Driessen-Mol, A., Pedron, S., Brizard, A. & Baaijens, F. 2011. Substrates for cardiovascular tissue engineering. *Advanced drug delivery reviews,* 63**,** 221-241.

Burdick, J. A., Mauck, R. L., Gorman, J. H., 3rd & Gorman, R. C. 2013. Acellular biomaterials: an evolving alternative to cell-based therapies. *Sci Transl Med,* 5**,** 176ps4.

Cao, Y. & Wang, B. 2009. Biodegradation of silk biomaterials. *International journal of molecular sciences,* 10**,** 1514-1524.

Cheng, Y., Chen, M.-H., Chang, W.-H., Huang, M.-Y. & Wang, T.-W. 2013. Neural stem cells encapsulated in a functionalized self-assembling peptide hydrogel for brain tissue engineering. *Biomaterials,* 34**,** 2005-2016.

Ciocci, M., Cacciotti, I., Seliktar, D. & Melino, S. 2017. Injectable silk fibroin hydrogels functionalized with microspheres as adult stem cells-carrier systems. *International journal of biological macromolecules*.

Dailey, T., Metcalf, C., Mosley, Y. I., Sullivan, R., Shinozuka, K., Tajiri, N., Pabon, M., Acosta, S., Kaneko, Y., Van Loveren, H. & Borlongan, C. V. 2013. An Update on Translating Stem Cell Therapy for Stroke from Bench to Bedside. *J Clin Med,* 2**,** 220-241.

Dalby, M. J., Gadegaard, N. & Oreffo, R. O. 2014. Harnessing nanotopography and integrin–matrix interactions to influence stem cell fate. *Nature materials,* 13**,** 558.

Darnell, M. & Mooney, D. J. 2017. Leveraging advances in biology to design biomaterials. *Nature materials,* 16**,** 1178.

Diez-Tejedor, E., Gutierrez-Fernandez, M., Martinez-Sanchez, P., Rodriguez-Frutos, B., Ruiz-Ares, G., Lara, M. L. & Gimeno, B. F. 2014. Reparative therapy for acute ischemic stroke with allogeneic mesenchymal stem cells from adipose tissue: a safety assessment: a phase II randomized, double-blind, placebo-controlled, single-center, pilot clinical trial. *J Stroke Cerebrovasc Dis,* 23**,** 2694-700.

Ding, X., Yang, G., Zhang, W., Li, G., Lin, S., Kaplan, D. L. & Jiang, X. 2017. Increased stem cells delivered using a silk gel/scaffold complex for enhanced bone regeneration. *Scientific Reports,* 7**,** 2175.

Discher, D. E., Mooney, D. J. & Zandstra, P. W. 2009. Growth factors, matrices, and forces combine and control stem cells. *Science,* 324**,** 1673-1677.

Dobkin, B. H. & Dorsch, A. 2013. New evidence for therapies in stroke rehabilitation. *Curr Atheroscler Rep,* 15**,** 331.

Dong, H. W. 2008. *The Allen reference atlas: A digital color brain atlas of the C57Bl/6J male mouse*, John Wiley & Sons Inc.

Emerich, D. F., Silva, E., Ali, O., Mooney, D., Bell, W., Yu, S. J., Kaneko, Y. & Borlongan, C. 2010. Injectable VEGF hydrogels produce near complete neurological and anatomical protection following cerebral ischemia in rats. *Cell Transplant.,* 19**,** 1063-71.

Engler, A. J., Sen, S., Sweeney, H. L. & Discher, D. E. 2006. Matrix elasticity directs stem cell lineage specification. *Cell,* 126**,** 677-689.

Faiz, K. W., Sundseth, A., Thommessen, B. & Ronning, O. M. 2018. Patient knowledge on stroke risk factors, symptoms and treatment options. *Vasc Health Risk Manag,* 14**,** 37-40.

Fernandez-Garcia, L., Mari-Buye, N., Barios, J. A., Madurga, R., Elices, M., Perez-Rigueiro, J., Ramos, M., Guinea, G. V. & Gonzalez-Nieto, D. 2016. Safety and tolerability of silk fibroin hydrogels implanted into the mouse brain. *Acta Biomater,* 45**,** 262-275.

Floren, M., Bonani, W., Dharmarajan, A., Motta, A., Migliaresi, C. & Tan, W. 2016a. Human mesenchymal stem cells cultured on silk hydrogels with variable stiffness and growth factor differentiate into mature smooth muscle cell phenotype. *Acta biomaterialia,* 31**,** 156-166.

Floren, M., Migliaresi, C. & Motta, A. 2016b. Processing techniques and applications of silk hydrogels in bioengineering. *Journal of functional biomaterials,* 7**,** 26.

Freudenberg, U., Hermann, A., Welzel, P. B., Stirl, K., Schwarz, S. C., Grimmer, M., Zieris, A., Panyanuwat, W., Zschoche, S., Meinhold, D., Storch, A. & Werner, C. 2009. A star-PEG-heparin hydrogel platform to aid cell replacement therapies for neurodegenerative diseases. *Biomaterials,* 30**,** 5049-60.

Gasperini, L., Mano, J. F. & Reis, R. L. 2014. Natural polymers for the microencapsulation of cells. *J. R. Soc. Interface,* 11**,** 20140817.

Georges, P. C., Miller, W. J., Meaney, D. F., Sawyer, E. S. & Janmey, P. A. 2006. Matrices with compliance comparable to that of brain tissue select neuronal over glial growth in mixed cortical cultures. *Biophysical journal,* 90**,** 3012-3018.

Ghuman, H., Gerwig, M., Nicholls, F. J., Liu, J. R., Donnelly, J., Badylak, S. F. & Modo, M. 2017. Long-term retention of ECM hydrogel after implantation into a sub-acute stroke cavity reduces lesion volume. *Acta Biomater.,* 63**,** 50-63.

Gorgieva, S. & Kokol, V. 2011. Collagen- vs. Gelatine-Based Biomaterials and Their Biocompatibility: Review and Perspectives. *In:* PIGNATELLO, R. (ed.) *Biomaterials Applications for Nanomedicine.* Rijeka, Croatia: InTech.

Gotoh, Y., Tsukada, M. & Minoura, N. 1998. Effect of the chemical modification of the arginyl residue in Bombyx mori silk fibroin on the attachment and growth of fibroblast cells. *Journal of Biomedical Materials Research Part A,* 39**,** 351-357.

Gutierrez-Fernandez, M., Rodriguez-Frutos, B., Alvarez-Grech, J., Vallejo-Cremades, M. T., Exposito-Alcaide, M., Merino, J., Roda, J. M. & Diez-Tejedor, E. 2011. Functional recovery after hematic administration of allogenic mesenchymal stem cells in acute ischemic stroke in rats. *Neuroscience,* 175**,** 394-405.

Ha, S.-W., Gracz, H. S., Tonelli, A. E. & Hudson, S. M. 2005. Structural Study of Irregular Amino Acid Sequences in the Heavy Chain of Bombyx m ori Silk Fibroin. *Biomacromolecules,* 6**,** 2563-2569.

Hamid, R., Rotshteyn, Y., Rabadi, L., Parikh, R. & Bullock, P. 2004. Comparison of AlamarBlue and MTT assays for high through-put screening. *Toxicology in vitro,* 18**,** 703-710.

Hao, L., Zou, Z., Tian, H., Zhang, Y., Zhou, H. & Liu, L. 2014. Stem cell-based therapies for ischemic stroke. *Biomed Res Int,* 2014**,** 468748.

Horan, R. L., Antle, K., Collette, A. L., Wang, Y., Huang, J., Moreau, J. E., Volloch, V., Kaplan, D. L. & Altman, G. H. 2005. In vitro degradation of silk fibroin. *Biomaterials,* 26**,** 3385-3393.

Howard, D., Buttery, L. D., Shakesheff, K. M. & Roberts, S. J. 2008. Tissue engineering: strategies, stem cells and scaffolds. *Journal of anatomy,* 213**,** 66-72.

Hu, X., Kaplan, D. & Cebe, P. 2006. Determining beta-sheet crystallinity in fibrous proteins by thermal analysis and infrared spectroscopy. *Macromolecules,* 39**,** 6161-6170.

Huang, P., Gebhart, N., Richelson, E., Brott, T. G., Meschia, J. F. & Zubair, A. C. 2014. Mechanism of mesenchymal stem cell-induced neuron recovery and anti-inflammation. *Cytotherapy,* 16**,** 1336-44.

Iadecola, C. & Anrather, J. 2011. The immunology of stroke: from mechanisms to translation. *Nat Med,* 17**,** 796-808.

Inouye, K., Kurokawa, M., Nishikawa, S. & Tsukada, M. 1998. Use of Bombyx mori silk fibroin as a substratum for cultivation of animal cells. *Journal of biochemical and biophysical methods,* 37**,** 159-164.

Jian, R.-L., Mao, L.-B., Xu, Y., Li, X.-F., Wang, F.-P., Luo, X.-G., Zhou, H., He, H.-P., Wang, N. & Zhang, T.-C. 2015. Generation of insulin-producing cells from C3H10T1/2 mesenchymal progenitor cells. *Gene,* 562**,** 107-116.

Jiang, M., Lv, L., Ji, H., Yang, X., Zhu, W., Cai, L., Gu, X., Chai, C., Huang, S., Sun, J. & Dong, Q. 2011. Induction of pluripotent stem cells transplantation therapy for ischemic stroke. *Mol Cell Biochem,* 354**,** 67-75.

Jin, H.-J. & Kaplan, D. L. 2003. Mechanism of silk processing in insects and spiders. *Nature,* 424**,** 1057.

Jin, R., Liu, L., Zhang, S., Nanda, A. & Li, G. 2013. Role of inflammation and its mediators in acute ischemic stroke. *J Cardiovasc Transl Res,* 6**,** 834-51.

Kaplan, C. V. a. D. 2007. Silk as a biomaterial. *progress in polymer science,* 32**,** 991-1007.

Kapoor, S. & Kundu, S. 2016. Silk protein-based hydrogels: promising advanced materials for biomedical applications. *Acta biomaterialia,* 31**,** 17-32.

Kapoor, S. & Kundu, S. C. 2016. Silk protein-based hydrogels: Promising advanced materials for biomedical applications. *Acta Biomater,* 31**,** 17-32.

Kim, U.-J., Park, J., Li, C., Jin, H.-J., Valluzzi, R. & Kaplan, D. L. 2004. Structure and properties of silk hydrogels. *Biomacromolecules,* 5**,** 786-792.

Krishna, O. D. & Kiick, K. L. 2010. Protein-and peptide-modified synthetic polymeric biomaterials. *Peptide Science,* 94**,** 32-48.

Kundu, B., Kurland, N. E., Yadavalli, V. K. & Kundu, S. C. 2014. Isolation and processing of silk proteins for biomedical applications. *International journal of biological macromolecules,* 70**,** 70-77.

Kundu, B., Rajkhowa, R., Kundu, S. C. & Wang, X. 2013. Silk fibroin biomaterials for tissue regenerations. *Adv Drug Deliv Rev,* 65**,** 457-70.

Kuraitis, D., Giordano, C., Ruel, M., Musarò, A. & Suuronen, E. J. 2012. Exploiting extracellular matrix-stem cell interactions: a review of natural materials for therapeutic muscle regeneration. *Biomaterials,* 33**,** 428-443.

Lam, J., Lowry, W. E., Carmichael, S. T. & Segura, T. 2014. Delivery of iPS-NPCs to the Stroke Cavity within a Hyaluronic Acid Matrix Promotes the Differentiation of Transplanted Cells. *Advanced functional materials,* 24**,** 7053-7062.

Lemmens, R. & Steinberg, G. K. 2013. Stem cell therapy for acute cerebral injury: what do we know and what will the future bring? *Curr Opin Neurol,* 26**,** 617-25.

Leng-Duei Koh, Y. C., Choon-Pengteng, Yin-Win Khin, Xian-Jun Loh, Si-Yintee, Michelle Low, Enyi Ye Hai-Dong Yua, Yong-Weizhang , Ming-Yong Han

2015. Structures, mechanical properties and applications of silk fibroin materials. *progress in polymer science,* 46**,** 86-110.

Li, C., Vepari, C., Jin, H.-J., Kim, H. J. & Kaplan, D. L. 2006. Electrospun silk-BMP-2 scaffolds for bone tissue engineering. *Biomaterials,* 27**,** 3115-3124.

Li, S., Nih, L. R., Bachman, H., Fei, P., Li, Y., Nam, E., Dimatteo, R., Carmichael, S. T., Barker, T. H. & Segura, T. 2017. Hydrogels with precisely controlled integrin activation dictate vascular patterning and permeability. *Nat. Mater.,* 16**,** 953-961.

Lindvall, O. & Kokaia, Z. 2010. Stem cells in human neurodegenerative disorders—time for clinical translation? *The Journal of clinical investigation,* 120**,** 29-40.

Liu, S., Yin, F., Zhang, J., Wicha, M. S., Chang, A. E., Fan, W., Chen, L., Fan, M. & Li, Q. 2014. Regulatory roles of miRNA in the human neural stem cell transformation to glioma stem cells. *J Cell Biochem,* 115**,** 1368-80.

Loya, K. 2014. chpater 11- stem cells. *Handbook of Pharmacogenomics and Stratified Medicine*.

M. Cai, Y. Z., B. Zhou, S. Lou 2014. Hypoxic conditioned medium from rat cerebral cortical cells enhances the proliferation and differentiation of neural stem cells mainly through P-K/Akt pathways.

Massensini, A., Ghuman, H., Saldin, L. T., Medberry, C. J., Keane, T. J., Nicholls, F. J., Velankar, S. S., Badylak, S. F. & Modo, M. 2015. Concentration-dependent rheological properties of ECM hydrogel for intracerebral delivery to a stroke cavity. *Acta biomaterialia,* 27**,** 116-130.

Matsumoto, A., Chen, J., Collette, A. L., Kim, U.-J., Altman, G. H., Cebe, P. & Kaplan, D. L. 2006. Mechanisms of silk fibroin sol− gel transitions. *The Journal of Physical Chemistry B,* 110**,** 21630-21638.

Meinel, L., Hofmann, S., Karageorgiou, V., Kirker-Head, C., Mccool, J., Gronowicz, G., Zichner, L., Langer, R., Vunjak-Novakovic, G. & Kaplan, D. L. 2005. The inflammatory responses to silk films in vitro and in vivo. *Biomaterials,* 26**,** 147-155.

Melke, J., Midha, S., Ghosh, S., Ito, K. & Hofmann, S. 2016. Silk fibroin as biomaterial for bone tissue engineering. *Acta biomaterialia,* 31**,** 1-16.

Miljan, E. A. & Sinden, J. D. 2009. Stem cell treatment of ischemic brain injury. *Curr Opin Mol Ther,* 11**,** 394-403.

Minoura, N., Aiba, S.-I., Higuchi, M., Gotoh, Y., Tsukada, M. & Imai, Y. 1995. Attachment and growth of fibroblast cells on silk fibroin. *Biochemical and biophysical research communications,* 208**,** 511-516.

Narita, Y., Yamawaki, A., Kagami, H., Ueda, M. & Ueda, Y. 2008. Effects of transforming growth factor-beta 1 and ascorbic acid on differentiation of human bone-marrow-derived mesenchymal stem cells into smooth muscle cell lineage. *Cell and tissue research,* 333**,** 449-459.

Nguyen, M. K. & Alsberg, E. 2014. Bioactive factor delivery strategies from engineered polymer hydrogels for therapeutic medicine. *Prog. Polym. Sci.,* 39**,** 1236-1265.

Nhs, U. 2017. STROKE.

Nicholls, F. J., Rotz, M. W., Ghuman, H., Macrenaris, K. W., Meade, T. J. & Modo, M. 2016. DNA–gadolinium–gold nanoparticles for in vivo T1 MR imaging of transplanted human neural stem cells. *Biomaterials,* 77**,** 291-306.

Nih, L. R., Carmichael, S. T. & Segura, T. 2016. Hydrogels for brain repair after stroke: an emerging treatment option. *Curr Opin Biotechnol,* 40**,** 155-163.

Padmanabhan, S. 2014. *Handbook of pharmacogenomics and stratified medicine,* Academic Press.

Pakulska, M. M., Ballios, B. G. & Shoichet, M. S. 2012. Injectable hydrogels for central nervous system therapy. *Biomed Mater,* 7**,** 024101.

Park, J. & Lakes, R. S. 2007. *Biomaterials: an introduction*, Springer Science & Business Media.

Partlow, B. P., Hanna, C. W., Rnjak-Kovacina, J., Moreau, J. E., Applegate, M. B., Burke, K. A., Marelli, B., Mitropoulos, A. N., Omenetto, F. G. & Kaplan, D. L. 2014. Highly tunable elastomeric silk biomaterials. *Advanced functional materials,* 24**,** 4615-4624.

Paul, G. & Anisimov, S. V. 2013. The secretome of mesenchymal stem cells: potential implications for neuroregeneration. *Biochimie,* 95**,** 2246-56.

Paulusse, J. M. & Sijbesma, R. P. 2006. Ultrasound in polymer chemistry: revival of an established technique. *Journal of Polymer Science Part A: Polymer Chemistry,* 44**,** 5445-5453.

Porter, F. V. D. 2009. Silks as ancient models for modern polymers. *Polymer* 50**,** 5623-5632.

Prewitz, M., Seib, F. P., Pompe, T. & Werner, C. 2012. Polymeric biomaterials for stem cell bioengineering. *Macromolecular rapid communications,* 33**,** 1420-1431.

Prewitz, M. C., Seib, F. P., Von Bonin, M., Friedrichs, J., Stissel, A., Niehage, C., Muller, K., Anastassiadis, K., Waskow, C., Hoflack, B., Bornhauser, M. & Werner, C. 2013. Tightly anchored tissue-mimetic matrices as instructive stem cell microenvironments. *Nat. Methods,* 10**,** 788-94.

Quertainmont, R., Cantinieaux, D., Botman, O., Sid, S., Schoenen, J. & Franzen, R. 2012. Mesenchymal stem cell graft improves recovery after spinal cord injury in adult rats through neurotrophic and pro-angiogenic actions. *PloS one,* 7**,** e39500.

Reis, C., Wilkinson, M., Reis, H., Akyol, O., Gospodarev, V., Araujo, C., Chen, S. & Zhang, J. H. 2017. A Look into Stem Cell Therapy: Exploring the Options for Treatment of Ischemic Stroke. *Stem Cells Int,* 2017**,** 3267352.

Reznikoff, C. A., Brankow, D. W. & Heidelberger, C. 1973. Establishment and characterization of a cloned line of C3H mouse embryo cells sensitive to postconfluence inhibition of division. *Cancer research,* 33**,** 3231-3238.

Robert Passier, C. M. 2003. Origin and use of embryonic and adult stem cells in differentiation and tissue repair. *cardiovascular research,* 58**,** 324-335.

Rockwood, D. N., Preda, R. C., Yucel, T., Wang, X., Lovett, M. L. & Kaplan, D. L. 2011. Materials fabrication from Bombyx mori silk fibroin. *Nat Protoc,* 6**,** 1612-31.

Rossignol, J., Fink, K., Davis, K., Clerc, S., Crane, A., Matchynski, J., Lowrance, S., Bombard, M., Dekorver, N., Lescaudron, L. & Dunbar, G. L. 2014. Transplants of adult mesenchymal and neural stem cells provide neuroprotection and behavioral sparing in a transgenic rat model of Huntington's disease. *Stem Cells,* 32**,** 500-9.

Seib, F. P. 2017. Silk nanoparticles-an emerging anticancer nanomedicine. *AIMS Bioengineering,* 42**,** 239-258.

Seib, F. P. & Kaplan, D. L. 2013. Silk for drug delivery applications: opportunities and challenges. *Israel Journal of Chemistry,* 53**,** 756-766.

Seib, F. P., Pritchard, E. M. & Kaplan, D. L. 2013. Self-Assembling Doxorubicin Silk Hydrogels for the Focal Treatment of Primary Breast Cancer. *Advanced functional materials,* 23**,** 58-65.

Seib, F. P. K., D. L 2013. Silk for Drug Delivery Applications: Opportunities and Challenges. *Israel Journal of Chemistry,* 53**,** 756-766.

Seib, P. 2018. Silk hydrogels for drug and cell delivery. *In:* IN T. R. R. SINGH, G. L. R. D. E. (ed.) *Hydrogels: Design, Synthesis and Application in Drug Delivery & Regenerative Medicine.* Boca Raton, Florida, USA.

Seliktar, D. 2012. Designing cell-compatible hydrogels for biomedical applications. *Science,* 336**,** 1124-8.

Sharma, R., Wang, E. T. H. & Yang, Y. P. 2015. Development of mRuby2-Transfected C3H10T1/2 Fibroblasts for Musculoskeletal Tissue Engineering. *PloS one,* 10**,** e0139054.

Shi, Z., Huang, H. & Feng, S. 2016. Stem cell-based therapies to treat spinal cord injury&58; a review. *Journal of Neurorestoratology,* 55**,** 125-131.

Shoichet, M. S., Tate, C. C., Baumann, M. D. & Laplaca, M. C. 2008. Strategies for Regeneration and Repair in the Injured Central Nervous System. *In:* REICHERT, W. M. (ed.) *Indwelling Neural Implants: Strategies for Contending with the In Vivo Environment.* Boca Raton (FL).

Sinden, J. D. & Muir, K. W. 2012. Stem cells in stroke treatment: the promise and the challenges. *Int J Stroke,* 7**,** 426-34.

Stefan Przyborski, S. a. H., Daniel J. Maltman. 2008. Mesenchymal stem cells as mediators of neural differentiation. *current stem cell research therapy,* 3**,** 43-52.

Stojkovic, M., Lako, M., Stojkovic, P., Stewart, R., Przyborski, S., Armstrong, L., Evans, J., Herbert, M., Hyslop, L., Ahmad, S., Murdoch, A. & Strachan, T.

2004. Derivation of human embryonic stem cells from day-8 blastocysts recovered after three-step in vitro culture. *Stem Cells,* 22**,** 790-7.

Stonesifer, C., Corey, S., Ghanekar, S., Diamandis, Z., Acosta, S. A. & Borlongan, C. V. 2017. Stem cell therapy for abrogating stroke-induced neuroinflammation and relevant secondary cell death mechanisms. *Prog Neurobiol,* 158**,** 94-131.

Strokeassociation, U. 2018. Stroke statistics. *State of the Nation: stroke statistics*.

Sugihara, A., Sugiura, K., Morita, H., Ninagawa, T., Tubouchi, K., Tobe, R., Izumiya, M., Horio, T., Abraham, N. G. & Ikehara, S. 2000. Promotive Effects of a Silk Film on Epidermal Recovery from Full-Thickness Skin Wounds. *Proceedings of the society for experimental biology and medicine,* 225**,** 58-64.

Sun, W., Incitti, T., Migliaresi, C., Quattrone, A., Casarosa, S. & Motta, A. 2017. Viability and neuronal differentiation of neural stem cells encapsulated in silk fibroin hydrogel functionalized with an IKVAV peptide. *J Tissue Eng Regen Med,* 11**,** 1532-1541.

Sun, W., Incitti, T., Quattrone, A., Casarosa, S., Motta, A. & Migliaresi, C. 2016a. Genipin-crosslinked gelatin-silk fibroin hydrogels for modulating the behaviour of pluripotent cells. *J Tissue Eng Regen Med,* 10**,** 876-887.

Sun, W., Motta, A., Shi, Y., Seekamp, A., Schmidt, H., Gorb, S. N., Migliaresi, C. & Fuchs, S. 2016b. Co-culture of outgrowth endothelial cells with human mesenchymal stem cells in silk fibroin hydrogels promotes angiogenesis. *Biomed Mater,* 11**,** 035009.

Suzuki, S., Narita, Y., Yamawaki, A., Murase, Y., Satake, M., Mutsuga, M., Okamoto, H., Kagami, H., Ueda, M. & Ueda, Y. 2010. Effects of extracellular matrix on differentiation of human bone marrow-derived mesenchymal stem cells into smooth muscle cell lineage: utility for cardiovascular tissue engineering. *Cells Tissues Organs,* 191**,** 269-280.

Sylvester, P. W. 2011. Optimization of the tetrazolium dye (MTT) colorimetric assay for cellular growth and viability. *Drug Design and Discovery.* Springer.

Takahashi, K. & Yamanaka, S. 2006. Induction of pluripotent stem cells from mouse embryonic and adult fibroblast cultures by defined factors. *Cell,* 126**,** 663-76.

Tam, R. Y., Fuehrmann, T., Mitrousis, N. & Shoichet, M. S. 2014. Regenerative therapies for central nervous system diseases: a biomaterials approach. *Neuropsychopharmacology,* 39**,** 169-88.

Teo, W. E. & Ramakrishna, S. 2006. A review on electrospinning design and nanofibre assemblies. *Nanotechnology,* 17**,** R89-R106.

Thonhoff, J. R., Lou, D. I., Jordan, P. M., Zhao, X. & Wu, P. 2008. Compatibility of human fetal neural stem cells with hydrogel biomaterials in vitro. *Brain Res.,* 1187**,** 42-51.

Thurber, A. E., Omenetto, F. G. & Kaplan, D. L. 2015. In vivo bioresponses to silk proteins. *Biomaterials,* 71**,** 145-157.

Tseng, T. C., Tao, L., Hsieh, F. Y., Wei, Y., Chiu, I. M. & Hsu, S. H. 2015. An Injectable, Self-Healing Hydrogel to Repair the Central Nervous System. *Adv. Mater.,* 27**,** 3518-24.

Uludag, H., De Vos, P. & Tresco, P. A. 2000. Technology of mammalian cell encapsulation. *Advanced drug delivery reviews,* 42**,** 29-64.

Vining, K. H. & Mooney, D. J. 2017. Mechanical forces direct stem cell behaviour in development and regeneration. *Nature Reviews Molecular Cell Biology,* 18**,** 728.

Vu, T., Xue, Y., Vuong, T., Erbe, M., Bennet, C., Palazzo, B., Popielski, L., Rodriguez, N. & Hu, X. 2016. Comparative study of ultrasonication-induced and naturally self-assembled silk fibroin-wool keratin hydrogel biomaterials. *International journal of molecular sciences,* 17**,** 1497.

Wang, J., Yang, W., Xie, H., Song, Y., Li, Y. & Wang, L. 2014. Ischemic stroke and repair: current trends in research and tissue engineering treatments. *Regenerative medicine research,* 2**,** 3.

Wang, X., Kluge, J. A., Leisk, G. G. & Kaplan, D. L. 2008. Sonication-induced gelation of silk fibroin for cell encapsulation. *Biomaterials,* 29**,** 1054-64.

Wechsler, L. R. 2009. Clinical trials of stroke therapy: which cells, which patients? *Stroke,* 40**,** S149-51.

Werner, C. & Engelhard, K. 2007. Pathophysiology of traumatic brain injury. *Br J Anaesth,* 99**,** 4-9.

Yilmaz, G. & Granger, D. N. 2010. Leukocyte recruitment and ischemic brain injury. *Neuromolecular medicine,* 12**,** 193-204.

Zhang, H.-L., Xie, X.-F., Xiong, Y.-Q., Liu, S.-M., Hu, G.-Z., Cao, W.-F. & Wu, X.-M. 2017. Comparisons of the therapeutic effects of three different routes of bone marrow mesenchymal stem cell transplantation in cerebral ischemic rats. *Brain research*.

Zhang, J., Tokatlian, T., Zhong, J., Ng, Q. K., Patterson, M., Lowry, W. E., Carmichael, S. T. & Segura, T. 2011. Physically Associated Synthetic Hydrogels with Long-Term Covalent Stabilization for Cell Culture and Stem Cell Transplantation. *Advanced Materials,* 23**,** 5098-5103.

Zhang, P., Li, J., Liu, Y., Chen, X., Lu, H., Kang, Q., Li, W. & Gao, M. 2011. Human embryonic neural stem cell transplantation increases subventricular zone cell proliferation and promotes peri-infarct angiogenesis after focal cerebral ischemia. *Neuropathology,* 31**,** 384-91.

Zhang, R. L., Chopp, M., Roberts, C., Liu, X., Wei, M., Nejad-Davarani, S. P., Wang, X. & Zhang, Z. G. 2014. Stroke increases neural stem cells and angiogenesis in the neurogenic niche of the adult mouse. *PLoS One,* 9**,** e113972.

Zhang, Y., Ying, G., Ren, C., Jizhang, Y., Brogan, D., Liu, Z., Li, S., Ding, Y., Borlongan, C. V., Zhang, J. & Ji, X. 2015. Administration of human platelet-rich plasma reduces infarction volume and improves motor function in adult rats with focal ischemic stroke. *Brain Res,* 1594**,** 267-73.